Development of ROS-Modulating Nanoparticles for Anti-Inflammatory Therapies

Amandine Courtemanche

A thesis submitted to the University of Ottawa in partial fulfillment of the requirements for the Master of Science degree in Cellular and Molecular Medicine

Department of Cellular and Molecular Medicine

Faculty of Medicine

University of Ottawa, Ontario, Canada

Table of contents

List of Figures ..... **v**
Abbreviations ..... **vi**
Abstract ..... **viii**
Acknowledgements / Preface ..... **ix**
1. Introduction **1**
1.1. Inflammation 1
1.2. Chronic inflammatory diseases (CID) 1
1.2.1. CIDs and prevalence 1
1.2.2. Current treatments for CIDs 2
1.3. Reactive oxygen species (ROS) 3
1.3.1. What are ROS? 3
1.3.2. Oxidative stress 4
1.3.3. Oxidative damage to macromolecules 4
1.3.4. Sources of ROS production 5
1.3.5. Methods of ROS regulation 7
1.3.6. ROS signaling and physiological roles 9
1.3.7. ROS involvement in chronic inflammatory diseases 10
1.3.8. Current research on ROS-regulating strategies 11
1.4. Nanoparticles (NPs) 11
1.4.1. What are NPs? 11
1.4.2. Common types of nanoparticle compositions and structures 12
1.4.3. Advantages of NPs for drug delivery 13
1.4.4. Nanoparticle systemic circulation 15
1.4.5. Nanoparticle cellular uptake 16
1.5. Concept and structure of the NP system created 18
1.5.1. Rationale for the development of the NPs 18
1.5.2. Essential properties for the function of our NPs 19
1.5.3. NP structural components 19
1.5.4. Multi-functional approaches 25
1.6. Research hypothesis and objectives 25

2. Materials and Methods 26
2.1. Materials 26
2.2. Biomaterial synthesis 27
2.2.1. Boronic acid polymers: AC2, AC2N and AC2B polymer syntheses 27
2.2.2. Boronic acid polymers: AC4 polymer synthesis 28
2.2.3. AC3 polymer synthesis 28
2.2.4. AC5P and AC5 polymer syntheses 28
2.2.5. PEG-BA synthesis 29
2.2.6. CMDex-BA synthesis 29
2.2.7. PLGA-PEG-OH and PLGA-PEG-TPP polymer syntheses 30
2.3. In solution assays: Boronic ester bond formation and ROS-sensitivity 31
2.3.1. Boronic ester bond detection by fluorescence 31
2.3.2. Boronic ester bond detection by ^{1}H NMR 32
2.4. Nanoparticle assembly, optimization and property assessment 32
2.4.1. Optimization of NP ROS-scavenger content 32
2.4.2. Assembly of AC2 NP formulations selected for further studies 33
2.4.3. Assessment of NP stability 34
2.4.4. Nanoparticle visualization by transmission electron microscopy 34
2.4.5. Assessment of the NPs' ROS-sensitivity properties in solution 35
2.4.6. Assessment of the NP's ROS-scavenging properties in solution 35
2.5. Assessment of the NPs in vitro 36
2.5.1. Assessment of NP cellular uptake 36
2.5.2. Confirmation of NP cellular uptake and mitochondria targeting abilities 36
2.5.3. Assessment of NP cytotoxicity 37
2.5.4. Assessment of NP ROS-reduction abilities in vitro 38
2.5.5. Assessment of NP anti-inflammatory properties in vitro 39
3. Results 40
3.1. Confirmation of synthesis for the main biomaterials of interest 40
3.1.1. Synthesis of the AC2 polymer 40
3.1.2. Synthesis of the AC5P and AC5 polymer 41
3.1.3. Synthesis of the PLGA-PEG-OH and PLGA-PEG-TPP polymers 44
3.2. Confirmation of boronic ester bond formation by fluorescence 46

3.3. Confirmation of boronic ester bond formation and its ROS-sensitivity by NMR 48
3.4. Optimization of NP formulations 50
3.5. Characterization of selected NP formulations 51
3.6. NP visualization by transmission electron microscopy 53
3.7. Storage and biological stability of the NPs 53
3.8. Assessment of NPs ROS-sensitivity potential 54
3.9. Assessment of NPs ROS-scavenging potential 58
3.10. Assessment of NP cytotoxicity 59
3.11. NP cellular uptake 60
3.12. Confirmation of NP cellular uptake and mitochondrial targeting 61
3.13. Assessment of NP ROS-reduction in vitro 62
3.14. Assessment of NP inflammation reduction in vitro 63
4. Discussion 64
4.1. Biomaterial library synthesis 64
4.2. Monitoring of tannic acid fluorescence for confirmation of boronic ester bond formation 66
4.3. Confirmation of boronic ester bond formation and its ROS-sensitivity by NMR 69
4.4. Optimization of nanoparticle formulations 70
4.5. Physical characterization of the selected NP formulations 72
4.6. Stability of NPs for storage and biological conditions 74
4.7. Assessment of NPs ROS-sensitivity potential 76
4.8. Assessment of NPs ROS-scavenging potential 79
4.9. Nanoparticle cellular uptake and mitochondrial localization 82
4.10. Assessment of NP cytotoxicity 84
4.11. Assessment of NP ROS-reduction potential in vitro 85
4.12. Nanoparticle inflammation reduction 86
5. Future Directions 87
6. Conclusion 88
References 90

List of Figures

Figure 1. Schematic of cellular ROS production and regulation. 8
Figure 2. ROS-dependent NP properties 19
Figure 3. Structure and concept of the NP system. 24
Figure 4. Confirmation of successful synthesis for the AC2 polymer 41
Figure 5. Confirmation of synthesis for the AC5P and AC5 polymers 43
Figure 6. Confirmation of synthesis for PLGA-PEG-OH and PLGA-PEG-TPP 45
Figure 7. Fluorescence assessment of the complex formation between the polymer and the ROS-scavenger via boronic ester bond formation 47
Figure 8. ^{1}H NMR assessment of ROS-sensitive complex formation between boronic acid and the ROS-scavenger 49
Figure 9. Size and PDI optimization of the NPs' ROS-scavenger content 51
Figure 10. Characteristics of chosen NP systems 52
Figure 11. NP visualization by TEM 53
Figure 12. NP stability in storage and biological conditions 54
Figure 13. NP ROS-sensitivity in solution 57
Figure 14. NP potential for ROS-scavenging in solution 58
Figure 15. Assessment of NP cytotoxicity 59
Figure 16. NP cellular uptake via flow cytometry 60
Figure 17. NP cellular uptake and mitochondrial targeting microscopy studies 61
Figure 18. NP ROS-reduction potential in vitro 62
Figure 19. NP anti-inflammatory properties in vitro 63
Figure 20. Possible mechanism for the H_2O_2-induced breakage of the ROS-sensitive bond 76
Figure 21. ROS-scavenging mechanism 80

Abbreviations

ABCA1	ATP-binding cassette	**IFN-β**	Interferon-β
ACN	Acetonitrile	**IL-*X* (1β, 6, 8, 10, 12, 18)**	Interleukin
AD	Alzheimer's disease	**IMS**	Intermembrane space
AIBN	Azobisisobutyronitrile	**JAK/STAT**	Janus kinase/signal transducer and activator of transcription
APC	Allophycocyanin	**JNK**	Jun N-terminal kinase
$CDCl_3$	Deuterated chloroform	**kD**	kilodalton
cDNA	Complementary DNA	**LA**	Lactic acid
CID	Chronic inflammatory disease	**LDH**	Lactate dehydrogenase
COX	Cyclooxygenase	**LNP**	Lipid-based nanoparticle
CVD	Cardiovascular disease	**LPS**	Lipopolysaccharide
Cy5.5	Cyanine 5.5	**Mal**	Maleic anhydride polymer
DCF	Dichlorofluorescein	**MAPK**	Mitogen-activated protein kinase
DCFH—DA	2',7'-Dichlorofluorescein diacetate	**MDA**	Malondialdehyde
diBA	Benzene-1,4-diboronic acid	**MeOH**	Methanol
DLS	Dynamic light scattering	**miRNA**	Micro RNA
DMEM	Dulbecco's modified eagle medium	**MPO**	Myeloperoxidase
DMF	N,N-Dimethylformamide	**mRNA**	Messenger RNA
DMSO	Dimethyl sulfoxide	**Mw**	Molecular weight
DMSO-d6	Deuterated DMSO	**NADH**	Nicotinamide adenine dinucleotide
EG	Epigallocatechin gallate	**NADPH**	Nicotinamide adenine dinucleotide phosphate
EGNP	Epigallocatechin gallate nanoparticle	**NaOH**	Sodium hydroxide
eNP	Empty nanoparticle	**NF-κB**	Nuclear factor kappa B
ETC	Electron transport chain	**NMR**	Nuclear magnetic resonance
$FADH_2$	Flavin adenine dinucleotide	**NOS**	Nitric oxide synthase
FBS	Fetal bovine serum	**NOX**	NADPH oxidase
FDA	Food and drug administration	**NP**	Nanoparticle
FITC	Fluorescein isothiocyanate	**NSAID**	Non-steroidal anti-inflammatory drugs
FSC	Forward scatter	**PDI**	Polydispersity index
GA	Gallic acid	**PEG**	Poly(ethylene glycol)
GANP	Gallic acid nanoparticle	**PFA**	Paraformaldehyde
GlA	Glycolic acid	**PLGA**	Poly(lactic-co-glycolic acid)
GPX	Glutathione peroxidase	**PNP**	Polymeric nanoparticle
GSH	Glutathione	**ppm**	Parts per million
H_2O_2	Hydrogen peroxide	**PRX**	Peroxiredoxin
HOCl	Hypochlorous acid		

RAFT	Reversible addition-fragmentation chain transfer polymerization	**TEM**	Transmission electron microscopy
ROS	Reactive oxygen species	**THF**	Tetrahydrofuran
RT-qPCR	Quantitative reverse transcription polymerase chain reaction	**TNF-α**	Tumor necrosis factor alpha
SD	Standard deviation	**TOM20**	Translocase of outer mitochondrial membrane 20
SEM	Standard error of the mean	**TPP**	(4-Carboxybutyl)triphenylphosphonium bromide
siRNA	Silencing RNA	**VDAC**	Voltage dependant anionic channel
SOD	Superoxide dismutase	**WHO**	World health organization
SSC	Side scatter	**XO**	Xanthine oxidase
TANP	Tannic acid nanoparticle		

Abstract

Inflammation is a normal protective biological response mediated by a variety of pathways, many of which involve reactive oxygen species (ROS). ROS contribute to the progression of inflammation either by their involvement in inflammatory signaling, or via the oxidative stress they produce when present in elevated levels. As a prospective therapy for ROS and inflammation reduction, a novel ROS-sensitive and ROS-scavenging nanoparticle (NP) system was developed in this project. To this end, a library of biomaterials was synthesized, characterized, and assessed for their potential in forming ROS-sensitive boronic ester bonds. NP systems were assembled using these synthesized polymers and 1 of 3 ROS-scavengers: tannic acid (TA), gallic acid (GA) and epigallocatechin gallate (EG). The NPs demonstrated ROS-dependent properties in solution and in vitro. Additionally, they exhibited good cellular uptake and low cytotoxicity. Thus, we have obtained an optimized system which successfully activates in high ROS conditions, reduces ROS levels in inflammatory conditions, and exhibits potential for inflammation reduction.

Acknowledgements / Preface

I would like to begin by acknowledging those who have supported me throughout my Master and have contributed to making possible the completion of this project. Firstly, thank you to my supervisor, Dr. Suresh Gadde, for his insight and guidance throughout my Master and for his patience at answering my innumerable questions. My time as part of the G-INCs Lab has challenged me and allowed me to learn so much, it will definitely be a memorable learning experience. Thank you as well to my TAC members, Dr. Diane Lagace and Dr. Mireille Khacho, for their feedback and advice.

Additionally, I would like to recognize the University of Ottawa core facilities, particularly the flow cytometry and virometry (FVC) core, the cell biology and image acquisition (CBIA) core and the transmission electron microscopy (TEM) core for their time in sharing their expertise as well as allowing us to use their equipment. I would also like to acknowledge the generous financial support from the Canadian Institutes of Health Research (CIHR) and the center for infection, immunity and inflammation (CI3), thanks for seeing the potential in me and my project.

Lastly, special thanks to Dr. Shireesha Manturthi for her patience and insightful help and guidance in chemistry as well as Redaet Daniel for her expertise, availability and patience in teaching me microscopy techniques. Thanks as well to my friends, lab mates and family who have always lent me an ear and offered me help and support through the ups and downs of the past 2 years. I couldn’t have done it without their support.

1. Introduction

1.1. Inflammation

Inflammation is a normal protective biological response initiated by the immune system to restore homeostasis following aversive physical, chemical or infectious events[1]. The acute inflammatory response is comprised of a vast array of pathways activated during an immune response[2]. These pathways recruit effectors responsible for resolving the issue at hand. Once the issue resolved, the upregulated pathways are typically attenuated, thus ending the inflammatory response[3]. In certain conditions, the acute inflammatory response may be activated unnecessarily, sustained despite resolution of the issue or may be unable to resolve the issue successfully, leading to its continuous activation[4]. In such cases, the uncontrolled inflammatory response may become chronic, causing detrimental outcomes as seen in chronic inflammatory disease cases[2].

1.2. Chronic inflammatory diseases (CID)

1.2.1. CIDs and prevalence

Chronic inflammatory diseases encompass a large variety of disease conditions, including diabetes, cardiovascular diseases (CVDs) (such as atherosclerosis), neurodegenerative diseases (such as Alzheimer's disease), arthritis and chronic kidney diseases amongst many others[3,4]. In addition to their high variety, the prevalence of such diseases is notable. Indeed, in 2021, an estimated 10.5% of the world's population was living with diabetes with a predicted rise to 11.3% by 2030[5]. As for Alzheimer's disease (AD) it is believed to affect 22% of people over 50 years of age globally, whereas rheumatoid arthritis was estimated to affect 17.6 million people worldwide in 2020 with a projected to increase to 31.7 million by 2050[6,7]. Thus, CIDs affect a great number of individuals directly and indirectly in addition to posing a heavy burden on the healthcare system and economy.

Not only are CIDs prevalent, but they are also very deadly. The World Health Organization (WHO) considers noncommunicable diseases, diseases which aren't transmitted from one individual to another, many of which are CIDs, as one of the highest threats to global health in 2019. Indeed, over 50% of all deaths may be linked back to inflammation-related diseases[3,8].

Certain risk factors for the development of CIDs have been identified including age, obesity, diet and genetics[4,9]. Some sources even suggest that the high prevalence of CIDs may be linked to urbanization and the reduced exposure to pathogens in infancy[9]. This evolutionary medicine point of view claims that this reduced exposure may result in an overly sensitive and thus overly aggressive immune response later in life, causing CIDs[9].

1.2.2. Current treatments for CIDs

Currently, treatments options for patients with CIDs remain limited. Possible avenues include dietary changes, implementation of physical exercise and the use of anti-inflammatory or disease specific drugs. Dietary recommendations for CIDs patients include reducing the intake of foods with high glycemic indexes as they are related to higher risks of cardiovascular diseases (CVD) and diabetes, as well as reducing total fat intake with a focus on reduction of saturated and trans fat which aggravate inflammation[4]. Dietary changes also focus on increasing the intake of fruits, vegetables and some teas high in antioxidants and polyphenols, thus offering protection against inflammation. Incorporating micronutrients which are known for their anti-inflammatory properties, such as magnesium and vitamin D, or for their antioxidant properties, such as vitamin E, zinc and selenium, may also be beneficial [4].

As for prescribed medications, they vary a lot depending on the specific disease condition. They mainly include drugs such as metformin for diabetes, statins for CVDs and corticosteroids

or non-steroidal anti-inflammatory drugs (NSAIDs) for arthritis[4]. Unfortunately, currently available treatments for CIDs are insufficient. Notably, only a minority of rheumatoid arthritis patients reach a sustained clinical remission[10]. Reasons explaining why most anti-inflammatory drugs used for CIDs prove to be insufficient include the large doses required, their systemic distribution, possible toxicity, the focus of some medication on symptom relief rather than addressing disease cause, the variety of cytokines involved in inflammatory pathways and the complexity of their downstream effects as well as the complexity of the disease-specific pathology[10,11]. Thus, the development of novel therapies for CIDs remains a strong topic of interest[11].

1.3. Reactive oxygen species (ROS)

1.3.1. What are ROS?

Reactive oxygen species (ROS) are highly reactive, oxygen-containing molecules often involved as signaling molecules in crucial cellular processes such as inflammation, cellular proliferation and cellular differentiation[12]. ROS include molecules such as the superoxide anion, the hydroxyl radical and hydrogen peroxide (H_2O_2) all of which are free radicals or free radical precursors making them very reactive[12]. Indeed, free radicals are characterized by the presence of unpaired electrons which may negatively interact with cellular components to stabilize themselves, causing damages as seen in certain pathological conditions such as chronic inflammatory diseases[13,14]. In healthy individuals, ROS levels are typically kept within a homeostatic range by endogenous antioxidants and enzyme systems to limit their damaging effects and enable them to maintain their intended physiological function[15]. Thus, the link between ROS and inflammation is dual; ROS is involved in signaling within the inflammatory cascade, but it may also be a source of oxidative stress, thus involving it in both physiological and pathological conditions[16,17].

1.3.2. Oxidative stress

In disease conditions, either through ROS overproduction or reduced antioxidant defense, a redox imbalance may occur in which ROS levels surpass their regulation capacity, this is known as oxidative stress[17]. In such instances, ROS are more likely to negatively interact and damage various macromolecules such as lipids, proteins and DNA leading to tissue damage and persisting inflammation[14]. When reacting with these macromolecules, ROS are successfully able to stabilize themselves but in turn create a novel radical species which will itself negatively interact with other macromolecules. This step of the radical chain reaction, known as propagation, can create substantial damage[13]. Without restauration of a sufficient antioxidant defence, termination of the chain doesn't occur, and thus free radical propagation and damages persist, resulting in inflammation[14].

1.3.3. Oxidative damage to macromolecules

When ROS interact with nucleic acids, they may interact with a nucleotide's base or sugar component (ribose or deoxyribose)[18]. The most common ROS-induced nucleic acid damage is the oxidation of a guanine nucleotide by a hydroxyl radical to 8-oxoguanine, a biomarker for ROS-induced DNA damage[18–21]. In DNA, the presence of 8-oxoguanine may lead to a transversion mutation, ultimately leading to a double stranded break post DNA replication[22]. Single-strand and double-strand DNA breaks may also result from ROS interaction with deoxyribose components[18]. These breaks, if not repaired correctly, may lead to mutations, cell death and even carcinogenesis[18]. In RNA, oxidative damage may interfere with protein production and the function of noncoding RNAs[19].

In the case of its interaction with lipids, ROS, mainly the hydroxyl radical, may lead to lipid peroxidation. This process is characterized by the oxidation of unsaturated lipid chains which, when occurring at the cell membrane, can alter membrane integrity, fluidity and may

even induce cell death[18]. In addition, lipid peroxidation byproducts, such as malondialdehyde (MDA) may be harmful due to their toxicity and mutagenic tendencies[18].

As for their interactions with proteins, ROS-induced damages include amino acid oxidation and cleavage of certain peptide bonds which can impede correct protein folding[18,22]. This may lead to protein aggregation or prevent the correct function of their catalytic sites[18]. As proteins are crucial actors of cellular pathways, notably as receptors and enzymes, this can have immense impact on cell function and well-being. Degradation of oxidized proteins is possible by proteasomal and lysosomal function, but these typical protein degradation mechanisms are incapable of degrading protein aggregates, leading to enhanced protein aggregation[23].

1.3.4. Sources of ROS production

Given the high oxidative and damaging potential of ROS, it is interesting to delve into the conditions surrounding its production. Energy production in eukaryotic cells mainly occurs thanks to the mitochondria's role in cellular respiration. As an aerobic process, cellular respiration requires oxygen as the final electron acceptor of the electron transport chain (ETC). Oxidative phosphorylation requires NADH and $FADH_2$ electron carriers to undergo oxidation and donate their electrons at various points for transport through the ETC's coenzyme Q, cytochrome C and 4 complexes embedded within the inner mitochondrial membrane. As they progress through the chain, electrons may leak from the complexes and associate with oxygen molecules leading to the formation of superoxide anions[24]. Complexes I, II and III of the ETC all leak electrons towards the mitochondrial matrix whereas complex III also leaks electrons in the intermembrane space (IMS). Within the ETC, complex III is regarded as the main site for ROS production as it is the site of ubisemiquinone production, a radical intermediate of coenzyme Q[24]. This compound's autooxidation potential renders it capable of reducing oxygen molecules to

superoxide anions. Alongside complex III, complex I is regarded as a significant ROS production site whereas complex II, while still a debated topic, is typically disregarded as a significant contributor to ROS levels partly due to its function as a succinate electron acceptor and the fact that succinate levels are usually low in tissues[25,26]. Overall, through this electron leakage phenomenon, the mitochondria is responsible for producing approximately 90% of cellular ROS, making it the main ROS producer in the cell (Figure 1)[24].

After the mitochondrial ETC, NADPH oxidase (NOX) enzymes are the next most significant contributors to cellular ROS levels as their main function consists of controlled ROS production[27]. The NOX enzyme family consists of 7 different enzymes, all of which are transmembrane proteins[27,28]. Depending on the cell type and specific enzyme, NOX may be found in the plasma, mitochondrial and nuclear membranes as well as in the endoplasmic reticulum, lipid rafts and focal adhesions[27]. NOX generate ROS via the transfer of electrons from NADPH to molecular oxygen thus reducing it and yielding either the superoxide anion or H_2O_2[27]. The ROS produced by NOX are typically involved in cellular signaling pathways such as cell proliferation or differentiation or may be used for oxidative bursts in certain cell types[27]. Cells also possess other potential ROS producers such as xanthine oxidase (XO), cytochrome p450, myeloperoxidase (MPO), cyclooxygenases (COXs), nitric oxide synthase (NOS) and transition metals amongst others, all of which contribute to total ROS levels at a much lesser extent[27,29].

The presence of ROS may also stem from exogenous factors. Notably, certain sources, such as cigarette smoke, contain oxidizing molecules themselves which may lead to oxidative stress once inside the body. In other cases, sources such as radiation, cancer chemotherapy, food,

alcohol and drugs may cause the formation of ROS or induce it's production by the cells themselves[29].

1.3.5. Methods of ROS regulation

In the mitochondria, the superoxide anions produced from the ETC's electron leakage will be found mostly in the mitochondrial matrix but also in the IMS[15]. As they cannot cross the inner mitochondrial membrane due to their negative charge, superoxide anions from the mitochondrial matrix will undergo a conversion to H_2O_2 by the superoxide dismutase 2 (SOD2)[16,18]. This H_2O_2 may then undergo one of two fates: diffusion to the cytosol through the mitochondrial membranes or conversion to water by glutathione peroxidases (GPX) or peroxiredoxins (PRX)[15,30]. Mitochondrial matrix H_2O_2 may also use aquaporins on the inner mitochondrial membrane to reach the IMS before diffusing to the cytosol[16,30]. The IMS superoxide anions from complex III can diffuse to the cytosol via voltage-dependent anion channels (VDAC) where it can be converted to H_2O_2 this time by the superoxide dismutase 1 (SOD1)[15]. Cytosolic superoxide anions produced by NOX will be converted to H_2O_2 by SOD1 as well. The cytosolic H_2O_2 from the various mitochondrial compartments may then be used for redox signaling and pathway activation or be converted to water by cytosolic GPXs or PRXs (Figure 1)[15]. This H_2O_2 may also be converted to HOCl by myeloperoxidases (MPO) or to hydroxide radicals via Fenton's reaction which involves the Fe^{2+} cation[16].

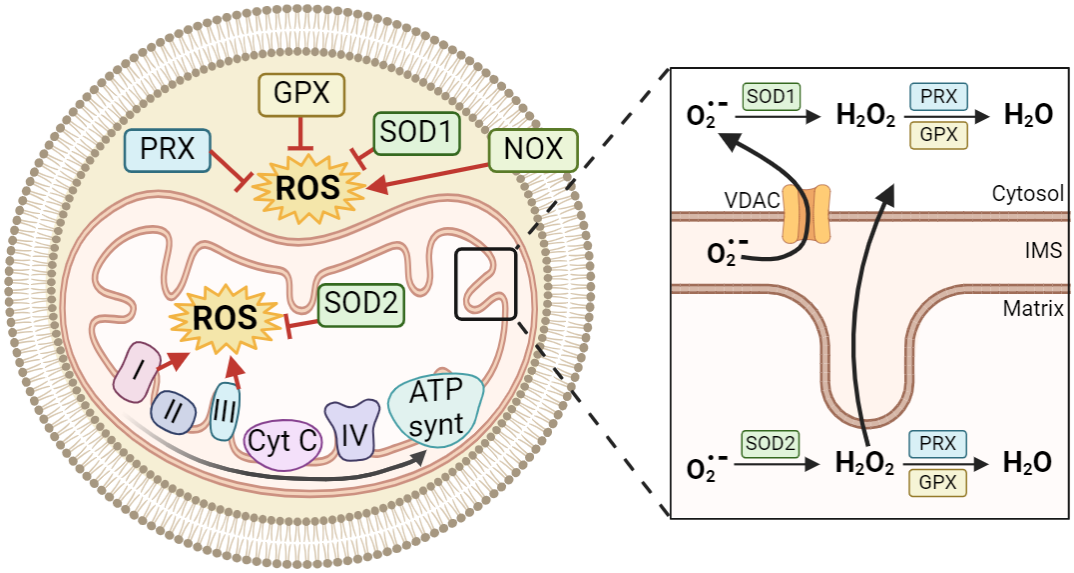

Figure 1. Schematic of cellular ROS production and regulation. Cellular ROS production occurs in the cytoplasm mainly due to the NOX enzyme and is eliminated by SOD1, GPX and PRX. In the mitochondria, ROS such as the superoxide anion are mainly produced by the electron transport chain's complex I in the matrix and complex III in the matrix and intermembrane space (IMS). Mitochondrial matrix superoxide anion can be converted to hydrogen peroxide by SOD2. This hydrogen peroxide can either diffuse to the cytosol or be converted to water by PRX and GPX. IMS superoxide anion can diffuse through the cytosol via voltage-dependent anion channels (VDAC) where it can undergo similar processes to the mitochondrial superoxide anion. (NOX: NADPH oxidase, SOD1: superoxide dismutase 1, SOD2: superoxide dismutase 2, PRX: peroxiredoxin, GPX: glutathione peroxidase).

The cellular ROS regulation process also involves various non-enzymatic antioxidants, such as glutathione and vitamins. Glutathione can be found in either its reduced (GSH) or oxidized (GSSG) forms. In typical healthy cells, GSH prevails and can be converted to GSSG following its oxidation, notably by H_2O_2[31]. This leads to the production of H_2O and O_2 from H_2O_2, thus reducing ROS levels[20]. This GSH/GSSG ratio is oftentimes used as a marker of oxidative stress where the lower the ratio, the more GSH is being oxidized to GSSG by ROS, and thus the higher the oxidative stress is in the cell[32]. In addition, GSH serves as a cofactor for the function of antioxidant enzymes such as GPX[20].

Other major contributors to non-enzymatic ROS regulation are vitamins. Vitamin E can scavenge ROS by donating hydrogens, thus interrupting lipid peroxidation. Similarly to vitamin E, vitamin C can prevent lipid peroxidation, reduce radicals directly and regenerate vitamin E and other antioxidants[20].

Dietary polyphenols such as flavonoids, phenolic acids, tannins and diferuloylmethane (the class to which belongs curcumin) may also serve as antioxidants, which is why some dietary recommendations for CIDs include foods high in polyphenols[33,34]. Despite this, the concentration of polyphenols in systemic circulation is low as they are readily metabolised[35]. Thus, some believe their low levels prevent them from having significant antioxidant effects and maintain that raising their levels to a threshold where they would exert an effect might actually be harmful[35,36].

1.3.6. ROS signaling and physiological roles

Although they may be a cause for oxidative stress and cellular damage, ROS' contribution to inflammation goes beyond their intrinsic damaging potential; ROS affect actors of key inflammatory pathways and thus induce inflammation[37]. Notably, ROS has targets in the NF-kB, MAPK, JAK/STAT and NLRP3 inflammasome signaling pathways and can thus induce inflammation via these routes[37,38]. Their effect on these pathways doesn't solely increase the cell expression of certain cytokines and chemokines but may also drive certain cellular phenomena to occur. Notably, NF-kB and MAPK activation can drive cell polarization, activation of the NLRP3 can induce pyroptosis and JAK/STAT activation can cause differentiation and apoptosis in certain cell types. Additionally, these pathways induce the expression mainly of pro-inflammatory molecules including TNF-α, IL-1β, IL-6, IL-8, IL-12, IL-18 and COX2[37]. However, certain pathways may also induce the expression of anti-inflammatory cytokines IL-10

and IFN- β, likely in an attempt to resolve inflammation and thus reinstate a homeostatic, non-inflammatory state within the cells[39].

In phagocytic immune cells such as macrophages, ROS production may serve functions beyond redox signaling known as respiratory bursts. Respiratory bursts are a defense mechanism of the innate immune system which help phagocytic cells kill pathogens[15,40]. When pathogens interact with surface molecules on phagocytic cells, this triggers a signaling cascade, leading notably to the strong activation of NOX enzymes during phagocytosis and thus a large ROS production[29,40]. The ROS produced will then be released by the cells into either the phagosomes or extracellular space to help degrade pathogens such as bacteria[29].

1.3.7. ROS involvement in chronic inflammatory diseases

As described, ROS' implication in inflammation is dual; it causes inflammation via damages caused by the oxidative stress it generates but also via the direct activation of inflammatory signaling pathways. In cases of redox imbalance, that is when ROS levels surpass the antioxidant capacity, ROS levels become abnormally elevated thus exacerbating these effects. Indeed, because of its role in signaling pathways, abnormally elevated ROS levels may activate inflammatory pathways in a dysregulated manner, leading to disease conditions[37]. Diseases related to the dysregulation of NF-kB, MAPK, JAK/STAT and NLRP3 inflammasome include CIDs such as Alzheimer's disease, arthritis and atherosclerosis[37,38]. This corroborates the characteristic redox imbalance states and increased serum ROS levels observed in CID and ROS-mediated disease patients[41–43].

1.3.8. Current research on ROS-regulating strategies

As the link between ROS and inflammation, particularly in the case of redox imbalances and CIDs, is well established, there have been studies conducted on the development of ROS-reducing strategies to alleviate CIDs. Notably, ROS-scavenging biomaterials, referring to biomaterials capable of ROS reduction, have been developed either in the form of enzymes that mimic or enhance endogenous ROS-reducing enzymatic functions, biomaterials that reduce produced ROS and biomaterials that reduce ROS production[37]. Within the realm of ROS-scavenging strategies for already produced ROS, numerous potential candidates are being assessed. Despite this, no such ROS-mediated system is currently approved for therapeutic use, attesting to the need for further research to be conducted on this topic. Indeed, when considering the broad therapeutic potential and the various customizable parameters of such systems, it is clear that more work is needed and that a lot of discoveries are left to be made.

1.4. Nanoparticles (NPs)

1.4.1. What are NPs?

As mentioned, we seek to create nanoparticles (NP) as a therapeutic avenue for the control of ROS and inflammation. NPs are small particles in the nanoscale size range (from 1nm to 100nm in diameter) with a wide array of different uses[44]. Their small size allows them to exhibit different physical and chemical properties than materials of bigger size, making them interesting to explore notably for electronic, agricultural, medical and pharmaceutical industries[44]. In the biomedical field, NPs are commonly used as drug delivery tools. These particles can be made from different materials including polymers and lipids according to their intended function. The use of NPs as drug delivery vehicles confers a variety of advantages including enhanced drug bioavailability, avenues for targeted drug delivery and potential for controlled drug release[45,46].

1.4.2. Common types of NP compositions and structures

NPs typically possess certain characteristic structural components including a core, the innermost part of the system, a shell layer which delineates the core, and a surface layer which coats the NPs[44]. By varying what makes up these structural components, NP properties can be adjusted to favour certain abilities and accomplish certain functions. For example, depending on the NP type, the core can be made either hydrophobic or hydrophilic to accommodate drugs of interest. Additionally, the NP surface layer can be modified to reduce agglomeration and interactions with biological components as well as target NPs to sites of interest[47]. Drug delivery NPs can be categorized based on their composition where 2 main NP types prevail: lipid-based NPs (LNPs) and polymeric NPs (PNPs). Although both are great delivery tools, the exact purpose and intended outcome expected can help determine which system should be used.

One common type of LNPs used are liposomes. Liposomes possess a phospholipid bilayer structures, thus resembling the cell membrane. Not only does this structure render them biocompatible, but it also enables them to easily cross the cell membrane to deliver their payload inside cells[48]. This structure also allows for versatile payload options as hydrophobic drugs can be encapsulated within the hydrophobic bilayer whereas hydrophilic drugs can be encapsulated within the NP core[48,49]. Unfortunately, liposomes present certain concerns, notably regarding their stability and upscaling of their production[49]. Stability is crucial for drug delivery systems as without stability, drugs may leak from the system or the system may degrade prematurely, defying the purpose of its use. In addition, when exploring the translational potential of a novel therapeutic, it is important to consider how to scale up its production. In the case of liposomes, elements such as access to high amounts of quality lipids, reproducibility, liposome sterilization and equipment availability become challenging. Some of these challenges even apply to all LNPs in general, making their use more difficult. As promising solutions are currently being explored

to remedy these challenges and given their good properties and vast potential, LNPs remain very useful tools to explore for drug delivery.

In contrast, PNPs are made from polymers rather than lipids, but remain biocompatible. Types of PNPs include nanocapsules in which the core is a cavity surrounded by the NP shell and surface molecules and nanospheres where the core is composed of a polymeric matrix[50]. The use of polymers makes these NPs more stable than liposomes and their structure allows for better customizability of the system[48]. Indeed, PNPs are a better choice for systems focusing on controlled drug release and requiring surface modifications[48]. In addition, as is the case with liposomes, polymeric NPs can encapsulate both hydrophobic and hydrophilic drugs depending on the polymer used and its properties. According to the system's intended function, drugs can be either within the PNP or on its surface, bound to the polymer or encapsulated in the core[50]. In addition, PNP formulations are simple and protocols for their fabrication are easy to reproduce, thus reducing batch to batch variability[48,50]. Unfortunately, the high molecular weight of the polymers used as well as their structure which differs from typical endogenous structures make PNPs more likely to induce immune responses. In addition, PNPs may exhibit a lower drug encapsulation efficiency[48].

1.4.3. Advantages of NPs for drug delivery

An important part of a drug's therapeutic efficacy depends on its ability to reach its site of action. NP properties can contribute to this end in multiple ways. Firstly, NPs can accommodate drugs that have more difficult properties to work with in biological models. They can notably help stabilize less stable drugs and prevent therapeutics such as nucleic acid or protein-based treatments from premature degradation[50,51]. They can also solubilize insoluble drugs for their delivery[50]. Indeed, NPs containing hydrophilic surface molecules may also

possess hydrophobic sections in their structure enabling them to carry an otherwise insoluble drug load. By changing the characteristics to be considered for the delivery of a particular drug, the use of NPs also enables compounds to cross certain biological barriers, such as cellular, mitochondrial and nuclear membranes, that they otherwise would be unable to cross[50,52]. In addition, these modification in properties can provide more flexibility in the modes of administration of certain treatments[50].

From a systemic point of view, NPs can protect drugs in a way that increases their bioavailability and systemic circulation time, thus allowing for a better proportion of drugs reaching their site of action[45,50]. In addition, NPs can help protect drugs to ensure they reach diseased sites in therapeutically relevant concentrations[46]. They can also ensure the concentration of multiple drugs at a disease site corresponds to the optimal synergistic ratios by encapsulating multiple drugs in a single system and thus delivering drugs at that optimal ratio. NPs can also help reduce toxicity and side effects linked to the use of high drug concentrations as by protecting the drugs, a lower initial dosage can lead to the same amount of drug reaching the site of interest and thus the same therapeutic effects[46].

The types of NPs and variety of materials that can be used makes NPs very adjustable to implement desired properties to the system. For example, modifications to a NP's surface can enable it to target certain organs, tissues, cell types or intracellular sites of interest[50,53]. Not only does this reduce a drug's off-target effects and toxicity, but it also makes them more efficient by increasing the probability they reach the desired target[54]. Drug release using NPs can also be controlled to create selectively activated systems, once again optimizing a drugs concentration at the site of interest and reducing possible toxicity. In addition, controlling a NPs biodegradability rate may also enable a slower drug release, increasing patient outcome. Indeed, slower release

rates may translate to lower dosage and reduced frequency of re-administration[46]. Thus, NPs have great drug delivery potential which, alongside the use of effective drugs, can revolutionize their therapeutic efficacy.

1.4.4. NP systemic circulation

NP treatments may be administered via a multitude of routes according to their properties and site of action. The choice of administration route comes with important considerations as not only will the NP affect the body, but the body will affect the NP as well. Intravenous injections are one of the main administration routes employed for NP treatments. Intravenous injections are favored as they are a simple and accessible administration route. This route allows for a systemic drug distribution and ensures a high concentration of circulating drug without them having to withstand treacherous environments such as the digestive system[55].

NP development must consider how NPs interact with the body in the context of a systemic distribution. For example, as the NPs circulate, they are coated by neighboring proteins, leading to the formation of a protein corona around the system[56]. This protein corona's composition depends on the NP's properties and may affect how NPs behave in the body[57]. Notably, they may hinder NP targeting abilities, promote NP opsonization, cause immune responses and modify the likelihood of cellular uptake either positively or negatively[57–59]. In addition, NP properties such as size are important to protect NPs against certain biological outcomes. For example, NPs below 5nm-10nm in size are likely to be rapidly excreted by the kidneys due to the size of the glomerular pores involved in blood filtration[60,61]. However, NPs above 200nm in size may activate the immune system. In addition, numerous studies find 50nm NP sizes to give good results in terms of cellular uptake and drug delivery, thus, NP sizes between 50-200nm are usually preferred[50].

In order to exit the systemic circulation and reach their intended location, NPs take advantage of the effect of disease on endothelial vascular walls. Disease conditions such as inflammation and cancer can increase levels of inflammatory markers leading to abnormally large gaps in the vascular wall. NPs can thus exit through these gaps reaching the extracellular matrix through which they travel until they reach their cellular target[62].

1.4.5. NP cellular uptake

Once they reach cells, NPs can be taken up via various processes. NP cellular uptake begins at its interaction with the cell membrane which may differ according to the cell type as well as the composition of the protein corona and the properties of the NP such as size, shape and surface charge[50,63]. In addition, characteristics of the cell membrane are dynamic as membrane fluidity and the distribution of proteins and lipid rafts is variable. Thus, the mode of NP entry depends on the location of the interaction on the membrane as well as the cell's state at the time of interaction[50].

The main route of cellular uptake is endocytosis (both phagocytosis and pinocytosis) where the cellular membrane engulfs the NPs for their internalization. This results in the formation of intracellular vesicles carrying the NPs. Phagocytosis is usually performed by phagocytic cells and requires the opsonization of the substrate taken up, therefore opsonins must be present on the protein corona to allow NP uptake via this route. Typically, the phagocytic process can take from 30 minutes to several hours and is favorable for the uptake of bigger NPs[63].

Multiple types of pinocytosis exist, all of which can enable NP internalization in cells. When the interaction between NP and cell occurs on membrane sites high in clathrin, clathrin-mediated endocytosis is favored. In this process, specific proteins are recruited to the interaction

site for formation of clathrin-coated vesicles between 100-150nm in size containing the internalized NPs[63]. As for caveolae-mediated NP entry, it occurs when NPs interact with caveolae, a type of cell membrane invagination ranging from 50-80nm in size. These caveolae are lined with caveolin proteins which recruit actors permitting NP internalization in vesicles[63]. For both clathrin and caveolae-mediated NP entry routes, the NP-loaded vesicles fuse with early endosomes[64]. Thus, NPs must either be made to escape endosomes or survive the acidification of endosomes and the lysosomal enzymes involved in lysosomal degradation[63]. Forms of NP endosomal escape techniques include using complex nanoparticle structures or pH-dependent mechanisms of endosomal membrane disruption[50].

Other forms of pinocytosis include clathrin/caveolae-independent endocytosis and macropinocytosis. The clathrin/caveolae-independent process occurs in cells that contain neither of these surface proteins and is the route of choice for folate-coated NPs and their delivery to the cytoplasm [63]. As for macropinocytosis, it entails the formation of membrane projections folding back onto the cell thus forming vesicles between 200nm-5000nm in size non-selectively containing all types of particles present in the extracellular space. Thanks to the large size of the vesicles formed, macropinocytosis is regarded as an important entry route for NPs too large for other pinocytic pathways[63].

Although NP uptake is a major step of their success in drug delivery, many NPs must still reach and surpass other intracellular biological barriers, such as the mitochondria or the nucleus, to have their intended effect.[50] It is thus important for these barrier-crossing NPs' properties to remain intact after the cellular uptake process.

1.5. Concept and structure of the NP system created

1.5.1. Rationale for the development of the NPs

To explore novel avenues for anti-inflammatory therapies, we opted for the development of a NP system possessing intrinsic ROS mediated properties. As many cellular processes and CIDs involve ROS, the development of a NP system capable of ROS-dependant activation (ROS-sensitivity) and ROS reduction (ROS-scavenging) is promising for the treatment of multiple disease conditions. To achieve this, polymeric NPs were used as they allow us to harness the NP's structure itself for a controlled therapeutic effect. As our goal focuses on the development of the NP system itself, it allows for the establishment of foundations to build upon for the development of efficient and tailored systems against specific cellular processes and disease conditions.

In relation to currently conducted studies on the topic, our system specifically aims at reaching a reduction of ROS levels back down to a homeostatic range, hence the different scavenging molecules employed. Additionally, many of the system's components were specifically synthesized to be tailored to our system and its intended use. Thus, their joint use creates a unique combination and a unique type of system. The need for novel ROS-regulation systems is clear as no currently available therapies use this ROS-reduction angle to alleviate inflammation, thus justifying the creation of our novel, unique system. Additionally, the vast potential for drug encapsulation within the system, which is unique in itself thanks to the particular properties of our synthesized biomaterials, enables an even broader scope of possibilities to tailor our system and render it more unique. Thus, the work we have set out to do is much needed in the field and will allows for the formation of a novel and potentially more efficient ROS-modulated NP system.

1.5.2. Essential properties for the function of our NPs

To create a system that works as intended, the NPs structure was designed to possess two key properties: ROS-sensitivity and ROS-scavenging (Figure 2). ROS-sensitivity refers to our NP's ability to disassemble in high ROS conditions. This occurs thanks to the presence of boronic ester bonds that will form within the NP system. In contrast, ROS-scavenging refers to the NP's ability to reduce ROS levels via the ROS-scavenger released during disassembly.

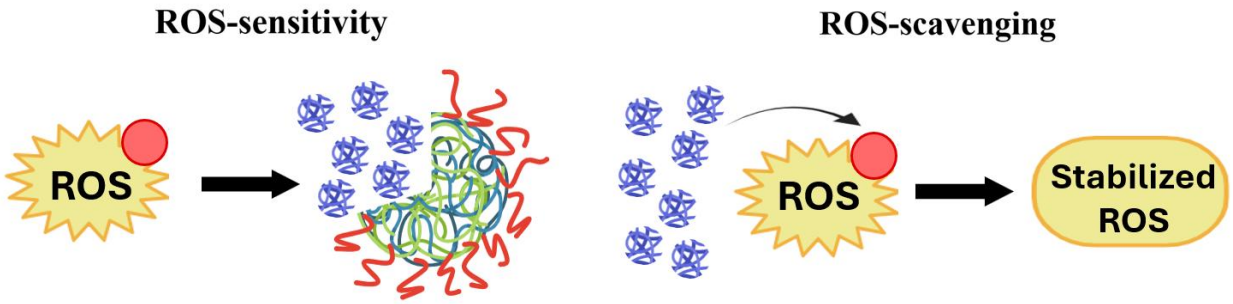

Figure 2. ROS-dependent NP properties. The NP structure should enable the system to have 2 ROS-dependent properties. ROS-sensitivity refers to the system's ability to break apart in high ROS conditions whereas ROS-scavenging refers to the released ROS-scavenger's ability to reduce ROS levels by stabilizing their unpaired electron (red circle), thus rendering them no longer reactive nor damaging.

1.5.3. NP structural components

1.5.3.1. ROS-scavengers

One of the main components of the system are the ROS-scavengers. ROS-scavengers can scavenger ROS by stabilizing free radicals, thus rendering them less reactive. These molecules are involved in both the ROS-sensitivity and ROS-scavenging aspects of the system. Therefore, varying which ROS-scavenger is used and eventually combining different ROS-scavengers will enable us to modulate the amount of boronic ester bonds formed and the ROS threshold needed to disassemble the system. We will thus be able to fine-tune the system for activation only in sites of abnormally elevated ROS levels and reduce these levels back down to a homeostatic

range. This way, we can ensure cellular ROS isn't completely depleted, allowing maintenance of non disease-related ROS effects. For this project, 3 ROS-scavengers of interest were selected based on their boronic ester bond formation potential and ROS-scavenging potential. These scavengers are tannic acid (TA), epigallocatechin gallate (EG) and gallic acid (GA) (Figure 3).

Our first scavenger of interest, TA, is a part of the tannin class of polyphenols, known for their high molecular weights[33,65]. It is a natural antioxidant found notably in red wine or tea and often used for leather coating, adhesives and pharmaceutical functions. As it is widely naturally present, TA is not expensive and thus advantageous to use. In addition, TA's structure possesses 10 hydroxyphenol (or galloyl) groups, making it the biggest of our ROS-scavengers of interest. Each group is capable of ROS-sensitive bond formation and ROS-scavenging. Thanks to these groups, it is very soluble in water, as well as biodegradable and biocompatible, important characteristics to ensure it can accomplish its function well once released from the NP system. Thus far, TA has been extensively researched for the development of various therapies, notably for hydrogel formation[66].

As for EG, it belongs to the flavonoids class of polyphenols and is a natural compound highly present in green tea[33,67]. When assessing the ROS-scavenging potential of various catechins, a study showed EG caused the highest free radical scavenging, attributable to its higher amount of hydroxyphenol groups than its catechin counterparts[67]. Despite it's potential for cancer treatments, EG is difficult to use as a cancer therapeutic as the acidic environment of tumor cells reduce its stability and impede its beneficial properties. In addition, EG shows low bioavailability and biodistribution and can thus not reach the sites of interest in sufficient amounts, a difficulty accentuated by its rapid metabolism. For these reasons, the development of

lipid nanocarriers for EG delivery is actively researched but polymeric NPs such as our own may also be able to help manage these difficult EG properties, increasing its usability[68].

Lastly, GA is a polyphenol part of the phenolic acids class of polyphenols[33]. It is known for its antioxidant properties and is naturally present in various fruits and medicinal plants[69]. It is the smallest of our ROS-scavengers of interest, possessing a single hydroxyphenol group. Despite this, it has been shown to be an efficient ROS-scavenger and a promising therapy for neurodegenerative diseases and neuroinflammation[69,70]. Unfortunately, it isn't used as a therapeutic tool as it faces limits due its poor water solubility, poor absorption, poor biodistribution and quick elimination[69]. Thankfully, most of these can be addressed via the use of NPs and make GA a great candidate for assessment of ROS and inflammation reduction.

In addition to their ROS-scavenging abilities, our ROS-scavengers of interest can reduce inflammation by acting on other steps of ROS production and inflammatory pathways, thus enhancing our NP's anti-inflammatory properties. Notably, polyphenols may induce the production of antioxidant enzymes such as GPX and SOD2 and inhibit the expression of ROS producing enzymes such as XO[35]. Polyphenols may also interfere with ROS mediated pro-inflammatory cytokines via JNK and NF-kB pathways[71,72]. Lastly, polyphenols also have the potential for complex formation to prevent the production of ROS via the Fenton reaction. Indeed, they can notably chelate Fe^{2+} which slows down the rate of the Fenton reaction[35,71].

1.5.3.2. Polymeric backbone

The NP's polymeric backbone is intended to provide structure to the system as well as provide the boronic acid functional groups for the formation of the boronic ester bond with the ROS-scavenger. Without the bond between the polymer and ROS-scavenger, the system would not hold together and thus the NPs would not assemble in the intended manner.

1.5.3.3. Surface molecules

The base NP system is coated with a PLGA-PEG copolymer, often used in the nanomedicine field. As a means to explore mitochondrial targeting, a TPP molecule was conjugated to the PLGA-PEG surface molecule. The first component used, poly(lactic-co-glycolic acid) (PLGA) is an FDA-approved polymer made from lactic acid (LA) and glycolic acid (GlA) moieties[73]. It is commonly used in drug delivery tools as it is soluble in common solvents, biocompatible, and its biodegradability allows it to be metabolized and excreted[73,74]. PLGA's biodegradation is mediated by its hydrolysis for which the rate differs for LA and GlA due to their different hydrophobicities. LA's methyl groups render it more hydrophilic resulting in slower hydrolysis than GlA[73]. Thus, PLGA's rate of biodegradation is adjustable by modifying its LA:GlA content ratio allowing for more control over the NP's properties and degradation[74]. For our system, modifying the LA:GlA content ratio of our PLGA and its degradation time can influence how our NPs respond and interact with H_2O_2.

As for the coating of PEG to the system, known as NP PEGylation, it is an FDA-approved method for enhancing NP properties in the body[75]. PEG's structure allows it to be flexible and water soluble[76]. Thanks to these properties, it helps reduce NP aggregation and immune recognition[76]. PEG also alters how NPs interact with biological proteins by causing steric hindrance thus reducing opsonization and phagocytosis as well as NP degradation and clearance[50,63,74–76]. Although this leads to an increased circulation time and NP biocompatibility, it may hinder, but not completely prevent, cellular uptake and drug release properties[50,60,74]. Thus it is important to ensure such properties are maintained within the intended range when using PEG. To do so, it is possible to vary the molecular weight of the PEG molecule used to optimize the NP's desired properties[76]. As our system is oxidation-sensitive, sufficient PEG protection is required to ensure NPs reach the cells before they disassemble and release their ROS-scavenger.

The mitochondrial targeting of the system is enabled by the incorporation of triphenylphosphonium (TPP) to the system. TPP is a mitochondria targeting agent widely used to promote the mitochondrial accumulation of various drugs and probes[77]. TPP is stable and has low reactivity in biological conditions. As a lipophilic and positively charged compound, it can cross the mitochondrial membrane thanks to its membrane potential and thus allow accumulation of conjugate drugs or NPs within the mitochondrial matrix[78]. The cell plasma membrane also possesses a slight negative membrane potential, therefore TPP may also contribute to NP cellular uptake. TPP is simple to synthesize and to conjugate to other compounds making it adaptable to different systems and uses. Variations in TPP's structure such as modifications of the carbon chain length can change its lipophilic properties, thus giving us greater abilities to modify the system's properties such as cellular uptake and site of NP accumulation. Its function for NP mitochondrial targeting has been previously shown in studies coating both liposomes and polymeric NPs with TPP[77]. In both cases, successful localization to the mitochondria was shown, making TPP a good avenue to enhance the mitochondrial localization of our NP system.

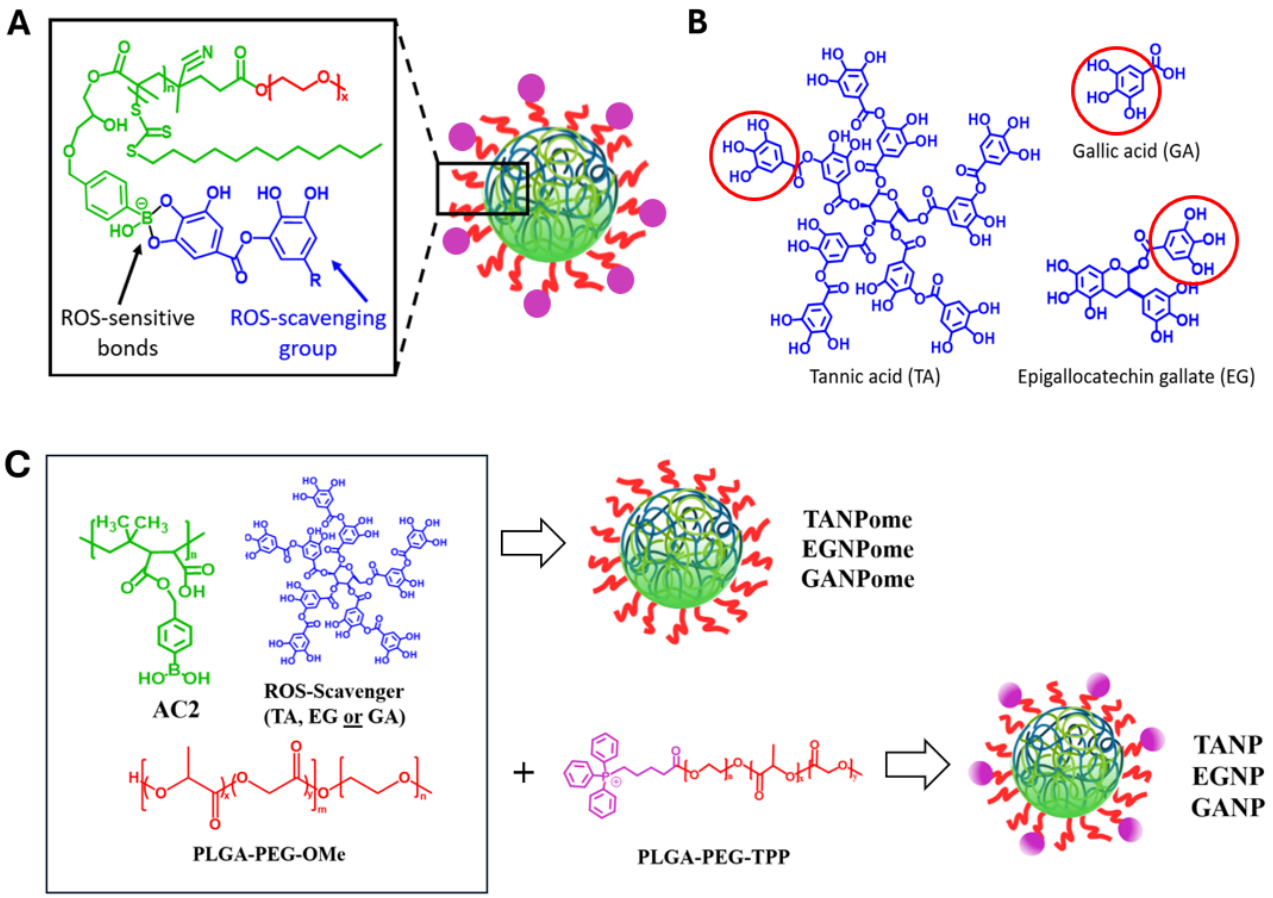

Figure 3. Structure and concept of the NP system. (**A) NP structure.** The NP system is comprised of a PEG-based surface molecule (red), a polymeric backbone containing a boronic acid functional group (green) and a ROS-scavenger (blue). The boronic acid functional group and the ROS-scavenger come together to form the ROS-sensitive boronic ester bond. Triphenylphosphonium (TPP) surface molecules may be added to the system to enable mitochondrial targeting (purple). (**B) ROS-scavengers of interest.** Tannic acid (TA), gallic acid (GA) and epigallocatechin gallate (EG) are the ROS-scavengers studied in this project. They each possess different amounts of catechol or hydroxyphenol groups (red) and thus varying potential for the formation of ROS-sensitive bonds and ROS-scavenging potential. (**C) Selected NP formulations.** The NPs used for the studies in this project contain the AC2 polymer, one of the three ROS-scavengers (TA, EG or GA) and PLGA-PEG-OMe, forming the TANPome, EGNPome and GANPome NPs, according to the ROS-scavenger used. For the mitochondria-targeting NPs, the same formulation was maintained with addition of PLGA-PEG-TPP.

1.5.4. Multi-functional approaches

With the use of this novel NP system exhibiting intrinsic ROS-sensitivity and ROS-scavenging properties, a certain level of ROS and inflammation reduction can be achieved. Yet, as do most other NP systems, our system still possesses its drug delivery potential which is currently unexploited. Combination approaches to combatting diseases can thus be explored by the encapsulation of anti-inflammatory drugs, disease specific drugs, and various RNA therapeutic agents (mRNA, miRNA and siRNA) in our system. Thus, we can achieve a multi-angle approach to the resolution of disease conditions by targeting different aspects of a same pathway, or different pathways of a same disease condition. Not only will our system enable delivery of these therapeutics in cells, but it will also enable a controlled, ROS-dependant release of the therapeutics, thus only delivering the agents to sites of enhanced inflammation.

1.6. Research hypothesis and objectives

We hypothesize that the system developed will successfully demonstrate ROS-sensitivity and ROS-scavenging properties. Additionally, we hypothesize that the development of a system with such properties will enable us to control inflammation by reducing ROS levels in CID cases. Lastly, we hypothesize that the system's ROS-sensitivity will enable stimuli-responsive delivery of therapeutic agents. To begin exploring this hypothesis, 3 main objectives were defined:

Objective 1: Biomaterials - Develop and characterize a library of potential biomaterials to be used for ROS-scavenging systems.

Objective 2: Nanoparticles - Assemble and optimize nanoparticle formulations and assess their properties in terms of ROS-sensitivity and ROS-scavenging potential.

Objective 3: Inflammation - Assess the nanoparticle system in vitro for its ROS-reduction and inflammation-reduction properties.

2. Materials and Methods

2.1. Materials:

For chemical synthesis and in solution assays:

The acetone, ACN and MeOH solvents were purchased from Fisher Chemical (respectively Cat#: A18-4, A21-4 and A412-4). DIC and diethyl ether were purchased from Sigma Aldrich (Cat#: D125407 and Cat#: 673811 respectively) and DMF and DMAP were purchased from Alfa Aesar (respectively Cat#: 43997 and Cat#: A13016). DCM was purchase from ThermoFisher Scientific (Cat#: 61005-0040), DMSO from VWR BDH Chemicals (Cat#: BDH1115) and ethanol from Greenfield Global (Cat#: P016EAAN). The PLGA-PEG-OMe polymer was bought from PolySciTech (Cat#: AK010) and PLGA-Cy5.5 was synthesized as part of a previous study[79]. The TA and GA ROS-scavengers of interest were obtained from Sigma Aldrich (TA Cat#: 403040; GA Cat#: 398225) and EG was obtained from Toronto Research Chemicals (EG Cat#: TRC-E588500). H_2O_2 was obtained from BioShop (Cat#: HYP001). For NMR, $CDCl_3$ and DMSO-d6 solvents were obtained respectively from Cambridge Isotope Laboratories (Cat#: DLM-7-100) and Sigma Aldrich (Cat#: 1.03424.0100). NMR tubes were obtained from Wilmad (Cat#: : Z565229).

For cell culture assays:

Cell culture assays were performed on RAW264.7 macrophages. Complete media is DMEM (Multicell, Cat#: 319-005-CL) supplemented with 10% fetal bovine serum (FBS) (Corning, Cat#: 35-077-CV) and 1% penicillin streptomycin L-glutamine (PEN) (Corning, Cat#: 30-009-

CI). Phenol red-free media used is DMEM (Multicell, Cat#: 319-051-CL). Other cell culture reagents used include phosphate buffered saline (Fisher bioreagents, Cat#: BP399-1) and TryplE (gibco, Cat#: 12604021).

2.2. Biomaterial synthesis

2.2.1. Boronic acid polymers: AC2, AC2N and AC2B polymer syntheses

Poly(isobutylene-*alt*-maleic anhydride) (424mg, 0.071mmol, Sigma Aldrich, Cat#: 531278) and 4-(hydroxymethyl)phenylboronic acid (426mg, 40 equivalents, Sigma Aldrich, Cat#: 512338) were combined with 5ml of DMSO in a reaction vial. The reaction was left to stir at room temperature for 24h yielding the AC2N compound. In another instance, NaOH (1ml, 0.1M, Sigma Aldrich) was added to the reaction vial after the 24h stirring to yield the AC2 polymer. Both compounds were purified by dialysis (Mw=1kD, Repligen, Cat#: 132104) in water for 48h with frequent water changes. AC2 and AC2N were collected, lyophilized and stored at -20^{o}C until needed. To form the AC2B polymer, the AC2 polymer (152.2mg) was initially dissolved in DMF (6ml) to which was added DIC (207.4ul, 1.339mmol), 4-(hydroxymethyl)phenylboronic acid (306.0mg, 2.01mmol, Sigma Aldrich, Cat#: 512338-1G) and DMAP (246.3mg, 2.01mmol). The vial was left to stir overnight, and the collected compound was dialyzed (Mw=1kD, Repligen, Cat#: 132104) for 48h in water and 24h in 5% ACN in Milli-Q water before ensuing lyophilization. For all three compounds, successful synthesis was confirmed by proton nuclear magnetic resonance (^{1}H NMR) using the Bruker AVANCE II 400 for AC2 (5.5mg in DMSO-d6) and AC2B (0.4mg in DMSO-d6) and the Bruker AVANCE III 600 for AC2N (8.5mg in DMSO-d6). The analysis of the NMR spectra was done using the MestReNova software.

2.2.2. Boronic acid polymers: AC4 polymer synthesis

Poly(isobutylene-*alt*-maleic anhydride) (121.4mg**,** 0.020mmol**,** Sigma Aldrich, Cat#: 531278), 4-(hydroxymethyl)phenylboronic acid (31.9mg, 10 equivalents, Sigma Aldrich, Cat#: 512338) and fluorescein sodium salt (231.1mg**,** 30 equivalents**,** Sigma Aldrich, Cat#: F6377) were combined in DMSO (4ml) and left to stir for 24h at room temperature. After stirring, the AC4 resulting compound was collected. It was then dialysed in Milli-Q water (Mw=1kD, Repligen, Cat#: 132104) and freeze dried for 48h. Successful compound synthesis was confirmed by ^{1}H NMR in DMSO-d6 using the AVANCE II 400. The NMR spectrum was visualized and analyzed using the MestReNova software.

2.2.3. AC3 polymer synthesis

Poly(isobutylene-*alt*-maleic anhydride) (404mg, 0.067mmol**,** Sigma Aldrich, Cat#: 531278) was combined to 4-Amino-2,2,6,6-tetramethylpiperidine (429mg**,** 40 equivalents**,** Sigma Aldrich, Cat#: 115738) in DMSO and left to stir overnight at room temperature. The compound was the collected, dialyzed in water for 48h and lyophilized. The product's structure was confirmed by ^{1}H NMR in DMSO-d6 by using the Bruker Avance II 400 and the MestReNova software.

2.2.4. AC5P and AC5 polymer syntheses

The AC5P polymer was synthesised by combining poly(ethylene glycol)methylether 4-cyano-4-[(dodecylsulfanylthiocarbonyl)sulfanyl]pentanoate (99.8mg, 0.01mmol, Sigma Aldrich, Cat#: 753033) with AIBN (1.8mg, 0.01mmol, Sigma Aldrich, Cat#: 441090) and glycidyl methacrylate (70ul, 0.513mmol, Sigma Aldrich, Cat#: 779342) in THF (2ml, Sigma Aldrich, Cat#: 186562). The vial was put in a nitrogen atmosphere and left to stir in an ice bath for 30 minutes. Subsequently, the vial was heated up to 70^{o}C and left to stir for 24h. For purification, the contents of the vial were transferred to a falcon tube containing excess hexane and

centrifuged at 2000rpm for 5 minutes. The supernatant was discarded, and the pellet was resuspended in hexane with vortexing before ensuing a second centrifugation. Multiple hexane washes were performed before the compound was collected and dried by vacuum overnight. Successful compound synthesis was confirmed by ^{1}H NMR in $CDCl_3$ using the Bruker AVANCE III 600. This AC5P synthesis protocol was inspired by a similar published synthesis[80].

For the formation of AC5, the AC5P polymer synthesized (93.2mg) was combined with 4-(hydroxymethyl)phenylboronic acid (40.7mg, Sigma Aldrich, Cat#: 512338) and combined to toluene (2ml, Fisher Chemical, Cat#: T3241) and ethanol (5ml). The solution was heated to 70^{o}C and left to stir overnight. Purification was conducted similarly to the reference protocol[80]. ^{1}H NMR was conducted in DMSO-d6 using the Bruker AVANCE II 400. The NMRs' analyses were performed using the MestReNova software.

2.2.5. PEG-BA synthesis

Formation of the PEG-BA polymer was done by dissolving 3-Carboxyphenylboronic acid (30mg, 0.209mmol**,** Sigma Aldrich, Cat#: 456764) in DMF (1ml) with stirring. DIC (56ul, 0.362mmol) and, 2-5 minutes later, poly(ethylene glycol) (average Mw=3400, 600mg, 0.176 mmol, Sigma Aldrich, Cat#: 373001) were added, followed by the addition of DMAP (46.2mg, 0.378mmol). The reaction mixture was left to react with stirring overnight. The resulting compound was dialyzed (Mw=1000) in water for 72h with frequent water changes. The resulting PEG-BA product was collected, lyophilized and analyzed by ^{1}H NMR in DMSO-d6 using the Bruker AVANCE AVII400 and MestReNova software.

2.2.6. CMDex-BA synthesis

The CMDex-BA polymer was synthesized by adding CM-Dextran 4 (105.5mg, 0.015mmol, TdBLabs, Cat#: CMD4) to a combination of DMSO (2ml) and DMF (2ml. DIC

(16.5ul, 0.106mmol) was added to the vial which was left to stir for 5 minutes before addition of 4-(hydroxymethyl)phenylboronic acid (24.6mg, 0.162mmol, Sigma Aldrich, Cat#: 512338) and DMAP (19.2mg, 0.157mmol). The mixture was left to react overnight with stirring. The resulting compound was collected and dialyzed in water for 72h with frequent water changes and in 5% ACN in water for 24h before proceeding with lyophilization. The dry CMDex-BA compound was analyzed by ^{1}H NMR in DMSO-d6 using the Bruker Avance II 400. The MestReNova software enabled visualization and analysis of the spectrum obtained.

2.2.7. PLGA-PEG-OH and PLGA-PEG-TPP polymer syntheses

The PLGA-PEG-OH polymer was synthesized by initially dissolving PLGA (1300mg, 0.05mmol, 50:50 LA:GlA) in DCM (7-10ml). Once dissolved, poly(ethylene glycol) (860mg, 0.19mmol, Sigma Aldrich, Cat#: 373001) and DMAP (26mg, 0.21mmol) were added to the mixture. The reaction was left to stir in an ice bath for 30 minutes during which was added DIC (29ul, 0.19mmol). The reaction was then removed from the ice bath and left to stir at room temperature overnight. The content of the vial was then put on a rotary evaporator to evaporate most of the solvent. Fresh DCM (1-3ml) was added to the vial to dissolve the compound and MeOH was added (10ml). The vial was placed at -20^{o}C until a precipitate formed from which the supernatant was decanted. A second wash was done on the precipitate by adding 1ml of DCM followed by 45ml of MeOH and placing the vial at -20^{o}C until precipitate formation. The precipitate was decanted once more and the collected precipitate was placed on vacuum overnight. The compound was dissolved in $CDCl_3$ and analyzed by ^{1}H NMR using the Bruker Avance III 600.

For the formation of PLGA-PEG-TPP, the synthesized PLGA-PEG-OH (1600mg) was dissolved in DCM (7ml). Subsequently, (4-Carboxybutyl)triphenylphosphonium bromide (TPP)

(132.5mg, 0.299mmol, Sigma Aldrich, Cat#: 157945) and DMAP (17.95mg, 0.164mmol) were added and the reaction was placed in an ice bath for 30 minutes with stirring during which was added DIC (45.5ul, 0.294mmol). The reaction was then left to stir overnight at room temperature. For the compound's purification, the solvents were evaporated using a rotary evaporator until 4ml was left in the vial. Diethyl ether was added to precipitate the polymer followed by 2 minutes of vortexing and a 5-minute centrifugation at 1300rpm. The resulting supernatant was decanted and MeOH (4ml) was added followed by diethyl ether (45ml), the resulting precipitate was decanted. The precipitate was washed multiple times by dissolving it in DCM (2ml), adding MeOH (4ml) and adding diethyl ether (40ml) and placing it at -20^{o}C until precipitate formation. The resulting compound was placed on a vacuum overnight and analyzed by ^{1}H NMR in $CDCl_3$ using the Bruker AVANCE III 600. For both syntheses, the protocol above was inspired by an already published similar synthesis[78]. The NMR spectra for both compounds were analyzed using the MestReNova software.

2.3. In solution assays: Boronic ester bond formation and ROS-sensitivity

2.3.1. Boronic ester bond detection by fluorescence

Solutions of AC2, maleic anhydride polymer (Poly(isobutylene-*alt*-maleic anhydride), Sigma Aldrich, Cat#: 531278) and tannic acid (TA) at a concentration of 0.5mg/ml were made in DMSO. A quartz cuvette (Hellma, Cat#: 101-QS) was filled with 1ml of TA solution to which was gradually added either AC2, maleic anhydride or DMSO in increments of 200ul until a total of 1ml was added. Four controls of 1ml of TA alone, AC2 alone, maleic anhydride polymer alone and DMSO alone were also made. The solutions were left to stir for 2 minutes before using the spectrophotometer (VARIAN Cary Eclipse) to excite the solution at 380nm and measure the resulting fluorescence at wavelengths from 430nm to 700nm.

2.3.2. Boronic ester bond detection by ^{1}H NMR

^{1}H NMR was performed in DMSO-d6 on samples of gallic acid (GA), benzene-1,4-diboronic acid (diBA) (Sigma Aldrich, Cat#: 417130) and a mix of 1:5 molar ratio of diBA: GA to assess for bond formation between the compounds. As for bond breakage, a 1:1 w/w ratio of GA and diBA were combined in DMSO-d6 and 10ul of 30% H_2O_2 was added. The NMR was ran about 1 week after the addition of the H_2O_2. All 4 NMRs were ran using the Bruker AVANCE II 400. NMR spectra were analyzed using the MestReNova software.

2.4. Nanoparticle assembly, optimization and property assessment

2.4.1. Optimization of NP ROS-scavenger content

NPs were made via nanoprecipitation by combining in an eppendorf, in order, one of the ROS-scavenger (2mM solutions in water for TA and GA, and in 3.4% DMSO and 96.6% water for EG, volume equivalent to 50nmol-1000nmol used accordingly), the AC2 polymer (100ul, 1mg/ml in 20.5% DMSO and 79.5% Milli-Q water), PLGA-PEG-TPP (50ul, 10mg/ml in acetone) and PLGA-PEG-OMe (50ul, 10mg/ml in acetone). The eppendorf's content was then added dropwise to stirring Milli-Q water and left to stir for 3h. The solution was collected and transferred to a 100k Mw filter centrifugal device (Microsep Advance centrifugal device, PALL Corporation, Cat#: MCP-100C46) for NP concentration. NPs were repeatedly centrifuged at 3000rpm for 10 minutes. After the first spin, NPs in the top solution were resuspended with the addition of 500ul of Milli-Q water. Resuspension without any solvent additions were conducted between the remaining spins. The top solution can be transferred to a new centrifugal device if the filter gets clogged, usually after the 3rd spin. This was repeated until 100ul-500ul of solution remains above the filter. This solution was collected and its exact volume was recorded. A 1.5ml disposable cuvette (BRAND GMBH+CO KG, Cat#: 759075D) was used to combine 1ml of

Milli-Q water and 7ul of concentrated NP for sizing and measurement of polydispersity index (PDI) by dynamic light scattering (DLS) using the Zetasizer Nano series (Malvern).

2.4.2. Assembly of AC2 NP formulations selected for further studies

The NP formulations selected for future studies were self-assembled via nanoprecipitation by combining, in order, one of the ROS-scavenger (for TANPs: 100ul TA, 2mM in Milli-Q water (200nmol); for EGNPs: 200ul EG (400nmol), 2mM in Milli-Q water; for GANPs: 500ul GA, 2mM in Milli-Q water (1000nmol)), the AC2 polymer (100ul, 1mg/ml in 20.5% DMSO and 79.5% Milli-Q water), PLGA-PEG-TPP (50ul, 10mg/ml in acetone) and PLGA-PEG-OMe (50ul, 10mg/ml in acetone) in an eppendorf tube with vortexing between each addition. For NPs without PLGA-PEG-TPP (TANPome, EGNPome and GANPome), only PLGA-PEG-OMe (100ul, 10mg/ml in acetone) was used. As for cy5.5-labelled NPs, PLGA-Cy5.5 (30ul, 10mg/ml in DMF), PLGA-PEG-TPP (35ul, 10mg/ml in acetone) and PLGA-PEG-OMe (35ul, 10mg/ml in acetone) were used. The eppendorf solution was then added dropwise to 3ml of stirring Milli-Q water and left to stir for 3h. The resulting NP solution was transferred to a 100k Mw filter centrifugal device (Microsep Advance centrifugal device, PALL Corporation, Cat#: MCP-100C46) for concentration. NPs were centrifuged at 3000rpm for 10 minutes and resuspended in the centrifugal device using 500ul of Milli-Q water. NPs were then centrifuged at 3000rpm in 10-minute intervals with resuspension of the solution in between until 100-500ul of solution remained above the filter. This solution was collected and its volume measured. If the volume stays the same after centrifugations, the filter might be clogged and thus the top solution can be transferred to a new centrifugal device, usually after the 3rd spin. Nanoparticles were sized and their PDI determined by dynamic light scattering (DLS) using Zetasizer Nano series (Malvern) by taking 7ul of concentrated NP solution and adding it to 1ml of Milli-Q water in

1.5ml disposable cuvettes (BRAND GMBH+CO KG, Cat#: 759075D). NP concentration was determined based on the initial quantity of ROS-scavenger added:

$$NP\ Concentration = \frac{(Concentration\ of\ ROS\ scavenger)(Volume\ of\ ROS\ scavenger)}{NP\ volume\ after\ concentrating}$$

In the formula, "Concentration of ROS-scavenger" is the concentration of the initial ROS-scavenger solution added to the eppendorf and "Volume of ROS-scavenger" is the volume of that ROS-scavenger solution initially added to the eppendorf.

2.4.3. Assessment of NP stability

TANP, EGNP, GANP, TANPome, EGNPome and GANPome nanoparticles were assembled and concentrated. For assessment of storage stability, nanoparticles were stored at 4^{o}C for 1 week. For assessment of stability in biological conditions, nanoparticles were incubated at 37^{o}C in 10% FBS for up to 48h. Nanoparticles were sized by dynamic light scattering using the Zetasizer Nano series (Malvern) at the start of the experiment and after 1 week (for storage stability) or 24 and 48h (for biological stability) by adding 8ul of nanoparticle sample to 1ml of Milli-Q water in 1.5ml disposable cuvettes (BRAND GMBH+CO KG, Cat#: 759075D). The percent variation of size between the initial sizing before incubation and each of the subsequent sizes were calculated.

2.4.4. NP visualization by transmission electron microscopy

TANP (containing 50ul of 2mM TA rather than 100ul), EGNP and GANP nanoparticles were assembled and concentrated. A 400-mesh copper grid (TED PELLA, INC., Cat#: 01822) was placed in droplets of the nanoparticle, UranyLess **(**Electron Microscopy Sciences, Cat#: 22409) and Milli-Q water consecutively for approximately 45 seconds in each with wicking

using a filter paper (VWR, Cat#: 28310-106) between each step. Grids were left to dry for at least 24h before their imaging via the JEM-1400Flash transmission electron microscope (TEM) and GATAN One View camera. Images were processed using the Fiji ImageJ software.

2.4.5. Assessment of the NPs' ROS-sensitivity properties in solution

The AC2 concentration of the TANPs, EGNPs and GANPs was calculated based on the concentrated NP volume. A volume equivalent to 5ug of AC2 was added to 800ul of either water or H_2O_2 in a cuvette (BRAND GMBH+CO KG, Cat#: 759075D) and periodically sized over 3 hours by DLS using a Zetasizer Nano series (Malvern). The percentage of size variation between the initial size and the size at each timepoint was measured and the absolute value was plotted with 0-10% variation considered as no variation. The size distribution by intensity as measured using the Zetasizer Nano series (Malvern) at key timepoints was also plotted.

2.4.6. Assessment of the NP's ROS-scavenging properties in solution

The ROS-scavengers and NPs' ROS-scavenging abilities were determined using the ROS-Glo H_2O_2 assay (Promega, Cat#: G8821). Wells from a white clear-bottom 96-well plate were filled with 60ul of H_2O_2 to which was added 20ul of treatment (TA, EG, GA, TANP, eNP or water for the untreated control) to form a final solution of 100uM H_2O_2 and 100uM of treatment per well. The NPs were left to interact with H_2O_2 for 20 mins before, as per the manufacturer's protocol, 20ul of 125uM H_2O_2 substrate solution was added to each well. The plate was left to incubate at room temperature for 1h. Following the incubation, 100ul of ROS-Glo detection solution was added to each well and incubated for 20 mins at room temperature. The resulting luminescence levels were measured using a plate reader (BioTek). Background luminescence was calculated using wells with 60ul of water and 20ul of each treatment and subtracted from the respective recorded luminescence values.

2.5. Assessment of the NPs in vitro

2.5.1. Assessment of NP cellular uptake

RAW264.7 macrophages were seeded in a 6-well plate at a density of 200k cells/well overnight using complete DMEM media before undergoing a 24h treatment with 20uM of cy5.5-TANPs, or a media change for the untreated cells. Cells were then washed with 1xPBS and lifted using TrypleE. The TrypleE was neutralized using complete DMEM media. Cells were collected and centrifuged at 1500rpm for 5 minutes and resuspended in 1x PBS. Cells were centrifuged again and resuspended in 400ul of 2% FBS in 1xPBS. Cells were then analyzed by flow cytometry using the BD LSRFortessa's (BD Biosciences) APC channel (640nm laser, 660/20 emission filter, voltages: FSC:286, SSC:231, APC:512) and the BD FACSDiva software (BD Biosciences) for detection of cy5.5-positive cells. The FLOWJO software was used to analyze the data. Initial gating used SSC-A/FSC-A to select live cells, and SSC-H/SSC-A to select a subpopulation of single cells. This subpopulation was placed in a histogram for the APC channel from which a gate of 0% cy5.5-positive cells was delineated from the untreated cell sample and applied to the treated cells to show the percentage of NP-positive cells. The geometric mean signal intensity was also determined by the software from the single cell population.

2.5.2. Confirmation of NP cellular uptake and mitochondria-targeting abilities

Round coverslips (MercedesScientific, Cat#: MER R00121.5) were dipped in 70% ethanol and left to dry. The coverslips were placed at the bottom of a 24-well plate and RAW264.7 cells in complete DMEM were seeded on top at a density of 30k cells/well. The next day, cells were treated with 20uM of cy5.5-TANPs for 24h. For their fixation, the cells were washed with 1x PBS followed by a 10-minute incubation with 4% PFA (Acros Organics, Cat#: 41678-5000) in 1x PBS. The PFA was aspirated and the cells washed 3 times with 1x PBS. Cells were then permeabilized using 0.5% triton in 1x PBS for 5 minutes followed by 3 1x PBS

washes. A blocking solution (0.05% saponin (EMD Millipore Corp, Cat#: 558255) and 20% FBS in 1x PBS) was added to the cells for 30 minutes during which a 1:200 dilution of TOM20 polyclonal antibody (Proteintech, Cat#: 11802-1-AP) was made in blocking solution. Cells were treated with 100ul of the TOM20 primary antibody per well in a humid environment for 1 hour. The coverslips were washed 3 times with 1x PBS before adding the AF488-conjugated secondary antibody (ThermoFisher Scientific, Cat#: A-11008), at a 1:500 dilution in 1x PBS for 1 hour. Cells were washed 3 times with 1x PBS before the nucleus was stained with 1:20 000 000 Hoechst (Molecular probes, Cat#: H1399) in 1x PBS for 1 minute. Cells were washed once again 3 times with 1x PBS. A drop of mounting media (Ibidi, Cat#: 50001) was placed on a microscopy slide cleaned with ethanol. The coverslip was placed face down on the mounting media (ThermoFisher Scientific, Cat#: P36980) and excess liquid was wiped away. The coverslip was sealed to the microscopy slide using nail polish and stored at 4^{o}C until imaging. Z-stack microscopy images were obtained with the Leica Thunder Imager and the LAS X software using the 63x objective. Hoechst was visualized using the DAPI filter (ex: 350/50, em:460/50), TOM20-AF488 using the GFP filter (ex: 470/40, em: 525/50) and cy5.5-TANPs using the Cy5 filter (ex: 620/60, em: 700/75). Images were processed using the small volume computational clearing from the LAS X software and the Fiji ImageJ software.

2.5.3. Assessment of NP cytotoxicity

RAW264.7 cells were seeded overnight in a 96-well plate at a density of 5000 cells per well using complete DMEM media. The LDH assay was conducted using the CyQUANT LDH Cytotoxicity Assay Kit (Invitrogen, Cat#: C20301) as per the manufacturer's protocol. In short, cells were treated for 24h in triplicates with 50ul of either sterile water (Multicell, Cat#: 809-115-CL) (for measurement of maximum LDH activity), phenol red-free DMEM media (for measurement of spontaneous LDH activity) or TANPs to a final well concentration of either

0uM (no treatment), 1uM, 5uM, 20uM or 100uM of NPs. After the 24h treatment, cells treated with water were treated with 10ul of 10X lysis buffer for 45 minutes at 37ºC to assess maximum LDH activity. Subsequently, 50ul of media from each well was transferred to a clear 96-well plate in duplicate to which 50ul of reaction mixture was added for a 30-minute incubation at room temperature. After incubation, 50ul of stop solution was added per well and absorbance of the wells was measured at 490nm and 680nm using a plate reader (BioTek). The technical duplicates were initially averaged to give an average absorbance readout. For each of the treated wells, the average absorbance readout at 680nm was subtracted from the average absorbance readout at 490nm to remove background and give an LDH activity value. The triplicates were then averaged and for each TANP concentration, the percentage of cell viability was measured as follows:

$$\%\ cell\ viability$$
$$= 100 - \left[\left(\frac{TANP\ treatment\ LDH\ activity\ -\ Spontaneous\ LDH\ activity}{Maximum\ LDH\ activity\ -\ Spontaneous\ LDH\ activity}\right)\ x100\right]$$

2.5.4. Assessment of NP ROS-reduction abilities in vitro

RAW264.7 cells were seeded at a density of 100k cells/well in a 12-well plate and left to adhere overnight. Cells were treated with 0uM (no treatment), 1uM, 5uM or 20uM of TANPs in complete DMEM media for 24h. Subsequently, LPS (Sigma Aldrich, Cat#: L4524) was added to the wells for a 6h treatment at a final concentration of 1ug/ml LPS in complete DMEM media. Following treatment, cells were washed with 1x PBS and treated with 10uM of DCFH-DA (Sigma Aldrich, Cat#: D6883) in serum-free DMEM for 30 minutes. Cells were then washed with 1x PBS and lifted using TrypLE. They were centrifuged at 1500rpm for 3 minutes and resuspended in fresh 1x PBS twice. Cells were analyzed by flow cytometry with the BD LSRFortessa (BD Biosciences) and BD FACSDiva software (BD Biosciences) using the FITC

channel (488nm laser, 530/30 emission filter, 400 voltage) for measurement of DCF signal intensity. The FLOWJO software enabled data analysis. Initial gating was done for the selection of live, single cells using the SSC (231 voltage) and FSC (voltage 286) channel data. The DCF signal intensity was assessed for this population. The fold change in geometric mean intensity for that population was also calculated using FLOWJO and plotted.

2.5.5. Assessment of NP anti-inflammatory properties in vitro

RAW264.7 cells were seeded at a density of 100k cells per well in a 12-well plate in complete DMEM media. The next day, cells underwent a 24h treatment with nanoparticles (1uM of TANPs or 20uM of EGNPs) in complete DMEM media. Subsequently, LPS was added to the wells to a final concentration of 100ng/ml for a 5h treatment. An RNA extraction was then performed on the cells using an RNeasy® Mini Kit (QIAGEN) as per the manufacturer's protocol. The resulting RNA's concentration was measured using a NanoDrop 2000/2000c spectrophotometer (Thermo Scientific). For cDNA synthesis, a volume of the extracted RNA equivalent to 900ng of RNA was added to 4ul of iScript Reverse Transcription Supermix (Bio-Rad, Cat#: 1708841), topped off to a total of 20ul using RNase-free water and placed in a thermal cycler (Bio-Rad). A mastermix was made by combining, for each well, 7ul of RNAse-free water, SYBR Green (appliedbiosystems, Cat#: 4309155) and forward and reverse primers for the markers of interest (0,5ul of each) with β-actin as the gene of reference (primer sequences, resuspended to 100uM: TNF-α FW: 5'-GAGAAGTTCCCAAATGGCCTCCC-3', REV: 5'-GTATGAGATAGCAAATCGGCTGACGG-3'; ABCA1 FW: 5'-GGAGCCTTTGTGGAACTCTTCC-3', REV: 5'-CGCTCTCTTCAGCCACTTTGAG-3'; β-Actin FW: 5'-GATCAAGATCATTGCTCCTCCTG-3', REV: 5'-AGGGTGTAAAACGCAGCTCA-3', Eurofins Genomics). A 96-well PCR plate was loaded in triplicates with 2ul of cDNA and 18ul of the correct mastermix in each well. It was sealed using

a Sealing Film (PureAmp, Cat#: P1001-Q), centrifuged at a quick pulse and placed in the CFX Opus 96 real-time PCR system for measurement of marker levels. Data was analyzed using the Livak method to find the fold change in relation to untreated cells.

3. Results

3.1. Confirmation of synthesis for the main biomaterials of interest

3.1.1. Synthesis of the AC2 polymer

Confirmation of successful synthesis for the AC2 polymer was done by ^{1}H NMR (Figure 4). The AC2 polymer was obtained by performing a spontaneous ring-opening reaction between a maleic anhydride polymer and 4-(hydroxymethyl)phenylboronic acid molecules to generate a boronic acid containing polymer. As successful compound synthesis involves the conjugation of repeating boronic acid units to the molecules, successful synthesis was determined based off the presence of characteristic peaks for the 4-(hydroxymethyl)phenylboronic acid moiety. ^{1}H NMRs give a characteristic peak for each hydrogen in a solution depending on their environment (surrounding atoms, functional groups, etc.). Thus, the easiest peaks from the added moiety to identify are the aromatic peaks as they are in a unique configuration compared to the other polymer hydrogens. Aromatic cycle hydrogens typically appear as doublets of doublets in the δ 7.0ppm-8.0ppm region. The results indeed show the presence of these characteristic peaks which were attributed as (a) at 7.70ppm and (b) at 7.23ppm. Thus, results support the successful synthesis of the AC2 polymer.

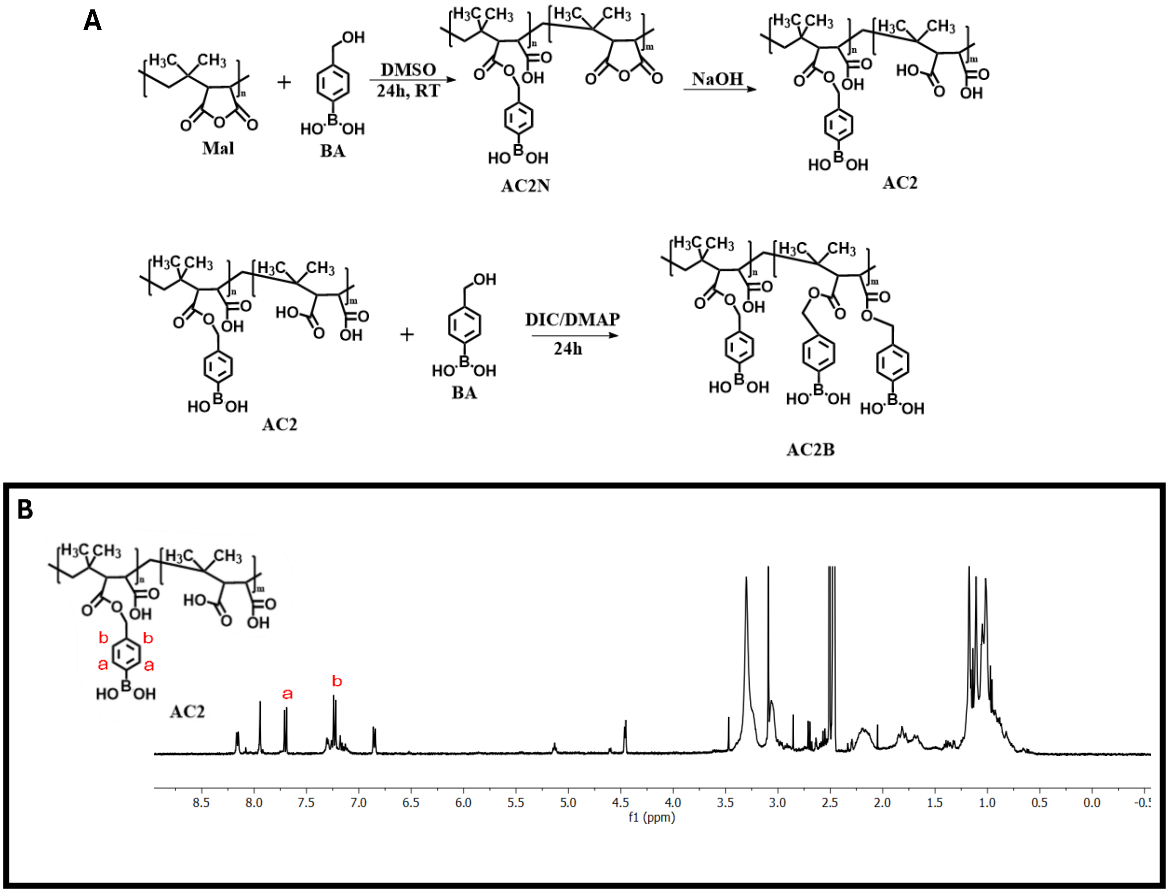

Figure 4. Confirmation of successful synthesis for the AC2 polymer. (A) Synthesis scheme. A maleic anhydride polymer (Poly(isobutylene-alt-maleic anhydride) (Mal) was used as a base to which was conjugated a boronic acid functional group (4-(hydroxymethyl)phenylboronic acid) by a spontaneous ring-opening reaction yielding the AC2N polymer. Unreacted maleic anhydride groups were opened using NaOH yielding the AC2 polymer. The polymer's new carboxylic acid groups were reacted, as part of a DIC/DMAP reaction, with 4-(hydroxymethyl)phenylboronic acid, resulting in the AC2B polymer. **(B) Confirmation of polymer structure.** The AC2 polymer's structure was confirmed by ^{1}H NMR in DMSO-d6. Successful synthesis was determined by the presence of the peaks (a) at δ 7.70ppm and (b) at δ 7.23ppm.

3.1.2. Synthesis of the AC5P and AC5 polymer

The confirmation of successful synthesis for the AC5P polymer was done via ^{1}H NMR (Figure 5). Initially, the methyl group (a) was attributed to a peak at δ 3.38ppm which served as the reference peak. Next, we identified the PEG peak (b) which appeared at its characteristic δ 3.65ppm range[81]. The integration of this peak gave 908H. To confirm the correct attribution of

the reference peak and of the PEG peak, PEG-macroCTA's Mw was used. As the biggest part of the molecule, the PEG polymer contributes to the majority of its ~10 000g/mol Mw. Thus, given the Mw of a single PEG molecule, which was calculated to ~ 44g/mol, it was determined that each PEG-macroCTA molecule is comprised of ~ 227 PEG repeating units. As each PEG molecule possesses 4 hydrogen atoms, its integration should be of 909H, which corresponds to the integration obtained. These peaks were then used to identify the amount of epoxy groups successfully conjugated to each PEG-macroCTA molecule, and thus the amount of epoxy groups on the AC5P polymer. To this end, the key hydrogens of the epoxy group were identified on the spectrum obtained by using a published spectrum for reference[82]. The first epoxy ring peak identified was (d) at δ 3.23ppm. As this peak only has 1 hydrogen, its integration is equal to the amount of epoxy groups on AC5P, which gave ~ 73 groups. Every epoxy ring has 2 hydrogens for peaks (e) at δ 2.64ppm and δ 2.84ppm while also having 2 hydrogens for peaks (c) at δ 3.82ppm and δ 4.29ppm. Thus, the integration ratio between hydrogens (d), (e) and (c) should be 1:2:2. This is indeed what is observed, with hydrogens (e) giving an integration of 149.89H and the peaks for (c) giving integrations of 69.92H and 78.30H.

The synthesis of the AC5 polymer was done by conjugating a boronic acid moiety to the epoxy groups of the AC5P polymer synthesized. As the ^{1}H NMR for AC5P confirmed its structure, the focus to confirm successful AC5 formation is on identifying peaks belonging to the novel moiety added, the phenylboronic acid group. As expected, peaks (f) at δ 7.70ppm and (g) at δ 7.23ppm appeared as a doublet of doublet, a characteristic presentation of aromatic cycles. Thus, this enabled us to confirm the conjugation of boronic acid to AC5P was successful in yielding the AC5 polymer.

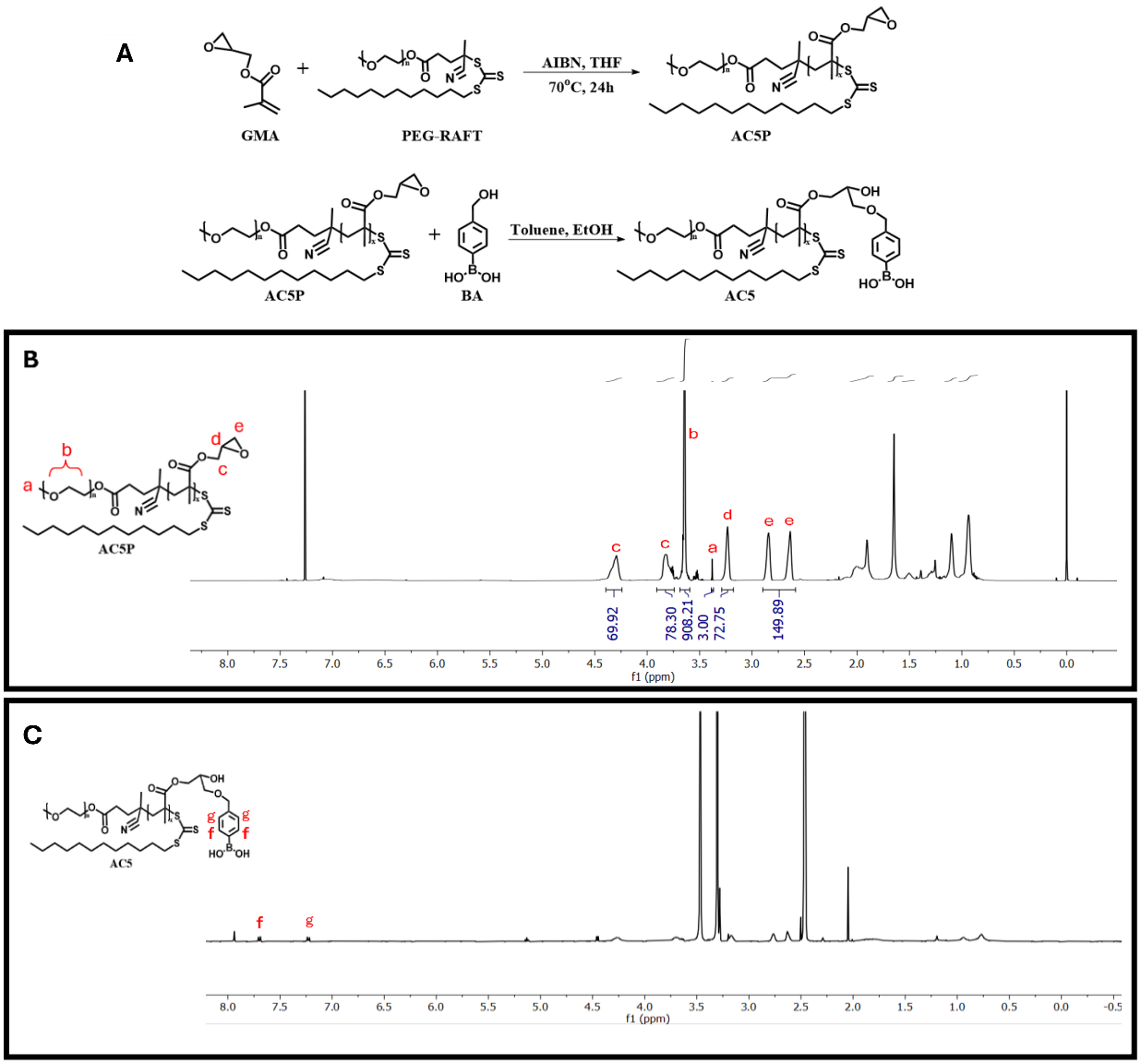

Figure 5. Confirmation of synthesis for the AC5P and AC5 polymers. (A) Synthesis scheme. An initial RAFT (Reversible addition-fragmentation chain-transfer) polymerization reaction occurred between glycidyl methacrylate (GMA) and PEG-RAFT (poly(ethylene glycol) methyl ether 4-cyano-4-[(dodecylsulfanylthiocarbonyl)sulfanyl]pentanoate) forming the AC5P intermediate. This polymer underwent an epoxide ring-opening reaction with 4-(hydroxymethyl)phenylboronic acid to add repeating boronic acid functional groups, yielding the AC5 polymer. **(B, C) Confirmation of polymer structure.** Both polymers were analyzed by ^{1}H NMR (B) in $CDCl_3$ for the AC5P polymer and (C) in DMSO-d6 for the AC5 polymer. Characteristic peaks (B) at (a): δ 3.38ppm; (b): δ 3.65ppm; (c): δ 3.82ppm and δ 4.29ppm; (d): δ 3.23ppm; (e): δ 2.64ppm and δ 2.84ppm for AC5P and (C) at (f): δ 7.70ppm and (g): δ 7.23ppm for AC5 enabled confirmation of synthesis.

3.1.3. Synthesis of the PLGA-PEG-OH and PLGA-PEG-TPP polymers

The confirmation of successful synthesis for both the PLGA-PEG-OH and PLGA-PEG-TPP polymers was done by ^{1}H NMR (Figure 6). The first synthesis was an esterification reaction between PLGA and PEG polymers. Thus, a successful synthesis would display the characteristic peaks for both of these compounds, which was indeed observed. Indeed, the first peak identified was for the PEG portion, which appears as a single peak around 3.65ppm[81]. It was identified as peak (d) at δ 3.67ppm on the spectrum obtained. As for the PLGA, it will appear as distinct peaks for the different units of the polymer. The glycolic acid moiety only possesses hydrogens as part of its CH_2 group, and thus a single peak will mark the presence of this group in the molecule. The glycolic acid peak was indeed visible in its characteristic region and identified as peak (a) at δ 4.67ppm – 4.94ppm. As for the lactic acid portion of PLGA, the methyl group (b) and the CH group (c) will tend to appear as separate peaks in their respective typical regions. Indeed, peaks were attributed as (b) at δ 1.60ppm and (c) at δ 5.15ppm-5.34ppm. Thus, these peaks indicate successful compound synthesis and enabled us to proceed to the second reaction for the conjugation of TPP.

The TPP conjugation reaction required a second esterification reaction this time between TPP and the PLGA-PEG-OH compound synthesized. Thus, the confirmation of successful synthesis depends on the presence of characteristic TPP peaks on the NMR spectra. TPP's structure is particular as it consists mainly of 3 equivalent aromatic cycles each containing 2 pairs of symmetrical hydrogens and one different hydrogen. Therefore, we should expect to see three peaks in this region, one for each pair and one for the CH, all appearing in the aromatic region between δ 7.0ppm-8.0ppm. It is indeed what has been observed with 3 peaks attributed as (e) at δ 7.80ppm, (f) at δ 7.88ppm and (g) at δ 7.71ppm. Thus, the second synthesis was deemed successful, enabling the use of the targeting agent in NP formulations.

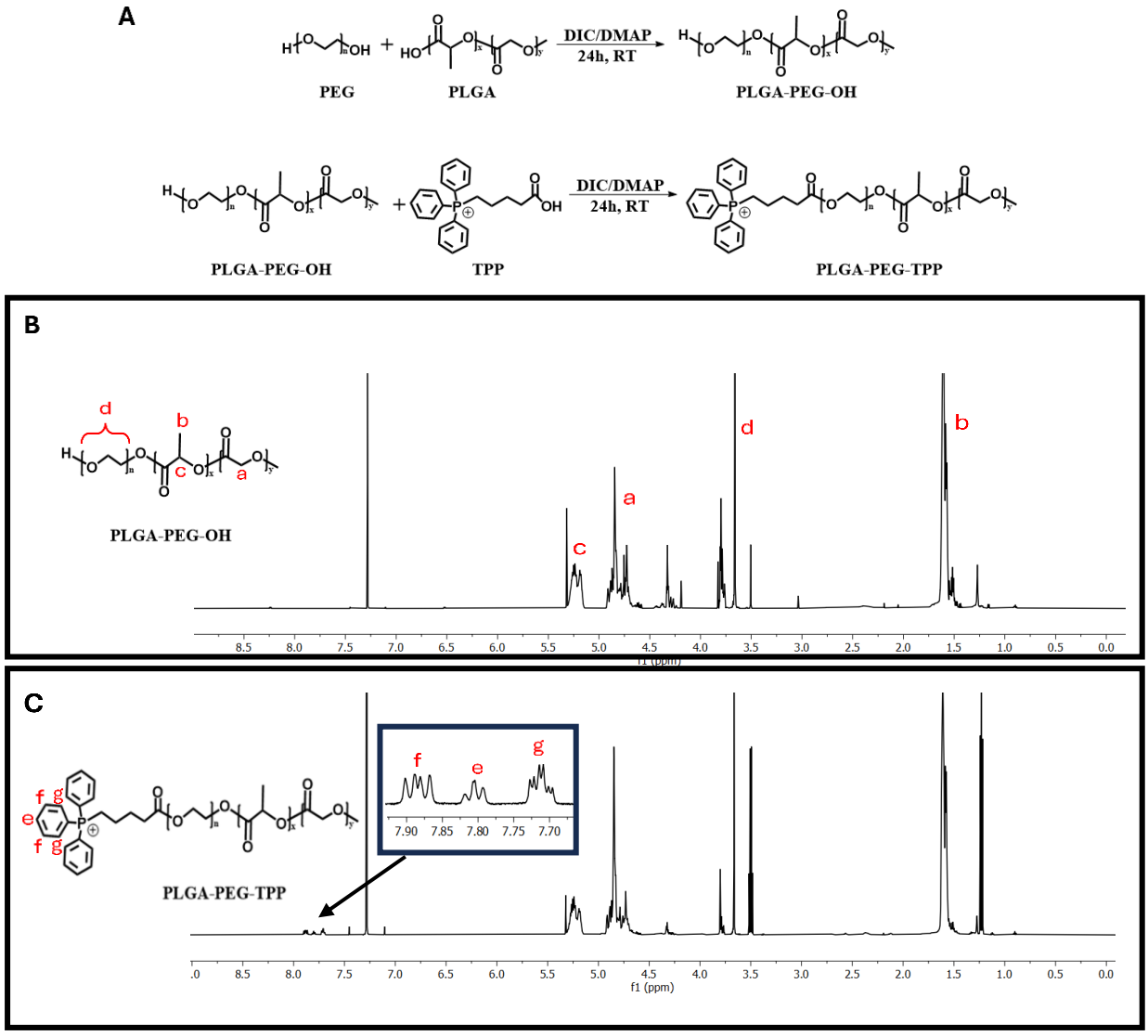

Figure 6. Confirmation of synthesis for PLGA-PEG-OH and PLGA-PEG-TPP. (A) Synthesis scheme. A DIC/DMAP esterification reaction between PEG and PLGA enabled the formation of PLGA-PEG-OH which underwent a second esterification reaction enabling the conjugation of the TPP mitochondria-targeting molecule. **(B, C) Confirmation of polymer structure.** ^{1}H NMR was performed in $CDCl_3$ on both compounds to confirm successful synthesis and evaluate compound purity. Characteristic peaks at (B) (a): δ 4.67ppm – 4.94ppm; (b): δ 1.60ppm; (c): δ 5.15ppm-5.34ppm; (d): δ 3.67ppm and at (C) (e): δ 7.80ppm; (f): δ 7.88ppm; (g): δ 7.71ppm enabled confirmation of synthesis and polymer structure.

3.2. Confirmation of boronic ester bond formation by fluorescence

The ROS-sensitive boronic ester bond, which constitutes the base of the NP system's function, is expected to form between the boronic acid functional group of the polymeric backbone and the ROS-scavenger's hydroxyphenol moieties. As we suspect TA to have a naturally quenched fluorescence due to its intramolecular and intermolecular interactions, we expect bond formation to affect these interactions, leading to an increase in fluorescence intensity[83]. The boronic ester bond's formation was assessed by fluorescence using a spectrophotometer to excite tannic acid at 380nm (Figure 7). Both the maximum amount assessed of TA alone (1ml, 500ug) and of the AC2 polymer alone (1ml, 500ug) show no fluorescence. Solutions containing both the AC2 polymer and TA do show fluorescence which increases in an AC2-dependent manner at emission wavelengths from 430nm to 470nm; as the amount of AC2 added increases, the level of fluorescence detected increases as well. With 500ug of TA, fluorescence levels following the addition of 100ug of AC2 remain low but increase greatly when 200ug of AC2 is added. From 300ug to 500ug of AC2, fluorescence levels do continue to increase but in smaller increments. The highest fluorescence intensity observed was at a 1:1 v/v ratio of AC2 and TA (Figure 7 A). As controls, increasing amounts of a maleic anhydride polymer (Mal), a reagent for the reaction forming the AC2 polymer, or DMSO were added to TA (1ml, 500ug) to assess the effect on fluorescence levels. Mal alone (1ml, 500ug) and DMSO alone (1ml) do not show any fluorescence emission at any wavelength. When looking at the 1:1 v/v ratio of TA with Mal or DMSO, a slight increase in fluorescence is observed up to 20 a.u.. However, the 1:1 v/v TA and AC2 solution has much higher fluorescence intensity at 80a.u. (Figure **7** B). When looking at the variation in fluorescence intensity at 436nm, TA incubated with increasing amounts of Mal or DMSO shows a small increase in fluorescence at 200ug (400ul) which

then remains consistent up to 500ug (1ml) of added compounds. However, when incubated with the AC2 polymer, the fluorescence intensity is sustainably increased up to the addition of 500ug (1ml) of AC2 (Figure 7 C).

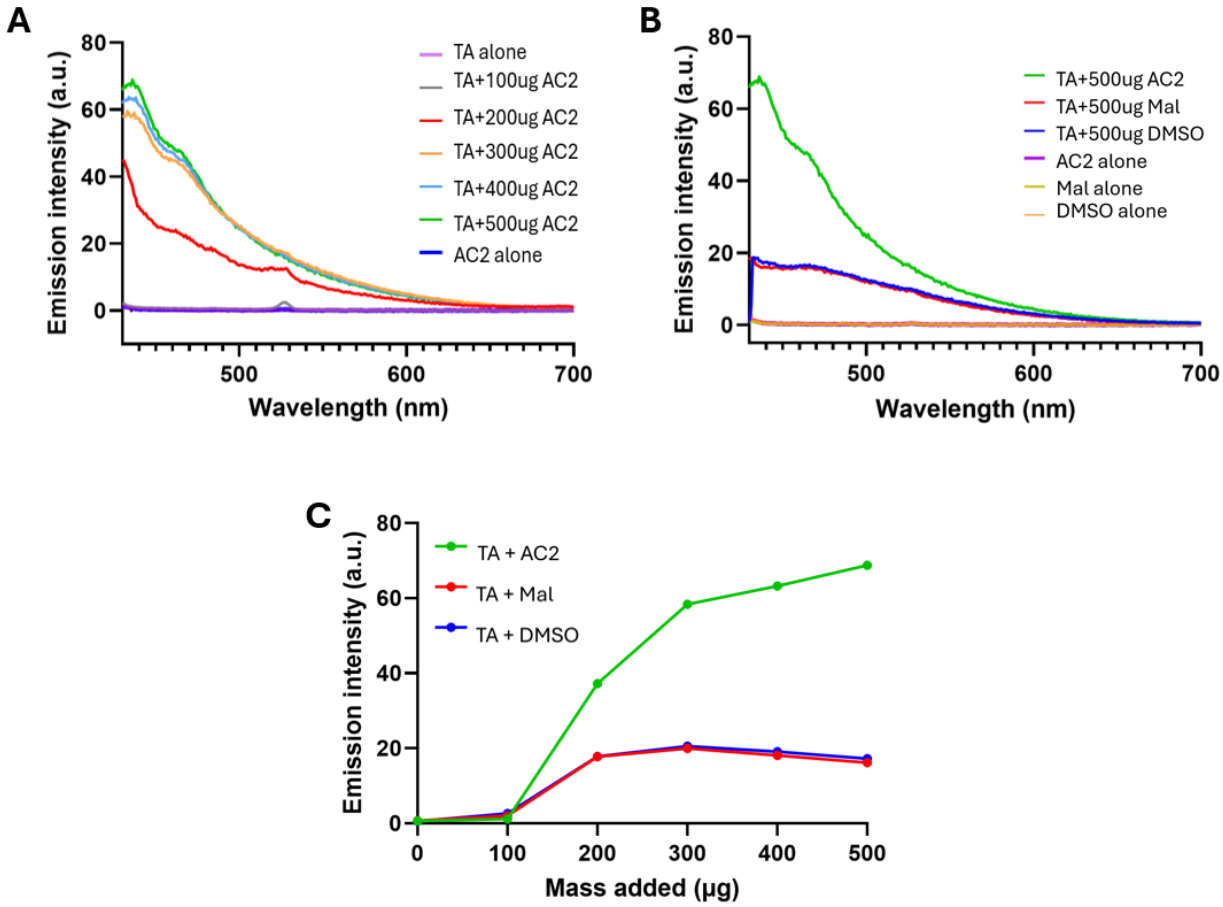

Figure 7. Fluorescence assessment of the complex formation between the polymer and the ROS-scavenger via boronic ester bond formation. Tannic acid (TA) fluorescence (ex:380nm) was monitored using a spectrophotometer. **(A) Effect of AC2 on TA fluorescence.** Tannic acid (1ml, 500ug) incubated with increasing amounts of AC2 polymer shows an AC2-dependant increase in fluorescence indicating boronic ester bond formation. **(B) Effect of non-boronic acid containing compounds on TA fluorescence.** Tannic acid (1ml, 500ug) incubation with the maleic anhydride polymer (Mal, 1ml, 500ug) or DMSO (1ml) controls does not result in a big increase in fluorescence in comparison to the AC2 polymer (1ml, 500ug). **(C) Variation of TA fluorescence at 436nm.** Monitoring tannic acid (1ml, 500ug) fluorescence at 436nm shows a sustained increase in fluorescence only with AC2 incubation but not with the Mal or DMSO controls. (n=1).

3.3. Confirmation of boronic ester bond formation and its ROS-sensitivity by NMR

^{1}H NMRs done on GA, diBA, 1:5 diBA:GA and following the addition of H_2O_2 to the compounds together were done to assess for the formation of boronic ester bonds between the compounds (Figure 8). Results obtained for the individual compounds showed all the expected peaks. For GA peaks were identified as (a) at δ 12.20ppm, (b) at δ 6.89ppm (c) at δ 9.16ppm and (d) at δ 8.81ppm. The peak integration matched with a 1:2:2:1 ratio respectively between the peaks. For diBA, peaks were identified as (e) at δ 7.99ppm and (f) δ 7.70ppm and integration showed the correct 1:1 ratio between the peaks. Signature solvent peaks for DMSO-d6 and water are visible at δ 2.5ppm and δ 3.35ppm respectively. Bound compounds (Figure 8, second track) will present a slightly varied structure, and thus peaks will accordingly shift in the ^{1}H NMR spectrum. This is mainly observed by the novel doublet of doublet appearing at δ 7.38ppm and δ 7.64ppm which indicate a structural change affecting the aromatic section of the compounds. Additionally, the bound compound's ^{1}H NMR presents increased peak intensities for (a), (c) and (d) hydrogens as well as broadened peaks for the (a) and (e) hydrogens. When adding in H_2O_2, the novel doublet of doublet disappears, showing that the structural changes which caused them to appear are no longer present. Additionally, the addition of H_2O_2 leads to many shifts and broadening of hydrogen peaks in both GA and diBA.

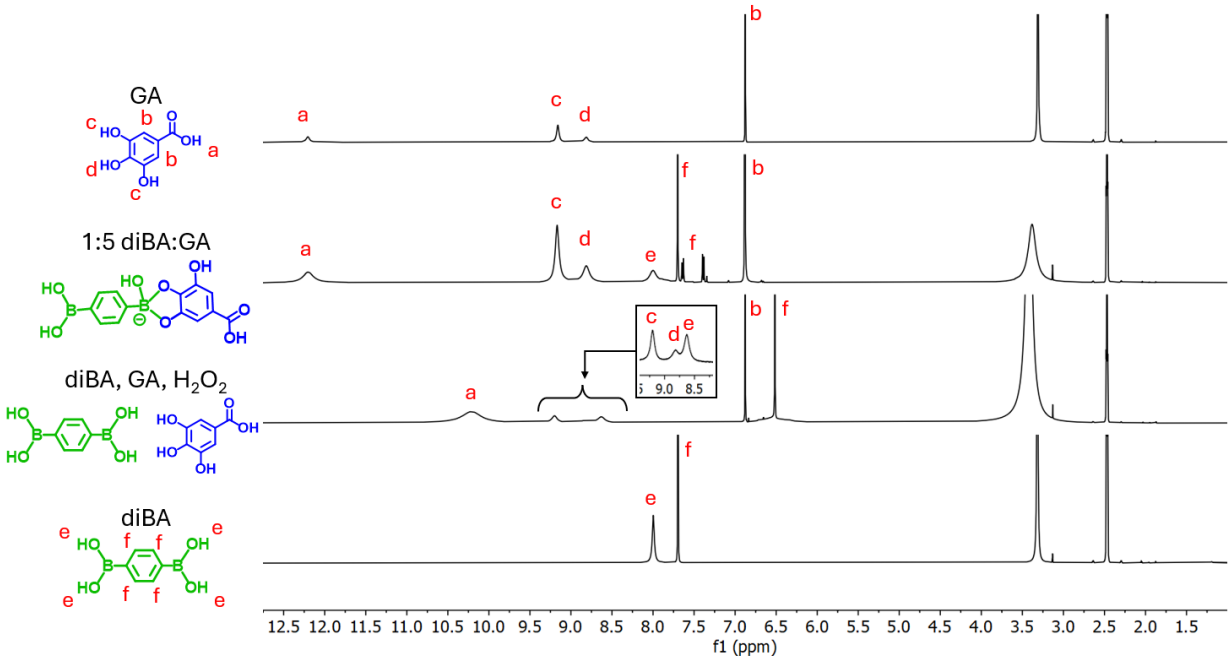

Figure 8. ^{1}H NMR assessment of ROS-sensitive complex formation between boronic acid and the ROS-scavenger. ^{1}H NMR was performed on gallic acid (GA), benzene-1,4-diboronic acid (diBA) as controls and on a combination of 1:5 molar ratio of diBA:GA in DMSO-d6. Formation of the bond is notably shown by the doublet of doublets (δ 7.38ppm and δ 7.64ppm) appearing in the 1:5 diBA:GA track. Following addition of 10ul of 30% H_2O_2 to a 1:1 w/w diBA:GA solution, the doublet of doublet disappears indicating loss of the boronic ester bond and thus ROS-sensitivity (n=1).

3.4. Optimization of NP formulations

The ROS-scavenger content of our NPs was optimized to obtain NPs with appropriate size and PDI values as measured by dynamic light scattering (DLS) (Figure 9). The amounts of ROS-scavenger assessed were higher for the smaller molecules (GA and EG) and lower for the bigger molecules (TA) to account for the variation in boronic ester bond formation potential and increase the likelihood of obtaining NPs with suitable physical characteristics. The NP formulations with smaller ROS-scavengers (EGNP and GANP) showed a slight inverse correlation between the amount of ROS-scavenger and size, whereas the TANPs showed a positive correlation between these parameters. As for the polydispersity index (PDI), which is a measure of the variation in NP sizes where smaller values correspond to less variation, no trend is observable for any of the NPs, apart from a very slight increase for the highest concentration of GA and TA used. When comparing the use of the same amount of ROS-scavenger (200nmol), we can see that the ROS-scavengers with similar sizes and a similar amount of hydroxyphenol groups generate NPs of similar size. In comparison, when the same amount of TA is used, the formulation resulted in much bigger NP sizes and a slightly bigger PDI. As all formulations displayed suitable characteristics (size between 50-200nm and PDI below 0.3), the NP formulations with the highest amount of each ROS-scavenger were the ones selected for future experiments.

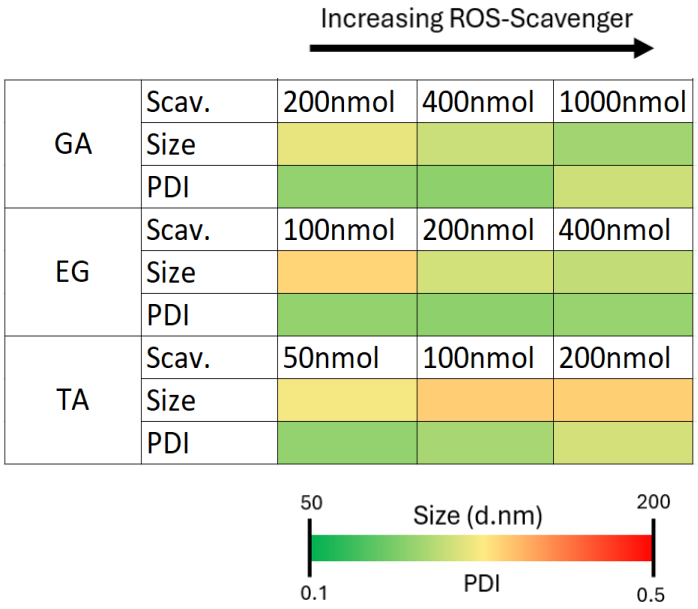

Figure 9. Size and PDI optimization of the NPs' ROS-scavenger content. NP systems for each ROS-scavenger of interest were made with varying amounts of ROS-scavenger content. Each formulation's suitability as candidate NP systems was assessed by size and PDI using dynamic light scattering (DLS). Results show the formation of NPs with suitable characteristics for various amounts of ROS-scavenger content as well as trends in size and PDI based on ROS-scavenger content. (Scav.: quantity of ROS-scavenger, GA: gallic acid, EG: epigallocatechin gallate, TA: tannic acid, PDI: polydispersity index) (n=3).

3.5. Characterization of selected NP formulations

The characterization of the selected NP formulations was done by looking at variations in size, PDI and size distribution (Figure 10). Nanoparticle sizing by DLS revealed that all formulations are between 50-150nm and that the mitochondria-targeted NPs (TANP, EGNP and GANP) are significantly larger than their non-targeted counterpart (TANPome, EGNPome, GANPome) for each ROS-scavenger. Indeed, the mitochondria-targeted NPs measure closer to 100nm whereas the non-targeted NPs are closer to the 50nm mark. Additionally, amongst the targeted NPs, TANPs showed a significant difference in size with EGNPs and GANPs, but the later don't present significant size differences from each other. However, amongst the non-targeted NPs, no significant size difference is observed regardless

of the ROS-scavenger used (figure 10 A). As for the NPs' PDIs, they vary within values of 0.2 to 0.3 for all formulations. No matter the ROS-scavenger used or whether the targeting agent is present or absent, no significant differences in PDIs are observed (figure 10 B). As for the NP's size distribution, all NP formulations assessed show a single population of NPs with sizes following a normal distribution. When comparing the targeted and non-targeted NPs for each ROS-scavenger, the shift in the peak of the curve attests to the change in size reported but also shows that this shift in size is the result of a shift of the entire NP population (figure 10 C).

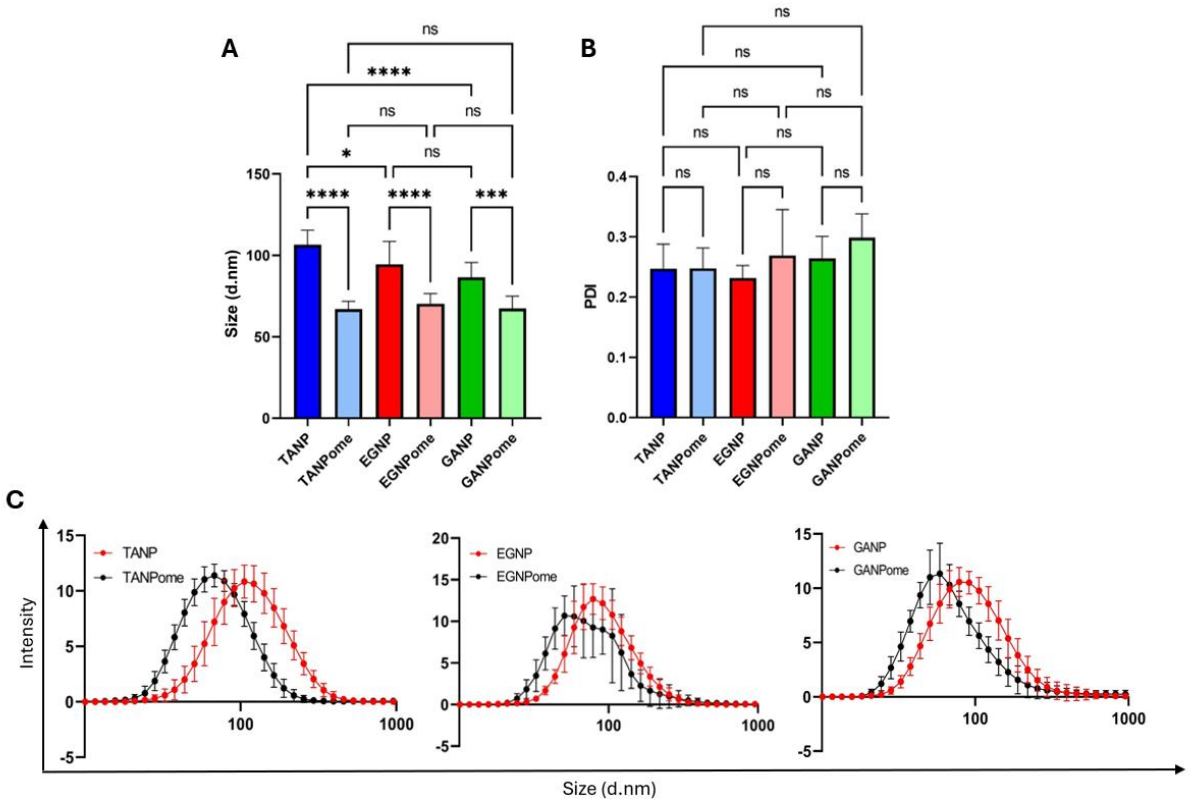

Figure 10. Characteristics of chosen NP systems. (A) NP size and (B) PDI. Size and PDI for selected formulations of targeted (TANP, EGNP, GANP) and non-targeted (TANPome, EGNPome and GANPome) NPs were assessed by dynamic light scattering (DLS). Results show adequate NP sizes and PDI. Results plotted as mean +/- SD. **(C). Comparaison of NP size distribution.** The size distribution by intensity as measured by DLS was plotted for the targeted and non-targeted NPs for the 3 ROS-scavengers. Data shows each formulation results in a single

population of NPs following a normal distribution. Results are plotted as mean +/- SD. (One-way ANOVA, non-significant (ns), *P<0.05, ***P<0.001, ****P<0.0001, n=10).

3.6. NP visualization by transmission electron microscopy

Visualization of the mitochondria-targeted NPs by TEM shows a homogenous population of NPs for all three ROS-scavengers (Figure 11). Images show the obtention of individual, spherical NPs independently of the ROS-scavenger used. The three NP formulations also display structural similarities as seen by the darker outer ring and lighter NP center.

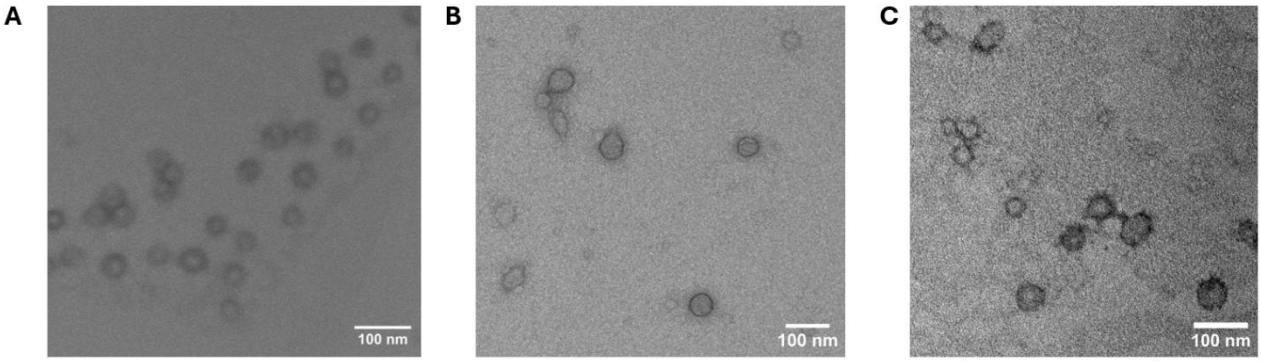

Figure 11. NP visualization by TEM. (A) TANPs (containing 100nmol of TA) (B) EGNPs and (C) GANPs were stained using UranyLess and visualized by TEM. Results show all three targeted NPs have a spherical shape (n=1).

3.7. Storage and biological stability of the NPs

NP stability was assessed in terms of percentage of size variation between the initial NP size and the size following an incubation period (Figure 12). For NP storage stability, NPs stored for 7 days at 4^{o}C showed size variations below 10% for all NP formulations, attesting to their high storage stability. In addition, the mean size variation for each NP formulation is within 5%, with the EGNP formulation appearing to show slightly more variation than its counterparts. As for biological stability, NPs were incubated in 10% FBS at 37^{o}C. A 24h incubation resulted in a slight variation in size for all NPs except for the TANPome NPs which showed a very high

variation in size. After 48h, the percentage of size variation seems to increase more for most NPs compared to the 24h data, mainly for TANPs and EGNPs.

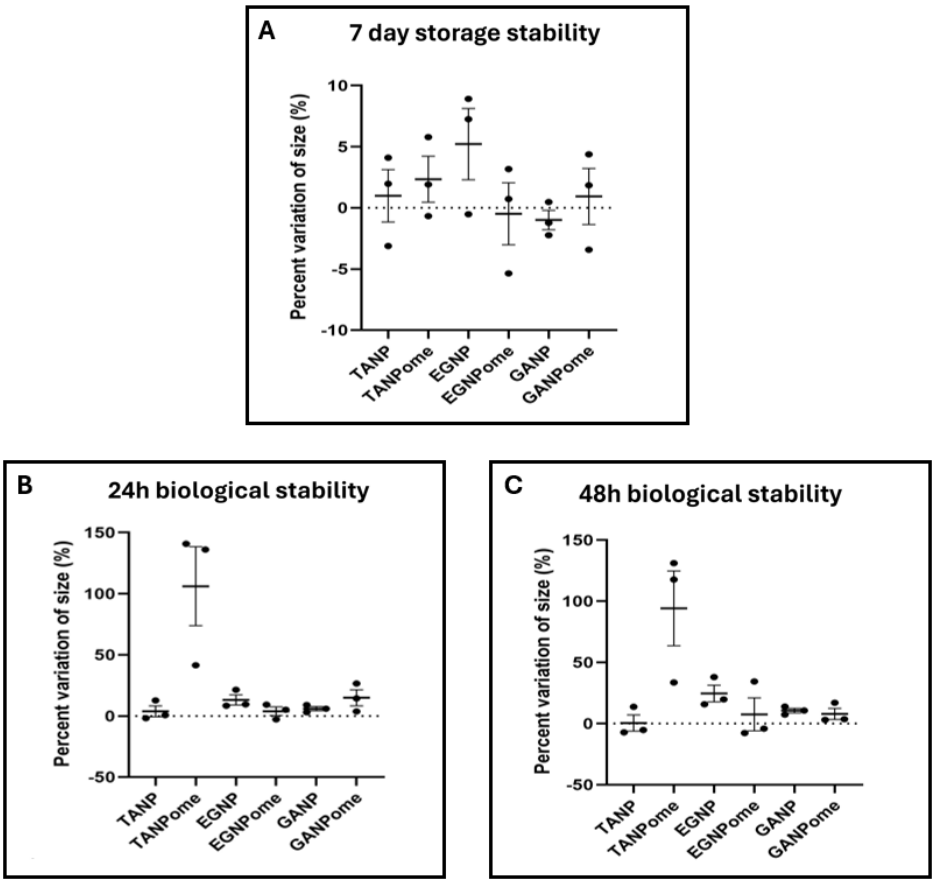

Figure 12. NP stability in storage and biological conditions. (A) NP storage stability. NP sizes were measured by DLS before and after storage at 4°C for 7 days and the percentage of size variation was plotted. Results show negligeable size variations all near or below 10%. **(B, C) NP stability in biological conditions.** NPs were measured by DLS using the before and after incubation at 37°C in 10% FBS for 24h (B) and 48h (C). Results showed some size variation. Results are presented as mean +/- SEM, with positive values indicating size increase and negative values indicating size decrease (n=3).

3.8. Assessment of NPs ROS-sensitivity potential

The assessment of the NPs ROS-sensitivity was done by measuring NP size periodically over a 3-hour incubation period in either water as a control or H_2O_2 as a model for ROS (Figure 13).

Percentage of size variation was initially assessed as an indication for ROS-induced structural modifications, which were used as an indication for ROS-sensitivity. Results show that all NP formulations, whether containing a ROS-scavenger or not, had no size variation over 10% during their incubation in water for the entirety of the 3h period. However, as expected, the results differ in H_2O_2. GANPs and TANPs showed a big variation in size as early as 5 minutes into the experiment. This was maintained for the entire 3-hour incubation period, with TANPs seemingly having a slightly higher size variation than GANPs. As for EGNPs, they showed the same initial trend in size variation until the 120-minute mark where the size variation seemed to decrease slightly. Lastly, as a control for the implication of the ROS-sensitive boronic ester bond in the size variation observed, eNPs, NPs without ROS-scavengers and thus without boronic ester bonds, were assessed. Again, in water, they showed no size variation above 10% over the 3-hour period. However, in H_2O_2, a slight variation in size, lower than that observed for the ROS-scavenger-containing NPs, was observed as of the 5-minute timepoint and remained stable throughout the 3 hours.

The size distribution as detected by intensity for each NP formulation was analyzed for the 5-minute, 60-minute and 180-minute timepoints. For the TANPs, the initial size distribution curve (0 min) resembled the curve for the NPs in water for all 3 timepoints, showing no change in the NP population. In these cases, the NP size distribution followed a normal distribution. In contrast, incubation of the TANPs in H_2O_2 resulted in a broadening and a shift of the peak towards bigger sizes. This was visible as of the 5-minute timepoint but was even more prominent at the 60-minute timepoint. Interestingly, this shift affected the entire NP population equally as the entire curve shifted while maintaining its normal distribution. At the 180-minute mark, the

size distribution curve starts to show 2 distinct populations, one main population of higher size around 1000nm and one very small population around 100nm.

The effect of H_2O_2 on the size distribution of the EGNPs and GANPs is similar. Both NPs show relatively similar size distributions around 100nm between the initially sized NPs and the sizes in water at different timepoints. Despite this, a small difference can be identified as the EGNPs seem to experience a slight broadening of the curve whilst the GANPs seem to show a slight narrowing of the curve, especially at 180 minutes. As for the H_2O_2 incubation sample, the size distribution curve split into 2 peaks as of the 5-minute mark, showing 2 distinct NP populations, one around 100nm and one closer to 1000nm. At the 60-minute mark, EGNPs showed more distinct peaks whilst GANPs have more NPs of intermediate size between the 2 main populations. After 180 minutes, the EGNPs' distribution curve shifts back to a normal distribution around 100nm, similar to the size distribution observed in water. In comparison, GANPs seem to have a similar shift of the 1000nm population back towards the original size distribution, but two distinct peaks are still visible.

As for the eNPs, once again the size distribution in water remains relatively constant throughout the duration of the experiment, with a very low intensity second peak visible at 5 minutes. In H_2O_2, although a second population starts forming at the 5-minute mark, it is of very low intensity and aligns with a peak also seen in water at that timepoint. At the 60-minute timepoint, that low intensity broader peak fuses with the main population peak and seems to drift back out slightly at the 180-minute mark. Despite these changes, the intensity of the second population peaks is much smaller for the eNPs than for the higher size peaks seen with the other

NPs. Overall, it is visible that the ROS-scavenger-containing NPs are more impacted by the high ROS environment whilst eNPs are also being affected but to a lower extent.

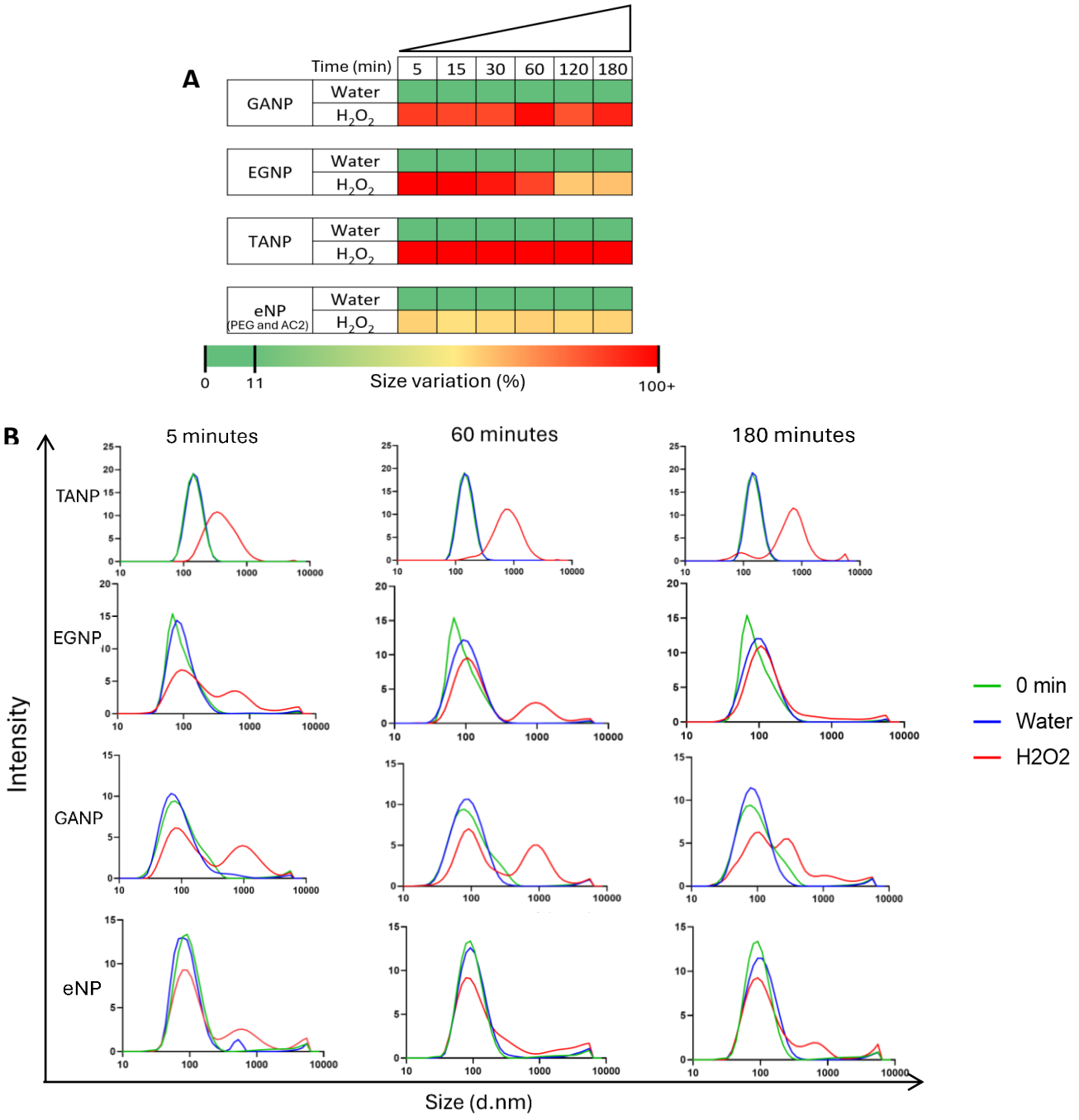

Figure 13. NP ROS-sensitivity in solution. (A) Variation in NP size. Nanoparticles were incubated in either water or 30% H_2O_2 and sized periodically by DLS over the course of 3h. A heatmap of the percentage of size variation is plotted with 0-10% variation considered as no variation (n=3). Data shows that our NP sizes are being affected by ROS and therefore ROS-

sensitivity is observed. (**B) Variation in NP size distribution.** TANP, EGNP, GANP and eNP (eNPs do not contain the ROS-scavenger) NPs' size distributions were assessed by DLS over the course of 3h and shows how the NP population changes during this incubation period, specifically at 5, 60 and 180 minutes. The data is presented as the average of the biological replicates. Results show new NP populations forming throughout ROS incubation, indicating ROS-sensitivity (n=3).

3.9. Assessment of NPs ROS-scavenging potential

The ROS-scavengers and NPs ROS-scavenging potentials were assessed by observing their ability to reduce H_2O_2 levels (Figure 14). The results show a significant decrease in H_2O_2 levels when using each of the 3 ROS-scavengers alone, confirming their abilities as ROS-scavengers. Additionally, TA reduced H_2O_2 levels significantly more than EG and GA. However, no significant difference in H_2O_2 reduction ability is visible when comparing EG to GA (Figure 14 A). As for the NP's H_2O_2 reduction abilities, TANPs showed a significant reduction in H_2O_2, but the reduction wasn't as pronounced as using free TA. Interestingly, eNPs, which lack the ROS-scavenger, showed a slightly significant increase in H_2O_2 levels compared to the untreated H_2O_2 control (Figure 14 B).

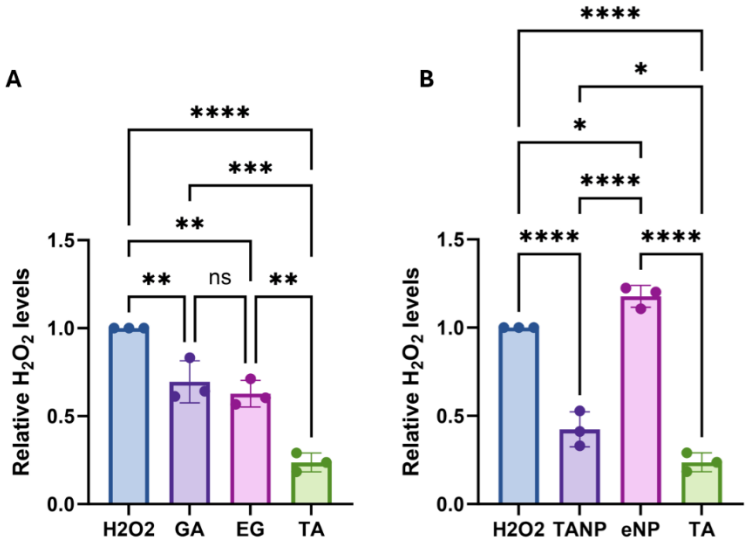

Figure 14. NP potential for ROS-scavenging in solution. (A) ROS-scavenger H_2O_2 reduction potential. The ROS-Glo H_2O_2 assay was used on 100uM of H_2O_2 treated with 100uM of GA, EG or TA ROS-scavengers. Luminescence levels were measured and results were normalized to the H_2O_2 untreated control. **(B) NP ROS-scavenging potential.** ROS-scavenging

potential of 100uM of TANPs and 100uM of eNPs (NPs with no ROS-scavengers) in 100uM of H_2O_2 was assessed using the ROS-Glo H_2O_2 assay and luminescence was measured. Results were normalized to the H_2O_2 untreated control. Luminescence was measured using a plate reader. Results presented are mean +/- SD. (One-way ANOVA, non-significant (ns), *P<0.05, **P<0.01, ***P<0.001, ****P<0.0001, n=3).

3.10. Assessment of NP cytotoxicity

An LDH cytotoxicity assay was conducted on RAW264.7 macrophages undergoing 24h TANP treatments at various concentrations (Figure 15). Results show no significant decrease in cell viability, and thus no cytotoxicity, for TANP treatment concentrations between 1uM and 20uM. At a 100uM concentration, TANPs do seem to show some statistically significant reduction in cell viability compared to the untreated control.

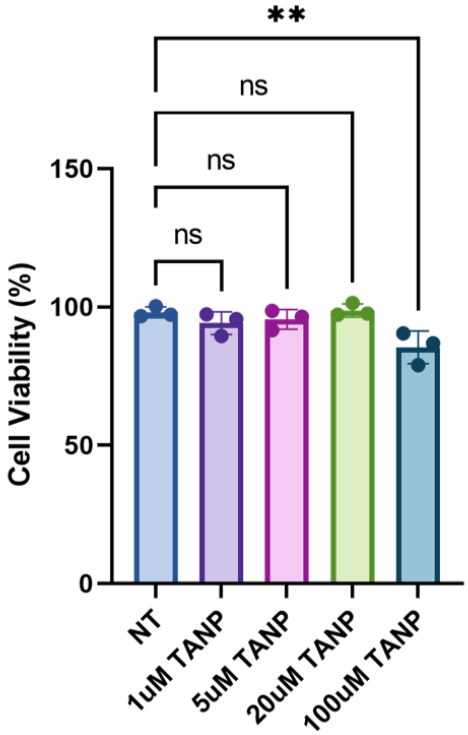

Figure 15. Assessment of NP cytotoxicity. RAW264.7 macrophages were treated with various concentrations of TANPs for 24h and the percentage of cell viability was determined using an LDH assay kit by measuring absorbance by plate reader at 490nm and 680nm to account for background. TANP treatments showed little to no toxicity compared to the untreated cells (NT). Results show mean +/- SD. (One-way ANOVA, non-significant (ns), **P<0.01, n=3).

3.11. NP cellular uptake

The NPs' cellular uptake was assessed notably by flow cytometry. Results showed a much higher cy5.5 signal intensity in the cy5.5-TANP treated cells than in the untreated cells. Another interesting observation is that the signal intensity seems to follow a relatively thin normal distribution curve (Figure 16 A). Additionally, measuring the percentage of cells positive for cy5.5 showed that with nearly 100% of all cells collected had taken up the TANPs (Figure 16 B).

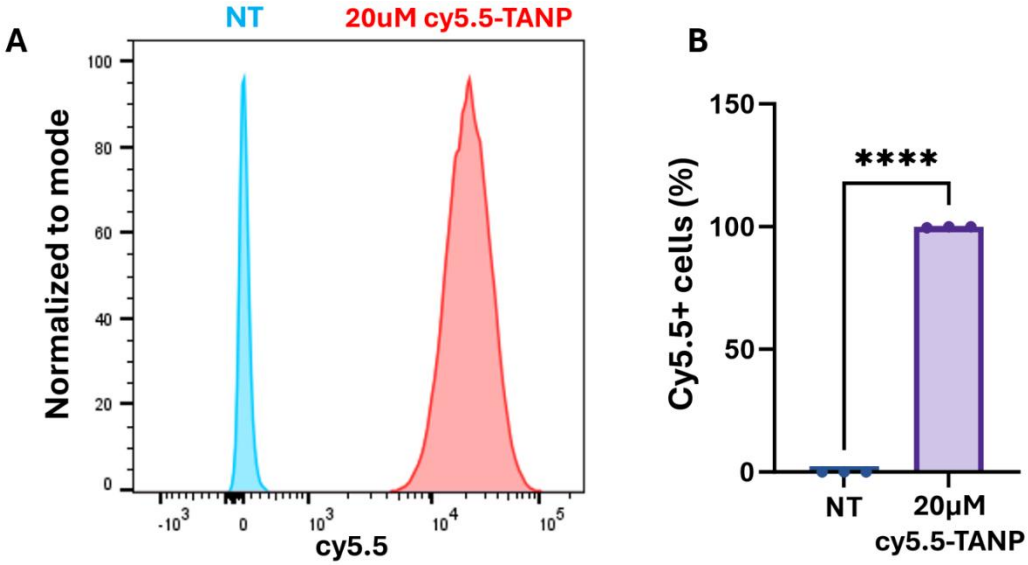

Figure 16. NP cellular uptake via flow cytometry. (A) Cy5.5 signal intensity in NP-treated cells. RAW264.7 cells were treated with 20uM of cy5.5-labelled TANPs for 24h or untreated (NT) as a negative control. Cells were evaluated by flow cytometry and a population of live and single cells was selected and assessed for cy5.5 signal intensity using the APC channel. A representative histogram of the results is shown where a high intensity of cy5.5 signal is observed in NP-treated cells. **(B) Percentage of cy5.5-positive cells.** Gates for the presence and absence of cy5.5 signal were made from the untreated (NT) cells and applied to the NP-treated cells to find the percentage of cy5.5-positive cells. Results show the presence of cy5.5 signal in nearly 100% of treated cells. Results are displayed as mean +/- SD. (Unpaired t-test, ****P<0.0001, n=3).

3.12. Confirmation of NP cellular uptake and mitochondrial targeting

Microscopy studies were conducted to confirm cellular uptake of the NPs (Figure 17). As expected, cy5.5-TANPs were detected within the RAW264.7 macrophages, and their internalization was confirmed using Z-stack imaging. The TANP's ability to reach the mitochondria was also assessed by labelling the cell's mitochondria and observing cy5.5-TANP fluorescence. Results show the mitochondrial labelling signal and the cy5.5 signal overlapping, suggesting localization of the TANPs near the mitochondria (Figure 17 A). A 3D reconstruction of the Z-stack images conducted to better understand the mitochondrial localization also confirmed interactions between the NPs and the mitochondria are occurring (Figure 17 B).

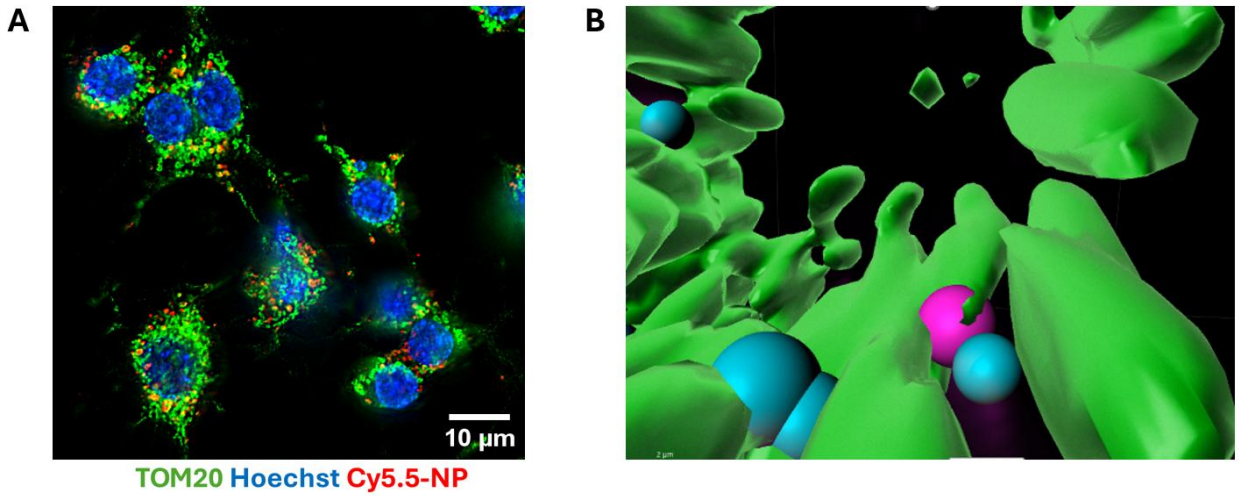

Figure 17. NP cellular uptake and mitochondrial targeting microscopy studies. (A) NP cellular uptake and mitochondria targeting. RAW264.7 cells were treated with 20uM of cy5.5-labelled TANPs for 24h. Cells were fixed and stained with TOM20 (green) for mitochondrial labelling and Hoechst (blue) for nucleus staining. Cells were observed using the Leica Thunder Imager and Z-stack images were obtained showing the NPs within the cells and NP signal overlapping with mitochondria labelling (n=2, one representative image shown). **(B) 3D reconstruction of NP-mitochondria interactions.** 3D reconstruction using Z-stack images enabled better visualization of the NP's mitochondria-targeting abilities (in green the mitochondria, in pink NPs considered to be interacting with the mitochondria and in blue NPs considered not to be interacting with the mitochondria based off their distance from the mitochondria) (n=1).

3.13. Assessment of NP ROS-reduction in vitro

Observing the reduction of lipopolysaccharide (LPS)-induced ROS levels in RAW264.7 macrophages allows for the verification of our NP's ROS-scavenging properties in vitro. Results show a shift towards a lower DCF fluorescence intensity, and thus lower ROS, in LPS-induced NP treated cells than LPS-induced untreated cells (Figure 18 A). When more specifically looking at the fold change in geometric mean intensity, we can see that LPS induced a very significant increase in ROS levels, and that TANP treatments at 1uM and 5uM showed a significant reduction in these levels. Although the 20uM treatment of TANPs' ROS-reduction isn't significant, most datapoints are in the same range as the 1uM and 5uM TANP results, and thus there still seems to be a trend towards a reduction at that concentration which may eventually reveal significance if more replicates are performed. Despite this, according to the fold change in geometric mean intensity observed, increasing TANP treatment concentration does not result in a greater decrease in ROS levels (Figure 18 B).

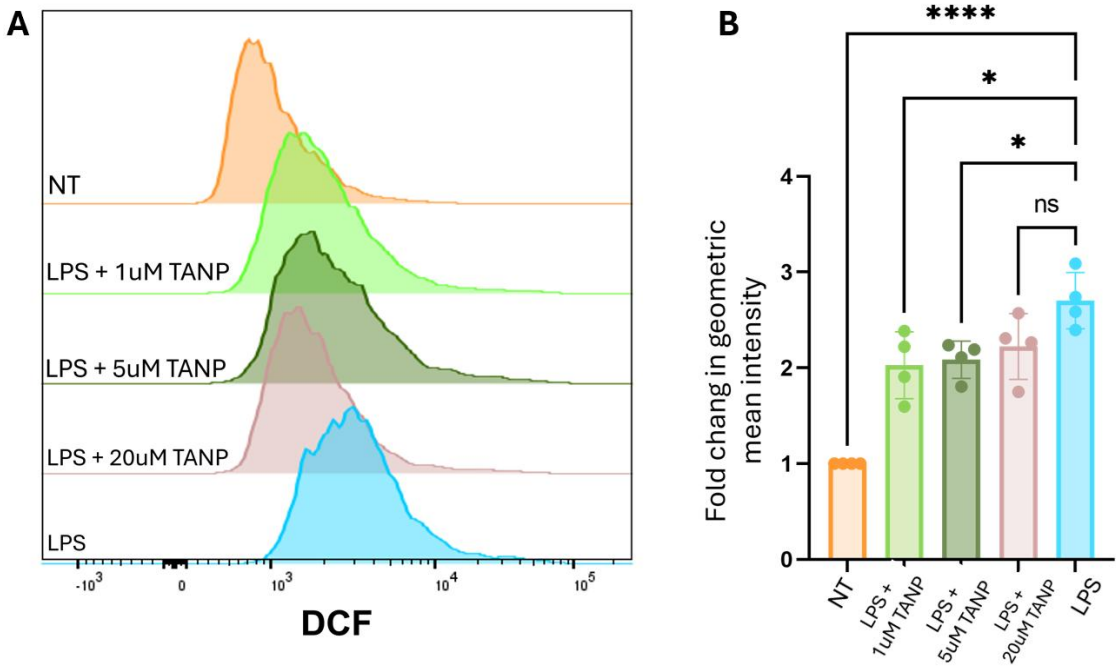

Figure 18. NP ROS-reduction potential in vitro. (A) Variation in DCF signal intensity. RAW264.7 cells were pre-treated with various concentrations of TANPs for 24h and subsequently treated with 1ug/ml LPS for 6h whereas the NT control remained untreated. A

DCFH-DA assay was performed to measure ROS levels in the cells and cells were assessed by flow cytometry. A representative histogram of the results obtained using the FITC channel is shown, showing DCF reduction with NP treatment**. (B) Fold change of DCF geometric mean intensity.** The geometric mean intensity of DCF signal was normalized to the untreated sample to plot the fold change in DCF level, showing a reduction in ROS levels with NP treatment. Results are displayed as mean +/- SD. (n=4, one-way ANOVA, *P<0.05, ****P<0.0001).

3.14. Assessment of NP inflammation reduction in vitro

TANPs and EGNPs were evaluated for their inflammation reduction potential by looking at their effect on pro-inflammatory and anti-inflammatory markers (Figure 19). Treatment of RAW264.7 cells with LPS resulted in a significant increase of TNF-α and ABCA1 levels. When treated with LPS and 1uM of TANPs, results showed a significant reduction of TNF-α levels. As for treatments using 20uM of EGNPs, no significant reduction of TNF-α was observed although some datapoints do show a reduction. As for ABCA1, there seems to be a trend towards its increase in cells treated with LPS and 1uM of TANPs, although the increase is non-significant.

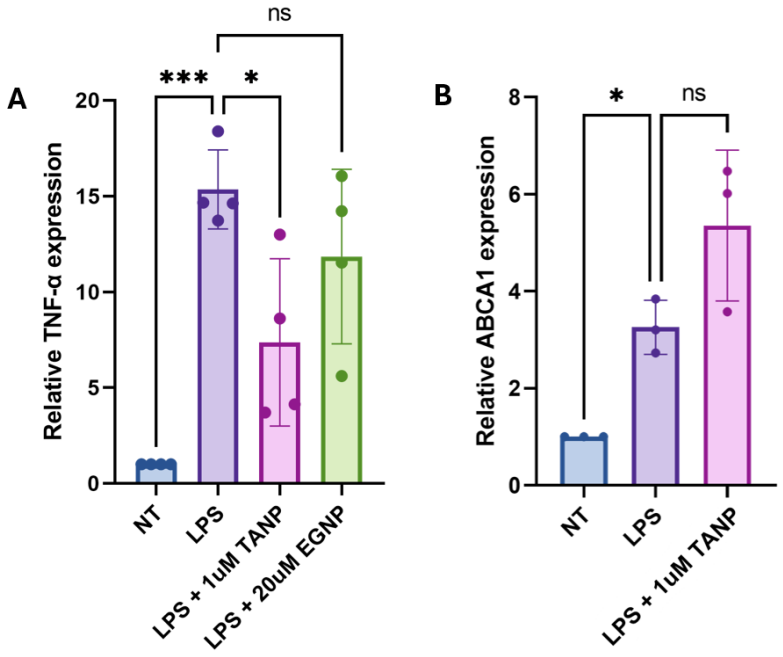

Figure 19. NP anti-inflammatory properties in vitro. (A) Effect of NPs on pro-inflammatory marker TNF-α. RAW264.7 macrophages were pre-treated with 1uM of TANPs or 20uM of EGNPs for 24h followed by a 5h 100ng/ml LPS treatment. Pro-inflammatory cytokine TNF-α levels were measured by RT-qPCR and showed trends towards a reduction of

inflammation. **(B) Effect of TANPs on anti-inflammatory marker ABCA1.** RAW264.7 cells pre-treated with 1uM of TANPs for 24h and treated with 100ng/ml of LPS for 5h. RT-qPCR enabled measurement of ABCA1 anti-inflammatory marker levels, showing trends towards an increase in ABCA1 levels with NP treatment. Results are displayed as mean +/- SD, with NT identifying untreated samples and LPS identifying cells treated with LPS but no NPs. ((A) n=4, (B) n=3, One-way ANOVA, non-significant (ns), *P<0.05, ***P<0.001).

4. Discussion

4.1. Biomaterial library synthesis

A library of various biomaterials was developed to have a set of potential candidates for the formation of the ROS-sensitive and ROS-scavenging NP systems. As boronic acid functional groups possess the ability to form ROS-sensitive bonds with ROS-scavengers, it was necessary to develop biomaterials possessing such groups. Additionally, as the main site of ROS production is the mitochondria, adding a mitochondrial targeting aspect to the system could further its potential. Thus, a mitochondria targeting PLGA-PEG surface molecule was also synthesized. Each of the polymers discussed below were synthesized and characterized by ^{1}H NMR to confirm obtention of the product. In each case, the significant peaks are present, attesting to successful synthesis.

Numerous characteristics of the biomaterials play a part in the formation of NP systems. Considerations such as the PLGA-PEG content and length, the amount of boronic acid functional groups, the other free functional groups on the polymer, and the polymer's physiochemical properties such as its molecular weight and polarity all play a part on how the NP system forms. Consequently, they affect NP properties such as size, surface charge and stability. Thus, having a library of biomaterials with varying properties allows for greater optimization potential. The main biomaterials of interest as polymeric backbones are the AC2 and AC5 polymers. AC2 was made from a maleic anhydride polymer whereas AC5 was made from a PEG-macroCTA

polymer. Thus, despite both containing repeating boronic acid units, they have different structures and physiochemical properties.

During the synthesis of the AC2 polymer, the maleic anhydride groups were opened via a spontaneous ring-opening reaction which, in addition to conjugating the boronic acid to the polymer, generates carboxylic acid functional groups (Figure 4). The carboxylic acid functional group is very hydrophilic and thus depending on the amount of groups present, they can influence the AC2 polymer's hydrophilicity and polarity[84]. Additionally, these functional groups are easily reacted with other compounds thus allowing for the potential conjugation of other molecules or even therapeutic drugs to the system[85]. In contrast, the AC5 polymer was synthesized by initially conjugating epoxy ring groups to a PEG-macroCTA polymer via a RAFT polymerization reaction (Figure 5). Subsequently, an epoxy ring-opening reaction was performed to conjugate the boronic acid functional groups to the polymer. AC5's particularity is it's PEG moiety which is already integrated in the polymer, eliminating the need for the addition of PLGA-PEG to the system.

In both systems, the amount of boronic acid groups added on the polymer can be controlled which gives more control over the polymer' ROS-mediated properties. However, the NP assembly process differs for each polymer. Indeed, AC5 simplifies the NP assembly process as PEG is already bound to the polymer and thus PLGA-PEG must not be added to the system. However this isn't the case for AC2 NPs. By having fewer materials and steps involved in their assembly, AC5 NPs may be advantaged in terms of reproducibility as there are fewer opportunities for variability. However, the presence of PEG on the polymer forces a certain PEG to boronic acid ratio which may affect the NPs stability. Indeed, there may be too little PEG available to stabilize the system, or too much PEG present which may destabilize the system.

Additionally, adding PEG separately makes it easier to change which PEG length and how much PEG is used to form NPs during NP optimization. The same is true for the incorporation of TPP to the system which is affected by the differences in biomaterial interactions and system configuration.

As for the synthesis of the PLGA-PEG-TPP targeting molecule, it was obtained following subsequent esterification reactions (Figure 6). The compound's properties will allow anchoring of the TPP molecule to the NP's surface, thus enabling mitochondrial targeting. Having a distinct targeting polymer allows more freedom in modifying the ratios with other surface molecules. Notably, using it in conjunction with the PLGA-PEG-OMe polymer enables optimization of the TPP content to ensure it is sufficient to direct NPs to the mitochondria but not excessive in a way that negatively affects surface charge and stability.

4.2. Monitoring of TA fluorescence for confirmation of boronic ester bond formation

As a crucial actor in the intended function of the NP system, the ROS-sensitive boronic ester bond's formation between the ROS-scavenger and AC2 polymer must be assessed. This was initially done via a fluorescence assay (Figure 7). According to their chemical structure, compounds may possess a variety of properties, including the potential for fluorescence. Fluorescence occurs when these compounds are excited at a particular wavelength. The photons absorbed prompt electrons to reach a higher energy state. As these excited electrons come back down to their ground state, they emit a photon of lower energy which can be detected as fluorescence.

Polyphenols have aromatic structures which favor fluorescence properties. In the case of TA, although it is a polyphenol, it's structure may permit the formation of intermolecular and intramolecular hydrogen bonding which can result in fluorescence quenching[83]. Thus, TA itself

shows low fluorescence intensity. However, bond formation between TA and other compounds may be able to change these interactions in a way that increases fluorescence[36]. Indeed, the formation of boronic ester bonds, which can occur between TA's hydroxyphenol moieties and the boronic acid functional groups of the AC2 polymer, may be sufficient to increase TA's fluorescence.

Thus, TA and AC2 were incubated together, and the resulting fluorescence intensity was measured using a spectrophotometer. As we increase the amount of AC2 polymer in solution, the potential for bond formation with TA increases as well. Literature shows that when excited at 380nm, TA possesses a fluorescence peak around 435nm and thus we chose the region between 430nm and 470nm as our main emission wavelength region of interest[86].

As expected, the more AC2 was added to the TA solution, the higher was the fluorescence intensity observed between 430nm and 470nm, with its peak being at 436nm. We can confirm this increase in fluorescence isn't due to the increase in AC2 as assessing the fluorescence intensity of 500ug of AC2 alone shows no fluorescence. At 100ug of AC2 in TA, no increase in fluorescence was observed which may be explained by the small amount of bonds formed and the sensitivity limits of the spectrophotometer. However, at 200ug, the increase in fluorescence intensity became much more noticeable, indicating that a significant amount of bonds were forming. The fluorescence intensity increased again at 300ug of AC2 but the subsequent AC2 additions resulted in lower increases. This may be the result of a saturation of the TA hydroxyphenol groups; most TA groups may already be involved in boronic ester bonds. The additional AC2 added may force some of the few remaining groups to react, explaining the noticeable but faint fluorescence increase (Figure 7A).

To ensure the fluorescence increase is due to the boronic ester bond formation, controls such as the maleic anhydride polymer (Mal) and DMSO were used. Mal is a precursor to the AC2 synthesis and thus has a similar structure. However, it lacks the boronic acid functional group and thus possesses no boronic ester bond formation potential. Similarly, DMSO is the solvent used for the fluorescence assays and thus should not affect TA fluorescence. Both Mal and DMSO alone show no fluorescence and thus we can determine that any variation in fluorescence resulting from their incubation with TA is due to TA. When incubating Mal or DMSO with TA, both solutions show a slight increase in fluorescence to 20a.u. indicating that both affect TA's fluorescence in the same manner. This may be explained by the variation in TA concentration as the volume of both Mal and DMSO added is the same, thus diluting TA to the same concentration and increasing its fluorescence. Indeed, a study monitoring the fluorescence of riboflavin shows an inverse relation between TA concentrations and riboflavin fluorescence[83]. Due to their aromatic rings, both structures can participate in π-π interactions as well as partake in hydrogen bonding thanks to their hydroxyl groups. These interactions can cause fluorescence quenching. Thus, it could be possible to see a similar phenomenon occur when looking at TA fluorescence itself as TA molecules can undergo the same interactions between each other. This also justifies why the TA alone control shows no fluorescence (Figure 7A). However, incubating TA with the same volume of AC2 results in a much higher fluorescence intensity. Thus, in this case, the resulting fluorescence is due to more than just the effect on TA concentration; the compounds are interacting, likely via boronic ester bond formation (Figure 7 B).

When looking specifically at the 436nm emission, the difference in AC2-TA and Mal-TA or DMSO-TA interactions is even more noticeable as we can clearly see that TA only shows a sustained increase in fluorescence with increased AC2 and not with the controls. The slight

increase in fluorescence at 200ug (400ul) of Mal and 400ul DMSO can be explained by the change in TA concentration which also applies to the AC2 sample yet AC2 still shows more fluorescence as boronic ester bonds are contributing to the fluorescence intensity. Although TA is more diluted as Mal and DMSO levels keep increasing, the TA fluorescence is stable near 20 a.u. which may simply mean that the interactions between the TA molecules are negligeable as of the addition of 400ul and thus don't change with the additional volume added (Figure 7C).

Overall, these results clearly show the impact of the boronic acid functional group in TA's fluorescence intensity and thus the interaction between the molecules. This supports our claim that boronic ester bonds are forming between TA and AC2. By this proof-of-concept experiment, we indirectly show that both GA and EG should behave similarly with boronic acid functional groups as they possess the same hydroxyphenol groups as TA. Thus, all ROS-scavengers of the project should form boronic ester bonds when combined with boronic acid polymers such as AC2.

4.3. Confirmation of boronic ester bond formation and its ROS-sensitivity by ^{1}H NMR

^{1}H NMRs were done for GA and diBA to better observe structural changes indicative of boronic ester bond formation (Figure 8). GA alone and diBA alone's ^{1}H NMRs were done as reference spectra to which we can compare the bound compounds spectrum (1:5 diBA:GA). When both compounds are placed together, their interaction will lead to peak shifts. The most striking indication of bond formation is the novel doublet of doublet appearing at δ 7.38ppm and δ 7.64ppm. Doublets of doublets are characteristic peaks of non-symmetrical aromatic cycles. Thus, these peaks show that the compounds are interacting in a way that disrupts the symmetricity of their aromatic cycle, likely via bond formation. In addition, the broadening of the (a) peak coincides with an increase in intensity for the (c) and (d) peaks. As all these peaks

belong to GA and the diBA:GA ratio favours a higher content of GA in solution, the increase in peak intensity could simply be explained by the higher GA concentration.

When H_2O_2 is added to the sample, the doublet of doublet is no longer visible, indicative of restoration of the aromatic cycle's symmetricities, and thus breakage of the boronic ester bond formed between the molecules. As H_2O_2 contains hydrogens, it can not only be picked up by the ^{1}H NMR but it may also interact via hydrogen bonding with the other compounds in solution, which can explain the multiple peak variations observed in this spectrum[87]. Thus, results show formation of ROS-sensitive boronic ester bonds between the boronic acid functional group and hydroxyphenol group on the ROS-scavenger. This data played a significant part in ensuring the NP system would form as designed and present the intended ROS-sensitivity properties. Thanks to these findings, we were able to proceed with the project by starting the NP assembly and optimization process.

4.4. Optimization of NP formulations

The importance of optimizing properties such as NP size includes reasons such as better systemic circulation, increased NP cellular uptake and decreased cellular toxicity. As for PDI, which is a measure for the variation in the NP population, its importance comes from the need for a homogenous NP population. Indeed, it is important to ensure all the NPs synthesized have similar characteristics to ensure they all behave the same way. This enables NP treatments to be more efficient as all NPs will contribute equally to the intended outcome, thus leading to more reproducibility in NP assembly and more control on treatment outcome.

The NP system forms thanks to interactions between the polymer and the hydroxyphenol moieties on the ROS-scavengers. Thus, as the different ROS-scavengers used have a different potential for bond formation, they may interact differently with the polymer and cause the other

components of the system to interact differently with the polymer as well. In addition, the ROS-scavengers' varying sizes and molecular weight can also influence the NPs structure and requires the consideration of concepts such as steric hindrance. In summary, different ROS-scavengers have different properties which can impact NP size and PDI.

In the optimization step of the project, NPs were made with varying amounts of each ROS-scavengers to assess how exactly ROS-scavengers influence NP size and PDI as well as to find optimal formulations in terms of these properties (Figure 9). To account for the varying sizes and bond formation potential of the ROS-scavengers, the experiment was done with higher amounts of the smaller ROS-scavengers (GA and EG) and smaller amounts of the bigger ROS-scavenger (TA). With increasing ROS-scavenger content, the smaller scavengers show a reduction of NP size. This may be justified by looking at the polymer to ROS-scavenger ratio. With less ROS-scavengers present, too few polymeric boronic acid groups may be binding to the ROS-scavenger, making the system harder to stabilize. This may cause NPs to contain more polymers and surface molecules for stability purposes which may yield bigger sizes. Thus, by increasing the amount of ROS-scavenger present, more boronic acid groups may bind to the scavengers, leading to the formation of more stable systems with a lower polymer to scavenger ratio. In addition, due to their small structure, the ROS-scavengers may be subject to less steric hindrance within the NP structure and be able to compact better, yielding smaller NP sizes.

However, in the case of TA, its much bigger and star-like structure might make it more likely to bind boronic acid groups on different polymer molecules rather than multiple groups on the same polymer molecule. By this logic, increasing the amount of TA would increase the quantity of polymers in the NP, in turn increasing NP size. Another explanation could be the steric hindrance generated by the TA molecules which can limit how small the NPs can be and can

explain why at quantities as small as 50nmol of TA, NP sizes are still bigger than 200nmol of the smaller scavengers. The potential effect of the ROS-scavenger's size and properties on NP assembly is even more noticeable when comparing the size of NPs made with the same amount of ROS-scavenger. GA and EG have a similar and much smaller NP size at 200nmol than TA.

As for the PDI, it stays relatively the same no matter the formulations and ROS-scavengers used, showing that no matter the amount or size of the scavenger, the NPs formed vary in size to the same extent. Although it may seem like the PDI slightly increases with the increase in ROS-scavenger for GA and TA, this could be explained by the fact that with more ROS-scavengers present, a higher variation in ROS-scavenger content of the system is possible. Thus, this may lead to a slight increase in the variation of the NP sizes within the solution.

As a result of this experiment, we have found that all formulations assessed fit within the 50nm-200nm size and ≤ 0.3 PDI ranges established, thus ensuring NPs would have optimal translational potential. In addition, the experiment led to choosing the 200nmol TANPs, 400nmol EGNPs and 1000nmol GANPs as the formulations of interest for further assessments. These were chosen as they had good properties but particularly because they possess the highest amount of ROS-scavenger and thus likely had the highest ROS-reduction potential.

4.5. Physical characterization of the selected NP formulations

When comparing specifically the formulations of interest, other aspects can be investigated such as the effect of the addition or not of the TPP targeting molecules (Figure 10). As both NPs for one ROS-scavenger with and without TPP otherwise have the exact same formulation, the significant difference in size observed for each pair is likely due to the addition of the TPP compound. Indeed, the higher sizes observed for the TPP containing NPs (TANP, EGNP and GANP) may be indicative of the successful incorporation of TPP to the system. This possible

explanation becomes increasingly plausible when considering the relatively high molecular weight and bulky structure of TPP. These attributes lead TPP to take up more space on the NP surface and have a higher potential for steric hindrance.

When comparing the formulations on the base of their ROS-scavenger, the non-targeted NPs show no significant variation in size, which can notably be due to the previous optimization experiment performed. Indeed, that experiment allowed us to alter the ROS-scavenger content of the different NPs to reduce differences and obtain similar suitable sizes for the different formulations. However, when adding TPP to the system, a significative difference emerges for the TANPs with the other systems, but not between EGNPs and GANPs. This can be explained by the different polymer to ROS-scavenger interactions enabled by the different scavengers. Indeed, because of their different interactions with the polymer, ROS-scavengers can also influence how many surface molecules are needed to stabilize the system, and how much of these can be the TPP-containing PLGA-PEG molecule (PLGA-PEG-TPP) or the non TPP-containing PLGA-PEG molecule (PLGA-PEG-OMe). Thus, with this in mind, it is logical that TANPs, as the sole NPs containing a much bigger scavenger, are the only ones displaying a significance in size difference with the GANPs and EGNPs.

As for the PDI, there are no significant differences in PDI values between the different NP formulations (Figure 10 B). This can also be seen by the size distribution data which follows a normal distribution (Figure 10 C). This indicates that the NP populations have the same magnitude of size variation independent of their formulation differences. This is advantageous as any variations in treatment outcome that could be due to the variation of the NP population will be the same for each formulation. The size distribution also allows us to see that the increase in size observed following the incorporation of TPP is applied to the whole population, thus

suggesting that all the targeting NPs synthesized do possess the TPP rather than only a subpopulation having incorporated it.

Additionally, the uniformity of the NPs suggested by the PDI and size distribution data was also visible by TEM (Figure 11). TEM analysis allowed confirmation that the NPs all had a similar spherical shape. This can be attributed to the different hydrophobic and hydrophilic interactions between the components of the NP system which better shield hydrophobic moieties from water when NPs adopt a spherical shape. The darker outer ring marks a more highly stained portion of the NPs, which may be attributed to the different composition of the NP's surface relative to its core.

4.6. Stability of NPs for storage and biological conditions

As for their stability, all systems were shown to be stable for up to 1 week of storage at 4°C, with variations in size below 10% (Figure 12). Indeed, a 10% variation on our NP sizes is considered negligeable as it corresponds to ~ 5-10nm size differences. These differences fit within the variations often observed for technical replicates when sizing a same NP sample and were thus determined as being negligeable.

In biological conditions, the systems still seem to be relatively stable for 24h with variations near the 10% negligeable threshold for most formulations. At the 48h timepoint, there seems to be an increase in size variation for many formulations (including TANP, EGNP and EGNPome) reaching about 10-40% (Figure 12). This slight increase visible can be attributed to several factors. Firstly, a longer incubation time increases the potential for detrimental interactions such as formation of a protein corona or NP aggregation. Additionally, the system created is ROS-sensitive and thus incubating it in biological conditions where ROS may be present even in small amounts, such as serum, can affect the system over time, explaining what is being observed[42].

Despite this, NPs may not need 48h of biological stability before being taken up by cells and producing their desired effect, especially as they can be administered via different routes to facilitate cellular uptake. For example, our project has shown successful NP uptake after a 24h treatment in vitro. Thus, if a local delivery was chosen, the NPs would be stable long enough in biological conditions to allow for their successful uptake and effect.

Interestingly, one formulation stands out from the rest with a variation in size of over 100% at both timepoints. Although the data shows this has been observed in 2 replicates, the third biological replicate shows a percentage of size variation much closer to those obtained for the other systems. The higher percentages of size variation may be due to a too low NP concentration resulting in the measurement of the FBS proteins in solution rather than the NPs themselves, or they may simply be other artifacts. Thus, it would be pertinent to repeat the assay in order to better understand what is being observed. In addition, looking at the size distribution of the NP population throughout the assay would also provide beneficial information. Size distribution data would allow us to know if there might be very big outlier particles in solution, such as FBS proteins, pulling up the NP average size and affecting the data obtained.

Lastly, it is important to note that although NP stability in biological settings ensures they carry out their intended effects, NPs are formulated with their degradation and the degradation of their components in mind. Indeed, this is necessary in order to prevent their accumulation and consequent detrimental effects. To this end, many NPs, including ours, contain biodegradable polymers as part of their formulation. Thus, the equilibrium between NP stability and degradation is one which must be carefully thought out.

4.7. Assessment of NP ROS-sensitivity potential

When incubating the NPs in water, their lack of size variation is indicative of their structural stability, which is logical as the NPs were assembled in water. However, in H_2O_2, the high variation in size displayed suggests structural changes induced by H_2O_2 are occurring. Thus, we believe these results to be indicative of ROS-sensitivity (Figure 13).

Indeed, when in presence of ROS, for example H_2O_2 as used here, the boronic ester bond formed between the hydroxyphenol groups of the ROS-scavenger and the boronic acid group on the AC2 polymer may be oxidized thus releasing a hydroxylated polymer moiety[88]. Following subsequent hydrolysis, the ROS-scavenger regains its initial structure and is freed from the system (Figure 20). This bond breakage will likely lead to a disassembly of the NP system as the ROS-scavenger is responsible for holding together the polymer molecules; without it, the polymers disperse, and the NP system is no longer present. This mechanism can justify the high variation in size observed for the NPs in H_2O_2.

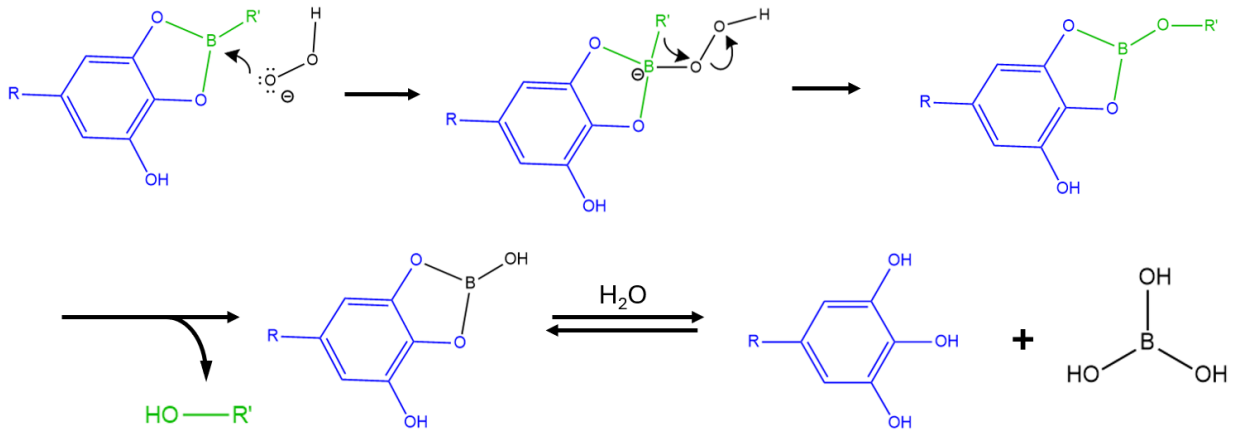

Figure 20. Possible mechanism for the H_2O_2-induced breakage of the ROS-sensitive bond. An arylboronic pinacol ester structure forms between the ROS-scavenger (blue) and AC2 polymer (green) which can be attacked by the electrons of H_2O_2. This leads to the oxidation of the bond, the hydroxylation of the AC2 polymer and the temporary formation of a pinacol borate[88]. This structure may then undergo a hydrolysis step, enabling the release of the ROS-

scavenger and of a non-toxic boric acid moiety[89]. Mechanism adapted from published literature[89,90].

As the different ROS-scavengers have different amounts of hydroxyphenol groups (Figure 3), they have the potential to form a different amount of ROS-sensitive bonds. Because of this, the rate of NP disassembly, H_2O_2 concentration required for disassembly and the level of disassembly can vary from one NP system to another depending on the ROS-scavenger used. The main differences observed indeed coincide with the variations in ROS-scavenger content. When looking at NP size distribution, the TANPs are the only NP system that exhibit a shift of the entire population following incubation in H_2O_2 (Figure 13 B). Indeed, at the 5- and 60-minute timepoints, the entire population peak shifts toward higher sizes whilst maintaining its normal distribution.

One possible explanation can pertain to the higher amount of AC2 binding sites on TA. Indeed, as more binding sites are involved in holding the system together, TA may play an important role in stabilizing and maintaining the system together. In contrast, smaller ROS-scavengers may not be as efficient at holding together the polymers due to their fewer binding sites, and thus the system may be arranged differently to favor stability despite this, for example by involving a different amount of surface molecules in each NP. Thus, the breaking of the ROS-sensitive bonds in TANPs could have a greater destabilizing effect than in the other NP systems, explaining the big peak shift observed.

The observation may also be explained by a previous hypothesis on the correlation between the increase in TA content and NP size. In this case, the increase in size was suggested to be linked to TA's structure favorizing binding with various polymer molecules rather than multiple

sites on the same polymer. By this logic, each polymer molecule is retained to the NP by fewer bonds than when smaller scavengers are used. Thus, fewer bonds must break to cause the loss of polymer from the system. Therefore, the resulting variation in size occurs faster and at a higher magnitude for TA than GA and EG. In comparison, the GANPs and EGNPs show similar trends as for both, a division of the NP population into 2 distinct population peaks is observed as of the 5-minute mark. As seen with TA, a trend towards an increase in size is observed with H_2O_2 incubation. Not seeing a shift of the entire population is likely an effect of the ROS-scavenger size which affects the system's ROS-sensitivity and may give systems with smaller ROS-scavengers less ROS-sensitivity. It would be interesting to further push the experiments to see the effect of using the same amount of ROS-scavenger in the different NP systems for this assay to have a better idea of the true reason behind this different behavior.

At the 180-minute timepoint, although the majority of the TANP population is still at a higher size range, a small proportion of the NPs appear at a peak similar in size to the initial population, which may be indicative of the NP's components in solution trying to reacquire a stable state or reassembling due to precipitation of the components over the incubation period. This is a constant observed in all scavenger-containing NPs at the 180-minute timepoint, which is logical as systems in solution usually adopt configurations to accommodate their properties and optimize their stability.

Lastly, it seems that eNPs are slightly being affected by the H_2O_2 in solution despite not containing any ROS-scavengers. This may be explained by the presence of the AC2 polymer in the system which contains the boronic acid functional group. This functional group may be able to interact in a certain way with the H_2O_2 leading to a reconfiguration of the NP system. Despite the slight variation in size and size distribution observed, the effects are much less significant

than with the scavenger-containing NPs, indicating that ROS-scavengers play an important role in the size variations observed. It would nonetheless be interesting to further explore what is being observed for the eNPs and whether this is observed without the presence of the AC2 polymer in the system. These results obtained allowed us to confirm the ROS-responsiveness of the system and to envision its use in in vitro settings.

4.8. Assessment of NP ROS-scavenging potential

As the NPs were designed as ROS-reducing drug delivery vehicles, assessing their ROS-reducing capacities is important to confirm our system has the desired effect (Figure 14). As highlighted previously, ROS can break the boronic ester bonds formed which causes the complete disassembly of the system and the release of the ROS-scavenger. To first validate our ROS-scavenger's ability to scavenge ROS, we assessed the free ROS-scavengers for H_2O_2 reduction potential (Figure 14 A). Interestingly, the level of ROS-reduction observed coincides with the size of the ROS-scavengers and their amount of available hydroxyphenol groups for ROS-scavenging.

This is logical as the hydroxyphenol groups are responsible for the ROS-scavenging. Indeed, these types of functional groups, where hydroxyl groups are bound to an aromatic cycle, confer to these molecules their antioxidant properties. Thanks to their structure, such molecules can neutralize free radicals such as ROS by donating an electron or a hydrogen atom thus stabilizing the free radical's unpaired electron by resonance (Figure 21)[35,71].

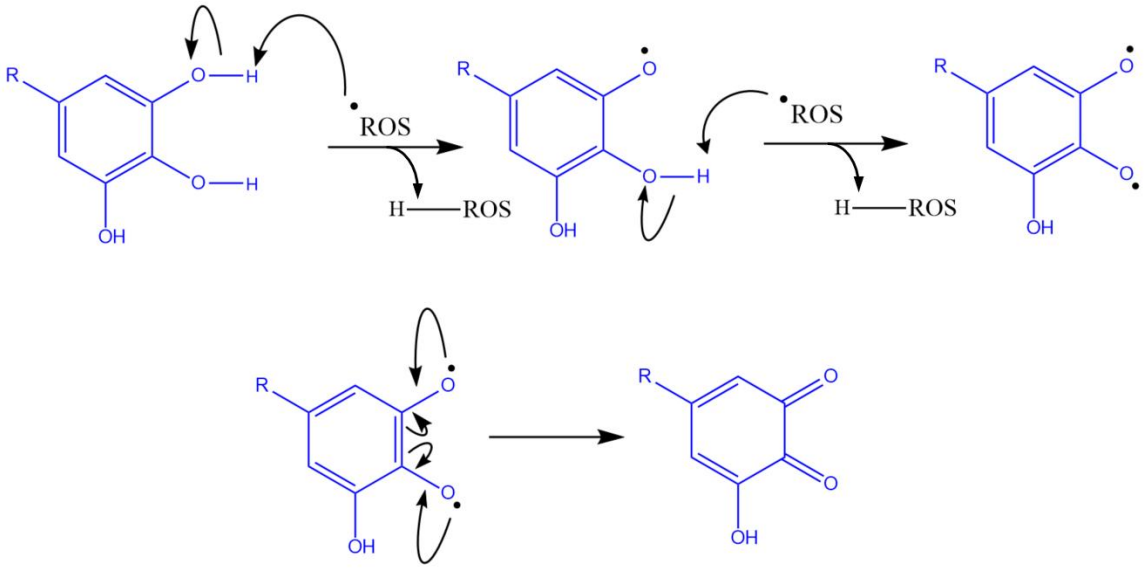

Figure 21. ROS-scavenging mechanism. The unpaired electron in free radicals (such as in many ROS) can be stabilized by hydroxyphenol (or catechol) groups (blue) thanks to their structure and resonance abilities[91]. In exchange, the ROS can receive a hydrogen atom. Having now lost its free electron, the ROS is no longer able to cause oxidative damage to macromolecules. Mechanism adapted from published literature[91].

Thus, by having a single galloyl hydroxyphenol moiety, GA showed the least amount of ROS-scavenging amongst the ROS-scavengers assessed. In comparison, EG has 3 ROS-scavenging hydroxyphenol groups and showed a slightly higher ROS-reduction than GA, although the difference observed is not statistically significant.

The small difference is logical as from EG's 3 hydroxyphenol groups, one is a galloyl and another a pyrogallol group where the hydroxyls are placed at the ortho and meta positions on the benzene[92,93]. EG's 3rd hydroxyphenol group resemble more a resorcinol group with hydroxyls at the meta position only[94]. A 2006 study, highlighted the effect of the positioning of hydroxyl groups on benzene rings on a compound's ROS-scavenging potential. This study found that hydroxyls at the para and ortho positions have a lower bond dissociation enthalpy and therefore

serve as better ROS-scavengers[94]. Therefore, EG's 3rd hydroxyphenol group doesn't contribute as much to reducing ROS levels as its only hydroxyl groups are in the meta position. This means there is no big difference between GA and EG in terms of their structural potential to scavenge ROS as EG only has one more galloyl group than GA. This explains the absence of significant difference in their reduction of H_2O_2 levels. As for TA, it has a significantly larger structure comprised of 10 galloyl groups, and can thus scavenge much more ROS, as shown in the data obtained where TA achieved by far the greatest decrease in H_2O_2 levels.

When looking at our NP's ROS-reduction abilities, we can see that our NPs do indeed significantly reduce ROS levels in solution (Figure 14 B). Interestingly, despite using the same concentration for the free TA and the TANPs, free TA seemed to reduce H_2O_2 levels to a greater extent than TANPs. Many reasons may explain this. Firstly, when making our NPs, considering TA is water-soluble, it is possible that not all of the TA added in the formulation is being used as part of the NP system. When calculating the concentration of TANPs, we assume all of the TA makes its way in the NPs but in reality any unused TA is lost during NP concentration. Thus, although we are treating with what should be 100uM of TANPs (which is 100uM of TA in the TANPs), this might not be the exact concentration used. Another explanation could be the ROS-sensitivity aspect of the system. As the system must be activated by high ROS levels to reduce them, the ROS-scavenging achieved by some NPs might prevent the activation of the other NPs in solution, thus hindering the TA's ROS-scavenging abilities. Lastly, the difference may just be due to a timing aspect. As the TANPs must first be activated to release the TA in solution, it may take more time before the TA from the NPs can start scavenging compared to free TA. Despite these considerations, the TANPs remain very efficient at H_2O_2 reduction.

Another interesting aspect of the data is the slight ROS increase observed when using the eNP control. As NPs that do not contain any ROS-scavengers, the eNPs should not be able to reduce ROS levels, which is what is observed. Despite that, it is interesting that the data rather suggests an increase in H_2O_2 levels. The eNPs do contain the AC2 polymer and its boronic acid functional groups. It may thus be possible that these free boronic acid groups interact with H_2O_2 in a certain way that slows down its degradation, resulting in higher H_2O_2 levels for the eNP-treated solution. This hypothesis aligns with the one proposed earlier to justify the small variation in eNP size during H_2O_2 incubation. Despite this theory, additional testing would have to be conducted to fully understand what is being observed.

4.9. NP cellular uptake and mitochondrial localization

RAW264.7 macrophages showed a high percentage of NP uptake with nearly 100% of all cells being positive for the NPs (Figure 16). Additionally, the high cy5.5 signal shows that many NPs made their way into the cells. Furthermore, the relatively thin normal distribution curve for the cy5.5 signal intensity indicates that the cells all uptake a similar number of NPs. Such consistency in NP uptake can suggest that the rate of NP uptake is the same for the whole cell population as the amount of NPs in the cells is the same at the given timepoint assessed. Additionally, consistency in NP uptake suggests that all the cells receiving the same treatment will be subject to the same magnitude of therapeutic effect from the NPs, helping obtain better consistency in both experimental results and in the outcome of their use as CID treatments.

As discussed previously, parameters of both the cell and the NPs are involved in successful NP cellular uptake. As professional phagocytic cells, it is not surprising to see such a high percentage of macrophages uptake NPs, and such a high signal for NPs in the cells[95]. A study by Qie et al does indeed suggests phagocytosis as the main method of NP uptake in macrophages,

although macrophages can also uptake NPs through various other cellular processes[95,96]. Again, this depends on how the interaction between the NP and cell occurs. As for the NPs themselves, their properties such as size and surface composition does greatly affect their uptake by macrophages[97]. Although studies show a reduced uptake of PEGylated NPs, the same study by Qie et al tested the extent of this reduction according to NP size[95]. This study showed that the largest PEGylated NPs assessed, which were 100nm in size, showed higher uptake in macrophages than their smaller-sized counterparts (30nm and 50nm). As the TANPs used in this assay are 100nm-sized PEGylated NPs, they should display successful NP uptake, which is indeed the case.

Although macrophages being phagocytic cells can seem like an unfair advantage when assessing NP cellular uptake, the rationale for their use as a cell model in the project surpasses this ability of theirs. Indeed, the use of macrophages is pertinent as they are one of the main cell types present at inflammatory sites in many inflammatory diseases. As they possess roles in the induction and resolution of inflammation, they are an ideal model for preliminary assessment of our NPs potential in CID cases, and thus assessing cellular uptake for this cell population is very insightful[98].

Additional microscopy experiments were performed and enabled us to confirm that the NPs were truly internalized by the cells, and not simply on the cell surface (Figure 17). Beyond that, microscopy studies confirmed that the NPs were able to reach the mitochondria. In our project, mitochondria targeting refers to the increased likelihood of the NPs reaching the mitochondria, and not their exclusive localization to the mitochondria. As previously explained, TPP enables mitochondrial targeting of the NP systems thanks to its positive charge and lipophilic nature[78]. Thus, the microscopy data obtained allowed us to confirm this NP property, conferring potential

to the system for mitochondrial ROS reduction, thus increasing its potential. Next steps in this direction may include assessing the NP's potential for the reduction of mitochondrial ROS specifically, in comparison to cytosolic ROS, and see if this varies the observed outcome on cellular ROS and inflammation.

4.10. Assessment of NP cytotoxicity

In order to ensure our NPs can accomplish their intended function in cells, it is important to ensure they do not cause cell toxicity. This is increasingly important as the NPs are made to reduce inflammation, and cell toxicity can follow from inflammation[99]. Thus, assessing cytotoxicity of the NPs is a first step at ensuring they do not induce inflammation. An absence of cytotoxicity was confirmed in RAW264.7 macrophages for TANP treatments at concentrations up to 20uM (Figure 15). This can notably be explained by the fact that NP-induced ROS production, caused by the NP's properties, plays an important part in NP-induced cytotoxicity. Indeed, most NP structures that do induce some cytotoxicity do so via the generation of ROS[100]. As our NPs are design to reduce ROS levels, it could be suggested that this may play a part in reducing the NP's cytotoxicity, thus resulting in no cytotoxicity observed.

In addition, the low cytotoxicity can be explained by the different components of the NP which were selected with this in mind. Notably, as previously discussed, PLGA and PEG are both FDA-approved biocompatible polymers, and thus would not cause cell toxicity[73]. Additionally, as stated earlier, TPP is a well researched, commonly used compound for mitochondria targeting, and is present on the structure of commercially available agents such as probes for mitochondrial labelling[77]. Thus, it is not a big cause for concern when it comes to cytotoxicity. As for the polymer, its cytotoxicity is difficult to estimate as it is a synthesized compound. However, given the cytotoxicity results obtained using the TANPs, the presence of

the polymer in the cells does not seem to have any toxic effects. Despite this, further testing could be done in order to confirm this. Lastly, the ROS-scavengers themselves, as natural ROS-scavenging antioxidants, should also not exert big cytotoxic effects but rather help reduce NP cytotoxicity. Despite the suggested low toxicity potential of the compounds used, when treating the cells with a higher concentration of TANPs, such as the 100uM of TANPs tested, there seemed be a slight decrease in cell viability. Although the difference is statistically significant, many studies do not consider a decrease in cell viability to values above 80% as a concern[101].

4.11. Assessment of NP ROS-reduction potential in vitro

As our NP system is designed to be ROS-scavenging, the assessment of its ROS-reduction abilities in vitro is an important step to the validation of our system (Figure 18). Thus, LPS induction was used to inflame RAW264.7 cells, causing a significant increase in ROS levels as confirmed by the data obtained. According to the DCFH-DA assay performed, the TANPs were able to reduce ROS levels in vitro in RAW264.7 macrophages. Interestingly, increasing the treatment concentration of TANPs doesn't lead to a greater ROS-reduction. Possible explanations include that the ROS levels in the LPS-induced cells may be insufficient to activate the entirety of treated NPs. In such a case, only a certain amount of treated NPs are activated, independent of the amount of NPs entering the cells. Another possible explanation could pertain to the saturation of the cellular uptake capacity; a maximum amount of NPs may be entering cells within the given treatment time[102,103]. This would once again result in the same number of NPs being activated within the cell, and thus explain the similar results obtained at different TANP treatment concentrations. An additional possible explanation could be linked to the location of the ROS in the cells. As the macrophages are activated with LPS, they will respond as they would in the case of a bacterial infection, and thus likely proceed to oxidative bursts. Thus, the NPs might be activated before they can reach ROS in other parts of the cell such as the

mitochondria. This may explain why the ROS levels are similar independently of the NP concentration used; they are unable to exert their ROS reduction function on mitochondrial ROS.

4.12. Assessment of NP anti-inflammatory properties in vitro

As described, ROS and inflammation are tightly interlinked and thus, we hope for our ROS-reducing system to be capable of inflammation reduction as well. To assess this, LPS-induced macrophages were treated with TANPs and EGNPs. Levels of TNF- α and ABCA1 were measured by RT-qPCR to observe fluctuations possibly indicative of inflammation reduction (Figure 19). TNF- α is a widely studied pro-inflammatory cytokine produced notably from the NF-kB and MAPK pathways which high ROS levels can dysregulate[37]. Thus, a reduction of ROS is expected to lead to a reduction of TNF- α levels. As expected, LPS treatment caused an inflammatory state in the cells as demonstrated by the increase in TNF-α levels observed[104]. In contrast, pre-treatment of the cells with both NPs showed lower TNF-α levels, with this difference showing statistical significance in the case of the TANPs. This indicates that a 24h TANP treatment can prevent inflammation. NPs are likely capable of scavenging ROS as they are produced, before they can influence the inflammatory signaling pathways or cause cellular oxidative damage.

A second measurement of inflammation reduction was done via the monitoring of ABCA1 levels. As an anti-inflammatory molecule, ABCA1 allowed us to assess how NPs affect the anti-inflammatory signals within a cell, enabling further assessment of inflammation reduction properties[105]. Interestingly, LPS treatment caused a slight significant increase in ABCA1 levels. This may seem counterintuitive as inflamed cells shouldn't exhibit increases in anti-inflammatory signals. However, as a response to an increase in inflammation, cells will eventually try to resolve their inflammatory state by increasing their expression of anti-

inflammatory molecules[39]. Thus, this may just be an effect of the timepoint, and concentration chosen for the LPS treatment. When using the TANPs, an even higher increase in ABCA1 levels is observed, although it does not display statistical significance in comparison to the inflamed state. Despite this, there is a high standard deviation for the NP treatment data, and one datapoint which seems to greatly differ from the others obtained. This may be the cause for the non-significance observed. Thus, repeating the assay to obtain more replicates could provide more clarity on the results obtained. This is true as well for the TNF-α data obtained which also show big standard deviations. Despite this, the preliminary data obtained shows promising indications of our NP system's anti-inflammatory properties. Confirmation of these properties by monitoring of a greater amount of inflammatory molecules would also be advisable to strengthen the anti-inflammatory capacities of the NP.

An additional advantage to assessing ABCA1 levels relates to its involvement in atherosclerosis. Indeed, ABCA1 is mainly known for its cholesterol efflux function[106]. Thus, assessing its levels provides some insight on the potential therapeutic value of our NP system in atherosclerosis disease cases. In this context, the increase in ABCA1 levels observed, although non-significant, provides indications that the NP system could have potential in the treatment of atherosclerosis. Indeed, increasing ABCA1 levels is viewed as a promising avenue for the treatment of atherosclerosis[107].

5. Future Directions

The system now established has great potential to be pushed further to better understand its abilities and better modulate them. Notably, one important next step would be to strengthen the anti-inflammatory data to better assess the anti-inflammatory effect of the ROS-reduction

achieved by the NPs. Looking at a broader range of NP concentrations for each of the NP formulations would give more insight on this intrinsic effect of the NPs.

Additionally, optimizing the ROS-sensitivity and ROS-scavenging properties of the system would allow us to better modulate the conditions of its activation as well as how much ROS they scavenge. By optimizing the system this way, it would be possible to create a system that selectively activates in high ROS conditions above a certain determined threshold and reduces ROS levels back down to a homeostatic range. Possible avenues also include combining multiple ROS-scavengers within a same system to see how customizable the system can become to a specific disease condition.

Furthermore, the NP's drug delivery potential has yet to be harnessed. Thus, looking at the NP's drug delivery properties such as encapsulation efficiency of drugs and RNA therapies could give insight on how to maximize the system's therapeutic potential. Possible options include encapsulating disease specific or anti-inflammatory drugs, or various mRNAs, miRNAs or siRNAs to interfere with cellular pathways involved in either inflammation or a specific disease condition. Consequently, assessing the NP in various cell lines more aligned with a specific disease condition, or even in in vivo models of ROS-mediated disease conditions, could shed even more light on its potential as a therapeutic agent.

6. Conclusion

In conclusion, whether as a symptom or the cause of a disease itself, inflammation is a common characteristic of many health conditions. Inflammation is tightly linked to ROS, especially in cases of CIDs where inflammation is a main pillar of the persisting disease condition, which also often presenting with signs of high oxidative stress. As a foundation for the development of novel CID treatments, this project set out to develop a NP system with intrinsic

ROS-sensitive and ROS-scavenging properties. The goal is for this newly developed system to be harnessed as an inflammation reduction and therapy delivery tool. In order to achieve this objective, 3 aims were delineated: the development of suitable biomaterials for NP assembly, the optimization and assessment of the NP system's properties and the system's assessment for ROS and inflammation reduction in vitro. A significant contribution was made to each aim of the project. Initially, a library of biomaterials including polymers and mitochondria targeting surface molecules were synthesized. Subsequently, the functional groups of interest were assessed to confirm their interactions and properties corresponded to the ones intended, and a variety of NP systems were then assembled for optimization purposes. NPs were shown to be non-toxic, have a good cellular uptake and be able to reach the mitochondria. In addition, they were shown to be ROS-sensitive, reduce ROS levels in vitro and reduce inflammatory signaling molecules in vitro as well. Thus, we have successfully developed NPs possessing the intended capabilities. As the system is entirely ROS-mediated, it can be harnessed for use in virtually any ROS-involving disease condition, making it an extremely versatile tool with high therapeutic potential. Thanks to this work, we hope to help pave the way to a new set of CID therapies.

Figures throughout this thesis were made using a combination of MestReNova, ChemDraw, GraphPad PRISM, FLOWJO, Biorender and FIJI ImageJ software.

References

(1) Arulselvan, P.; Fard, M. T.; Tan, W. S.; Gothai, S.; Fakurazi, S.; Norhaizan, M. E.; Kumar, S. S. Role of Antioxidants and Natural Products in Inflammation. *Oxid Med Cell Longev* **2016**, *2016*, 1–15. https://doi.org/10.1155/2016/5276130.

(2) Chen, L.; Deng, H.; Cui, H. Inflammatory Responses and Inflammation-Associated Diseases in Organs. *Oncotarget* **2018**, *9*, 7204–7218. https://doi.org/10.18632/oncotarget.23208.

(3) Furman, D.; Campisi, J.; Verdin, E.; Carrera-Bastos, P.; Targ, S.; Franceschi, C.; Ferrucci, L.; Gilroy, D. W.; Fasano, A.; Miller, G. W.; Miller, A. H.; Mantovani, A.; Weyand, C. M.; Barzilai, N.; Goronzy, J. J.; Rando, T. A.; Effros, R. B.; Lucia, A.; Kleinstreuer, N.; Slavich, G. M. Chronic Inflammation in the Etiology of Disease across the Life Span. *Nat Med* **2019**, *25*, 1822–1832. https://doi.org/10.1038/s41591-019-0675-0.

(4) Pahwa, R.; Jialal, I.; Goyal, A. Chronic Inflammation. StatPearls Publishing April 2023. https://www.ncbi.nlm.nih.gov/books/NBK493173/.

(5) Magliano, D. J.; Boyko, E. J. *IDF Diabetes Atlas*; International Diabetes Federation, 2021.

(6) Gustavsson, A.; Norton, N.; Fast, T.; Frölich, L.; Georges, J.; Holzapfel, D.; Kirabali, T.; Krolak-Salmon, P.; Rossini, P. M.; Ferretti, M. T.; Lanman, L.; Chadha, A. S.; van der Flier, W. M. Global Estimates on the Number of Persons across the Alzheimer's Disease Continuum. *Alzheimers Dement* **2022**, *19*, 658–670. https://doi.org/10.1002/alz.12694.

(7) Collaborators, G. B. D. 2021 R. A. Global, Regional, and National Burden of Rheumatoid Arthritis, 1990-2020, and Projections to 2050: A Systematic Analysis of the Global Burden of Disease Study 2021. *Lancet Rheumatol* **2023**, *5*, e594–e610. https://doi.org/10.1016/S2665-9913(23)00211-4.

(8) Benzian, H.; Beltrán-Aguilar, E.; Niederman, R. Global Health Threats Are Also Oral Health Threats. *The Journal of the American Dental Association* **2023**, *0*. https://doi.org/10.1016/j.adaj.2023.01.007.

(9) Straub, R. H.; Schradin, C. Chronic Inflammatory Systemic Diseases. *Evol Med Public Health* **2016**, *2016*, 37–51. https://doi.org/10.1093/emph/eow001.

(10) Zhang, Q.; Dehaini, D.; Zhang, Y.; Zhou, J.; Chen, X.; Zhang, L.; Fang, R. H.; Gao, W.; Zhang, L. Neutrophil Membrane-Coated Nanoparticles Inhibit Synovial Inflammation and Alleviate Joint Damage in Inflammatory Arthritis. *Nat Nanotechnol* **2018**, *13*, 1182–1190. https://doi.org/10.1038/s41565-018-0254-4.

(11) Patil, K. R.; Mahajan, U. B.; Unger, B. S.; Goyal, S. N.; Belemkar, S.; Surana, S. J.; Ojha, S.; Patil, C. R. Animal Models of Inflammation for Screening of Anti-Inflammatory Drugs: Implications for the Discovery and Development of Phytopharmaceuticals. *Int J Mol Sci* **2019**, *20*. https://doi.org/10.3390/ijms20184367.

(12) Ray, P. D.; Huang, B.-W.; Tsuji, Y. Reactive Oxygen Species (ROS) Homeostasis and Redox Regulation in Cellular Signaling. *Cell Signal* **2012**, *24*, 981–990. https://doi.org/10.1016/j.cellsig.2012.01.008.

(13) Phaniendra, A.; Jestadi, D. B.; Periyasamy, L. Free Radicals: Properties, Sources, Targets, and Their Implication in Various Diseases. *Indian Journal of Clinical Biochemistry* **2014**, *30*, 11–26. https://doi.org/10.1007/s12291-014-0446-0.

(14) Biswas, S. K. Does the Interdependence between Oxidative Stress and Inflammation Explain the Antioxidant Paradox? *Oxid Med Cell Longev* **2016**, *2016*, 1–9. https://doi.org/10.1155/2016/5698931.

(15) Sena, L. A.; Chandel, N. S. Physiological Roles of Mitochondrial Reactive Oxygen Species. *Mol Cell* **2012**, *48*, 158–167. https://doi.org/10.1016/j.molcel.2012.09.025.

(16) Mittal, M.; Siddiqui, M. R.; Tran, K.; Reddy, S. P.; Malik, A. B. Reactive Oxygen Species in Inflammation and Tissue Injury. *Antioxid Redox Signal* **2014**, *20*, 1126–1167. https://doi.org/10.1089/ars.2012.5149.

(17) Pizzino, G.; Irrera, N.; Cucinotta, M.; Pallio, G.; Mannino, F.; Arcoraci, V.; Squadrito, F.; Altavilla, D.; Bitto, A. Oxidative Stress: Harms and Benefits for Human Health. *Oxid Med Cell Longev* **2017**, *2017*, 1–13. https://doi.org/10.1155/2017/8416763.

(18) Juan, C. A.; de la Lastra, J. M.; Plou, F. J.; Pérez-Lebeña, E. The Chemistry of Reactive Oxygen Species (ROS) Revisited: Outlining Their Role in Biological Macromolecules (DNA, Lipids and Proteins) and Induced Pathologies. *Int J Mol Sci* **2021**, *22*, 4642. https://doi.org/10.3390/ijms22094642.

(19) Kong, Q.; Lin, C. G. Oxidative Damage to RNA: Mechanisms, Consequences, and Diseases. *Cellular and Molecular Life Sciences* **2010**, *67*, 1817–1829. https://doi.org/10.1007/s00018-010-0277-y.

(20) de Almeida, A. J. P. O.; de Oliveira, J. C. P. L.; da Silva Pontes, L. V.; de Souza Júnior, J. F.; Gonçalves, T. A. F.; Dantas, S. H.; de Almeida Feitosa, M. S.; Silva, A. O.; de Medeiros, I. A. ROS: Basic Concepts, Sources, Cellular Signaling, and Its Implications in Aging Pathways. *Oxid Med Cell Longev* **2022**, *2022*, 1–23. https://doi.org/10.1155/2022/1225578.

(21) Arnett, S. D.; Osbourn, D. M.; Moore, K. D.; Vandaveer, S. S.; Lunte, C. E. Determination of 8-Oxoguanine and 8-Hydroxy-2′-Deoxyguanosine in the Rat Cerebral Cortex Using Microdialysis Sampling and Capillary Electrophoresis with Electrochemical Detection. *Journal of Chromatography B* **2005**, *827*, 16–25. https://doi.org/10.1016/j.jchromb.2005.05.036.

(22) Shields, H. J.; Traa, A.; Van Raamsdonk, J. M. Beneficial and Detrimental Effects of Reactive Oxygen Species on Lifespan: A Comprehensive Review of Comparative and Experimental Studies. *Front Cell Dev Biol* **2021**, *9*. https://doi.org/10.3389/fcell.2021.628157.

(23) Cecarini, V.; Gee, J.; Fioretti, E.; Amici, M.; Angeletti, M.; Eleuteri, A. M.; Keller, J. N. Protein Oxidation and Cellular Homeostasis: Emphasis on Metabolism. *Biochimica et Biophysica Acta (BBA) - Molecular Cell Research* **2007**, *1773*, 93–104. https://doi.org/10.1016/j.bbamcr.2006.08.039.

(24) Tirichen, H.; Yaigoub, H.; Xu, W.; Wu, C.; Li, R.; Li, Y. Mitochondrial Reactive Oxygen Species and Their Contribution in Chronic Kidney Disease Progression Through Oxidative Stress. *Front Physiol* **2021**, *12*. https://doi.org/10.3389/fphys.2021.627837.

(25) Zorov, D. B.; Juhaszova, M.; Sollott, S. J. Mitochondrial Reactive Oxygen Species (ROS) and ROS-Induced ROS Release. *Physiol Rev* **2014**, *94*, 909–950. https://doi.org/10.1152/physrev.00026.2013.

(26) Bandara, A. B.; Drake, J. C.; Brown, D. A. Complex II Subunit SDHD Is Critical for Cell Growth and Metabolism, Which Can Be Partially Restored with a Synthetic Ubiquinone Analog. *BMC Mol Cell Biol* **2021**, *22*. https://doi.org/10.1186/s12860-021-00370-w.

(27) Skonieczna, M.; Hejmo, T.; Poterala-Hejmo, A.; Cieslar-Pobuda, A.; Buldak, R. J. NADPH Oxidases: Insights into Selected Functions and Mechanisms of Action in Cancer and Stem Cells. *Oxid Med Cell Longev* **2017**, *2017*, e9420539. https://doi.org/10.1155/2017/9420539.

(28) Pecchillo Cimmino, T.; Ammendola, R.; Cattaneo, F.; Esposito, G. NOX Dependent ROS Generation and Cell Metabolism. *Int J Mol Sci* **2023**, *24*, 2086. https://doi.org/10.3390/ijms24032086.

(29) Bhattacharyya, A.; Chattopadhyay, R.; Mitra, S.; Crowe, S. E. Oxidative Stress: An Essential Factor in the Pathogenesis of Gastrointestinal Mucosal Diseases. *Physiol Rev* **2014**, *94*, 329–354. https://doi.org/10.1152/physrev.00040.2012.

(30) Bienert, G. P.; Schjoerring, J. K.; Jahn, T. P. Membrane Transport of Hydrogen Peroxide. *Biochimica et Biophysica Acta (BBA) - Biomembranes* **2006**, *1758*, 994–1003. https://doi.org/10.1016/j.bbamem.2006.02.015.

(31) Jena, A. B.; Samal, R. R.; Bhol, N. K.; Duttaroy, A. K. Cellular Red-Ox System in Health and Disease: The Latest Update. *Biomedicine & Pharmacotherapy* **2023**, *162*, 114606. https://doi.org/10.1016/j.biopha.2023.114606.

(32) ZITKA, O.; SKALICKOVA, S.; GUMULEC, J.; MASARIK, M.; ADAM, V.; HUBALEK, J.; TRNKOVA, L.; KRUSEOVA, J.; ECKSCHLAGER, T.; KIZEK, R. Redox Status Expressed as GSH:GSSG Ratio as a Marker for Oxidative Stress in Paediatric Tumour Patients. *Oncol Lett* **2012**, *4*, 1247–1253. https://doi.org/10.3892/ol.2012.931.

(33) Han, X.; Shen, T.; Lou, H. Dietary Polyphenols and Their Biological Significance. *Int J Mol Sci* **2007**, *8*, 950.

(34) Jin, T. Curcumin and Dietary Polyphenol Research: Beyond Drug Discovery. *Acta Pharmacol Sin* **2018**, *39*, 779–786. https://doi.org/10.1038/aps.2017.179.

(35) Tsao, R. Chemistry and Biochemistry of Dietary Polyphenols. *Nutrients* **2010**, *2*, 1231–1246. https://doi.org/10.3390/nu2121231.

(36) Yeo, J.; Lee, J.; Yoon, S.; Kim, W. J. Tannic Acid-Based Nanogel as an Efficient Anti-Inflammatory Agent. *Biomater Sci* **2020**, *8*, 1148–1159. https://doi.org/10.1039/C9BM01384A.

(37) Liu, J.; Han, X.; Zhang, T.; Tian, K.; Li, Z.; Luo, F. Reactive Oxygen Species (ROS) Scavenging Biomaterials for Anti-Inflammatory Diseases: From Mechanism to Therapy. *J Hematol Oncol* **2023**, *16*.

(38) Baek, S.-H.; Park, T.; Kang, M.-G.; Park, D. Anti-Inflammatory Activity and ROS Regulation Effect of Sinapaldehyde in LPS-Stimulated RAW 264.7 Macrophages. *Molecules* **2020**, *25*, 4089. https://doi.org/10.3390/molecules25184089.

(39) Freire, M. O.; Van Dyke, T. E. Natural Resolution of Inflammation. *Periodontol 2000* **2013**, *63*, 149–164. https://doi.org/10.1111/prd.12034.

(40) Sargent, A. L.; Leedberg, J. A.; Burress, J. E.; Dalwadi, P. S.; O'Fallon, K. S.; Gaffney-Stomberg, E.; Gaines, P. C. W. Quantitatively Assessing the Respiratory Burst in Innate Immune Cells. *Methods Mol Biol* **2023**, *2614*, 47–70. https://doi.org/10.1007/978-1-0716-2914-7_4.

(41) Li, Z.; Xu, D.; Li, X.; Deng, Y.; Li, C. Redox Imbalance in Chronic Inflammatory Diseases. *Biomed Res Int* **2022**, *2022*, 1–3. https://doi.org/10.1155/2022/9813486.

(42) Hayashi, I.; Morishita, Y.; Imai, K.; Nakamura, M.; Nakachi, K.; Hayashi, T. High-Throughput Spectrophotometric Assay of Reactive Oxygen Species in Serum. *Mutation Research/Genetic Toxicology and Environmental Mutagenesis* **2007**, *631*, 55–61. https://doi.org/10.1016/j.mrgentox.2007.04.006.

(43) Sies, H.; Jones, D. P. Reactive Oxygen Species (ROS) as Pleiotropic Physiological Signalling Agents. *Nat Rev Mol Cell Biol* **2020**, *21*. https://doi.org/10.1038/s41580-020-0230-3.

(44) Joudeh, N.; Linke, D. Nanoparticle Classification, Physicochemical Properties, Characterization, and Applications: A Comprehensive Review for Biologists. *J Nanobiotechnology* **2022**, *20*. https://doi.org/10.1186/s12951-022-01477-8.

(45) Gwinn, M. R.; Vallyathan, V. Nanoparticles: Health Effects—Pros and Cons. *Environ Health Perspect* **2006**, *114*, 1818–1825. https://doi.org/10.1289/ehp.8871.

(46) Lee, J. H.; Yeo, Y. Controlled Drug Release from Pharmaceutical Nanocarriers. *Chem Eng Sci* **2015**, *125*, 75–84. https://doi.org/10.1016/j.ces.2014.08.046.

(47) Ahmad, F.; Salem-Bekhit, M. M.; Khan, F.; Alshehri, S.; Khan, A.; Ghoneim, M. M.; Wu, H.-F.; Taha, E. I.; Elbagory, I. Unique Properties of Surface-Functionalized Nanoparticles for Bio-Application: Functionalization Mechanisms and Importance in Application. *Nanomaterials* **2022**, *12*, 1333. https://doi.org/10.3390/nano12081333.

(48) Lu, H.; Zhang, S.; Wang, J.; Chen, Q. A Review on Polymer and Lipid-Based Nanocarriers and Its Application to Nano-Pharmaceutical and Food-Based Systems. *Front Nutr* **2021**, *8*. https://doi.org/10.3389/fnut.2021.783831.

(49) Guimarães, D.; Cavaco-Paulo, A.; Nogueira, E. Design of Liposomes as Drug Delivery System for Therapeutic Applications. *Int J Pharm* **2021**, *601*, 120571. https://doi.org/10.1016/j.ijpharm.2021.120571.

(50) Mitchell, M. J.; Billingsley, M. M.; Haley, R. M.; Wechsler, M. E.; Peppas, N. A.; Langer, R. Engineering Precision Nanoparticles for Drug Delivery. *Nat Rev Drug Discov* **2020**, *20*, 1–24. https://doi.org/10.1038/s41573-020-0090-8.

(51) Chenxi, Z.; Hemmat, A.; Thi, N.; Afrand, M. Nanoparticle-Enhanced Drug Delivery Systems: An up-to-Date Review. *J Mol Liq* **2025**, 126999. https://doi.org/10.1016/j.molliq.2025.126999.

(52) Blanco, E.; Shen, H.; Ferrari, M. Principles of Nanoparticle Design for Overcoming Biological Barriers to Drug Delivery. *Nat Biotechnol* **2015**, *33*, 941–951. https://doi.org/10.1038/nbt.3330.

(53) Zhang, J.; Shi, Y.; Zheng, Y.; Pan, C.; Yang, X.; Dou, T.; Wang, B.; Lu, W. Homing in on an Intracellular Target for Delivery of Loaded Nanoparticles Functionalized with a Histone Deacetylase Inhibitor. *Oncotarget* **2017**, *8*, 68242–68251. https://doi.org/10.18632/oncotarget.20021.

(54) De Jong, W. H.; Borm, P. J. A. Drug Delivery and Nanoparticles: Applications and Hazards. *Int J Nanomedicine* **2008**, *3*, 133. https://doi.org/10.2147/ijn.s596.

(55) Chen, Z.; Farag, M. A.; Zhong, Z.; Zhang, C.; Yang, Y.; Wang, S.; Wang, Y. Multifaceted Role of Phyto-Derived Polyphenols in Nanodrug Delivery Systems. *Adv Drug Deliv Rev* **2021**, 113870. https://doi.org/10.1016/j.addr.2021.113870.

(56) Chenthamara, D.; Subramaniam, S.; Ramakrishnan, S. G.; Krishnaswamy, S.; Essa, M. M.; Lin, F.-H.; Qoronfleh, M. W. Therapeutic Efficacy of Nanoparticles and Routes of Administration. *Biomater Res* **2019**, *23*. https://doi.org/10.1186/s40824-019-0166-x.

(57) Corbo, C.; Molinaro, R.; Parodi, A.; Toledano Furman, N. E.; Salvatore, F.; Tasciotti, E. The Impact of Nanoparticle Protein Corona on Cytotoxicity, Immunotoxicity and Target Drug Delivery. *Nanomedicine* **2016**, *11*, 81–100. https://doi.org/10.2217/nnm.15.188.

(58) Tavakol, M.; Hajipour, M. J.; Ferdousi, M.; Zanganeh, S.; Maurizi, L. Competition of Opsonins and Dysopsonins on the Nanoparticle Surface. *Nanoscale* **2023**, *15*, 17342–17349. https://doi.org/10.1039/d3nr03823h.

(59) OWENSIII, D.; PEPPAS, N. Opsonization, Biodistribution, and Pharmacokinetics of Polymeric Nanoparticles. *Int J Pharm* **2006**, *307*, 93–102. https://doi.org/10.1016/j.ijpharm.2005.10.010.

(60) Hoshyar, N.; Gray, S.; Han, H.; Bao, G. The Effect of Nanoparticle Size on in Vivo Pharmacokinetics and Cellular Interaction. *Nanomedicine* **2016**, *11*, 673–692. https://doi.org/10.2217/nnm.16.5.

(61) Dolai, J.; Mandal, K.; Jana, N. R. Nanoparticle Size Effects in Biomedical Applications. *ACS Appl Nano Mater* **2021**, *4*, 6471–6496. https://doi.org/10.1021/acsanm.1c00987.

(62) Barua, S.; Mitragotri, S. Challenges Associated with Penetration of Nanoparticles across Cell and Tissue Barriers: A Review of Current Status and Future Prospects. *Nano Today* **2014**, *9*, 223–243. https://doi.org/10.1016/j.nantod.2014.04.008.

(63) Behzadi, S.; Serpooshan, V.; Tao, W.; Hamaly, M. A.; Alkawareek, M. Y.; Dreaden, E. C.; Brown, D.; Alkilany, A. M.; Farokhzad, O. C.; Mahmoudi, M. Cellular Uptake of Nanoparticles: Journey inside the Cell. *Chem Soc Rev* **2017**, *46*, 4218–4244. https://doi.org/10.1039/c6cs00636a.

(64) Naslavsky, N.; Caplan, S. The Enigmatic Endosome – Sorting the Ins and Outs of Endocytic Trafficking. *J Cell Sci* **2018**, *131*. https://doi.org/10.1242/jcs.216499.

(65) Hagerman, A. E.; Riedl, K. M.; Jones, G. A.; Sovik, K. N.; Ritchard, N. T.; Hartzfeld, P. W.; Riechel, T. L. High Molecular Weight Plant Polyphenolics (Tannins) as Biological Antioxidants. *J Agric Food Chem* **1998**, *46*, 1887–1892. https://doi.org/10.1021/jf970975b.

(66) Chen, C.; Yang, H.; Yang, X.; Ma, Q. Tannic Acid: A Crosslinker Leading to Versatile Functional Polymeric Networks: A Review. *RSC Adv* **2022**, *12*, 7689–7711. https://doi.org/10.1039/D1RA07657D.

(67) He, J.; Xu, L.; Yang, L.; Wang, X. Epigallocatechin Gallate Is the Most Effective Catechin Against Antioxidant Stress via Hydrogen Peroxide and Radical Scavenging Activity. *Medical Science Monitor* **2018**, *24*, 8198–8206. https://doi.org/10.12659/msm.911175.

(68) Nag, S.; Bhunia, A.; Mohanto, S.; Ahmed, M. G.; Subramaniyan, V. Rising Potentials of Epigallocatechin Gallate (EGCG) Loaded Lipid-Based Delivery Platforms for Breast Cancer. *Discover Applied Sciences* **2024**, *6*. https://doi.org/10.1007/s42452-024-05878-2.

(69) Bhuia, M. S.; Rahaman, M. M.; Islam, T.; Bappi, M. H.; Sikder, M. I.; Hossain, K. N.; Akter, F.; Al Shamsh Prottay, A.; Rokonuzzman, M.; Gürer, E. S.; Calina, D.; Islam, M. T.; Sharifi-Rad, J. Neurobiological Effects of Gallic Acid: Current Perspectives. *Chin Med* **2023**, *18*, 27. https://doi.org/10.1186/s13020-023-00735-7.

(70) Laurano, R.; Torchio, A.; Ciardelli, G.; Boffito, M. In Situ Forming Bioartificial Hydrogels with ROS Scavenging Capability Induced by Gallic Acid Release with

Potential in Chronic Skin Wound Treatment. *Gels* **2023**, *9*, 731. https://doi.org/10.3390/gels9090731.

(71) Dzah, C. S.; Zhang, H.; Gobe, V.; Asante-Donyinah, D.; Duan, Y. Anti- and pro-Oxidant Properties of Polyphenols and Their Role in Modulating Glutathione Synthesis, Activity and Cellular Redox Potential: Potential Synergies for Disease Management. *Advances in Redox Research* **2024**, *11*, 100099. https://doi.org/10.1016/j.arres.2024.100099.

(72) Roy, P. K.; Rashid, F.; Bragg, J.; Ibdah, J. A.; Hepatology, D. of G.; and Medicine, U. of M. S. of; Columbia; Missouri; States, U. Role of the JNK Signal Transduction Pathway in Inflammatory Bowel Disease. *World J Gastroenterol* **2008**, *14*, 200. https://doi.org/10.3748/wjg.14.200.

(73) Makadia, H. K.; Siegel, S. J. Poly Lactic-Co-Glycolic Acid (PLGA) as Biodegradable Controlled Drug Delivery Carrier. *Polymers (Basel)* **2011**, *3*, 1377–1397. https://doi.org/10.3390/polym3031377.

(74) Ventola, C. L. The Nanomedicine Revolution: Part 1: Emerging Concepts. *Pharmacy and Therapeutics* **2012**, *37*, 512.

(75) Suk, J. S.; Xu, Q.; Kim, N.; Hanes, J.; Ensign, L. M. PEGylation as a Strategy for Improving Nanoparticle-Based Drug and Gene Delivery. *Adv Drug Deliv Rev* **2016**, *99*, 28–51. https://doi.org/10.1016/j.addr.2015.09.012.

(76) Padín-González, E.; Lancaster, P.; Bottini, M.; Gasco, P.; Tran, L.; Fadeel, B.; Wilkins, T.; Monopoli, M. P. Understanding the Role and Impact of Poly (Ethylene Glycol) (PEG) on Nanoparticle Formulation: Implications for COVID-19 Vaccines. *Front Bioeng Biotechnol* **2022**, *10*, 882363. https://doi.org/10.3389/fbioe.2022.882363.

(77) Zielonka, J.; Joseph, J.; Sikora, A.; Hardy, M.; Ouari, O.; Vasquez-Vivar, J.; Cheng, G.; Lopez, M.; Kalyanaraman, B. Mitochondria-Targeted Triphenylphosphonium-Based Compounds: Syntheses, Mechanisms of Action, and Therapeutic and Diagnostic Applications. *Chem Rev* **2017**, *117*, 10043–10120. https://doi.org/10.1021/acs.chemrev.7b00042.

(78) Marrache, S.; Pathak, R. K.; Dhar, S. Formulation and Optimization of Mitochondria-Targeted Polymeric Nanoparticles. *Methods in molecular biology* **2015**, 103–112. https://doi.org/10.1007/978-1-4939-2288-8_8.

(79) Patel, Y.; Manturthi, S.; Tiwari, S.; Gahunia, E.; Courtemanche, A.; Gandelman, M.; Côté, M.; Gadde, S. Development of Pro-Resolving and Pro-Efferocytic Nanoparticles for Atherosclerosis Therapy. *ACS Pharmacol Transl Sci* **2024**, *7*, 3086–3095. https://doi.org/10.1021/acsptsci.4c00292.

(80) Basak, S.; Khare, H. A.; Kempen, P. J.; Kamaly, N.; Almdal, K. Nanoconfined Anti-Oxidizing RAFT Nitroxide Radical Polymer for Reduction of Low-Density Lipoprotein Oxidation and Foam Cell Formation. *Nanoscale Adv* **2022**, *4*, 742–753. https://doi.org/10.1039/d1na00631b.

(81) Pasek-Allen, J. L.; Wilharm, R. K.; Bischof, J. C.; Pierre, V. C. NMR Characterization of Polyethylene Glycol Conjugates for Nanoparticle Functionalization. *ACS Omega* **2023**, *8*, 4331–4336. https://doi.org/10.1021/acsomega.2c07669.

(82) Hayek, A.; Xu, Y.; Okada, T.; Barlow, S.; Zhu, X.; Moon, J. H.; Marder, S. R.; Yang, S. Poly(Glycidyl Methacrylate)s with Controlled Molecular Weights as Low-Shrinkage Resins for 3D Multibeam Interference Lithography. *J Mater Chem* **2008**, *18*, 3316. https://doi.org/10.1039/b809656b.

(83) San Andrés, M. P.; Baños-Cabrera, M.; Gutiérrez-Fernández, L.; Díez-Pascual, A. M.; Vera-López, S. Fluorescence Study of Riboflavin Interactions with Graphene Dispersed in Bioactive Tannic Acid. *Int J Mol Sci* **2021**, *22*, 5270. https://doi.org/10.3390/ijms22105270.

(84) Gorbounov, M.; Halloran, P.; Masoudi Soltani, S. Hydrophobic and Hydrophilic Functional Groups and Their Impact on Physical Adsorption of CO2 in Presence of H2O: A Critical Review. *Journal of CO2 Utilization* **2024**, *86*, 102908. https://doi.org/10.1016/j.jcou.2024.102908.

(85) Eras, A.; Castillo, D.; Suárez, M.; Vispo, N. S.; Albericio, F.; Rodriguez, H. Chemical Conjugation in Drug Delivery Systems. *Front Chem* **2022**, *10*. https://doi.org/10.3389/fchem.2022.889083.

(86) Albu, M. G.; Ghica, M. V.; Giurginca, M.; Trandafir, V.; Cotrut, C. Spectral Characteristics and Antioxidant Properties of Tannic Acid Immobilized on Collagen Drug-Delivery Systems. *Revista de Chimie* **2009**, *60*, 666–672.

(87) Zarycz, M. N. C.; Fonseca Guerra, C. NMR ^{1}H-Shielding Constants of Hydrogen-Bond Donor Reflect Manifestation of the Pauli Principle. *J Phys Chem Lett* **2018**, *9*, 3720–3724. https://doi.org/10.1021/acs.jpclett.8b01502.

(88) Liang, J.; Liu, B. ROS-responsive Drug Delivery Systems. *Bioeng Transl Med* **2016**, *1*, 239–251. https://doi.org/10.1002/btm2.10014.

(89) Peiró Cadahía, J.; Previtali, V.; Troelsen, N. S.; Clausen, M. H. Prodrug Strategies for Targeted Therapy Triggered by Reactive Oxygen Species. *Medchemcomm* **2019**, *10*, 1531–1549. https://doi.org/10.1039/c9md00169g.

(90) Achilli, C.; Ciana, A.; Fagnoni, M.; Balduini, C.; Minetti, G. Susceptibility to Hydrolysis of Phenylboronic Pinacol Esters at Physiological PH. *Open Chem* **2012**, *11*, 137–139. https://doi.org/10.2478/s11532-012-0159-2.

(91) Zafar, S.; Ahmed, R.; Khan, R. Biotransformation: A Green and Efficient Way of Antioxidant Synthesis. *Free Radic Res* **2016**, *50*, 939–948. https://doi.org/10.1080/10715762.2016.1209745.

(92) Hosseini, M.; Moghaddam, L.; Barner, L.; Cometta, S.; Hutmacher, D. W.; Savi, F. M. The Multifaceted Role of Tannic Acid: From Its Extraction and Structure to Antibacterial

Properties and Applications. *Prog Polym Sci* **2024**, 101908. https://doi.org/10.1016/j.progpolymsci.2024.101908.

(93) Zwolak, I. Epigallocatechin Gallate for Management of Heavy Metal-Induced Oxidative Stress: Mechanisms of Action, Efficacy, and Concerns. *Int J Mol Sci* **2021**, *22*, 4027. https://doi.org/10.3390/ijms22084027.

(94) Thavasi, V.; Leong, L. P.; Bettens, R. P. A. Investigation of the Influence of Hydroxy Groups on the Radical Scavenging Ability of Polyphenols. *J Phys Chem A* **2006**, *110*, 4918–4923. https://doi.org/10.1021/jp057315r.

(95) Qie, Y.; Yuan, H.; von Roemeling, C. A.; Chen, Y.; Liu, X.; Shih, K. D.; Knight, J. A.; Tun, H. W.; Wharen, R. E.; Jiang, W.; Kim, B. Y. S. Surface Modification of Nanoparticles Enables Selective Evasion of Phagocytic Clearance by Distinct Macrophage Phenotypes. *Sci Rep* **2016**, *6*. https://doi.org/10.1038/srep26269.

(96) Ngo, W.; Ahmed, S.; Blackadar, C.; Bussin, B.; Ji, Q.; Mladjenovic, S. M.; Sepahi, Z.; Chan, W. C. W. Why Nanoparticles Prefer Liver Macrophage Cell Uptake in Vivo. *Adv Drug Deliv Rev* **2022**, *185*, 114238. https://doi.org/10.1016/j.addr.2022.114238.

(97) Walkey, C. D.; Olsen, J. B.; Guo, H.; Emili, A.; Chan, W. C. W. Nanoparticle Size and Surface Chemistry Determine Serum Protein Adsorption and Macrophage Uptake. *J Am Chem Soc* **2012**, *134*, 2139–2147. https://doi.org/10.1021/ja2084338.

(98) Fujiwara, N.; Kobayashi, K. Macrophages in Inflammation. *Current Drug Target - Inflammation & Allergy* **2005**, *4*, 281–286. https://doi.org/10.2174/1568010054022024.

(99) Yang, Y.; Jiang, G.; Zhang, P.; Fan, J. Programmed Cell Death and Its Role in Inflammation. *Mil Med Res* **2015**, *2*. https://doi.org/10.1186/s40779-015-0039-0.

(100) Fu, P. P.; Xia, Q.; Hwang, H.-M.; Ray, P. C.; Yu, H. Mechanisms of Nanotoxicity: Generation of Reactive Oxygen Species. *J Food Drug Anal* **2014**, *22*, 64–75. https://doi.org/10.1016/j.jfda.2014.01.005.

(101) López-García, J.; Lehocký, M.; Humpolíček, P.; Sáha, P. HaCaT Keratinocytes Response on Antimicrobial Atelocollagen Substrates: Extent of Cytotoxicity, Cell Viability and Proliferation. *J Funct Biomater* **2014**, *5*, 43–57. https://doi.org/10.3390/jfb5020043.

(102) Cartiera, M. S.; Johnson, K. M.; Rajendran, V.; Caplan, M. J.; Saltzman, W. M. The Uptake and Intracellular Fate of PLGA Nanoparticles in Epithelial Cells. *Biomaterials* **2009**, *30*, 2790–2798. https://doi.org/10.1016/j.biomaterials.2009.01.057.

(103) Chou, H.-C.; Chiu, S.-J.; Hu, T.-M. Quantitative Analysis of Macrophage Uptake and Retention of Fluorescent Organosilica Nanoparticles: Implications for Nanoparticle Delivery and Therapeutics. *ACS Appl Nano Mater* **2024**, *7*, 3656–3667. https://doi.org/10.1021/acsanm.3c05058.

(104) Rouzer, C. A.; Jacobs, A. T.; Nirodi, C. S.; Kingsley, P. J.; Morrow, J. D.; Marnett, L. J. RAW264.7 Cells Lack Prostaglandin-Dependent Autoregulation of Tumor Necrosis

Factor-α Secretion. *J Lipid Res* **2005**, *46*, 1027–1037. https://doi.org/10.1194/jlr.m500006-jlr200.

(105) Tang, C.; Liu, Y.; Kessler, P. S.; Vaughan, A. M.; Oram, J. F. The Macrophage Cholesterol Exporter ABCA1 Functions as an Anti-Inflammatory Receptor. **2009**, *284*, 32336–32343. https://doi.org/10.1074/jbc.m109.047472.

(106) Matsuo, M. ABCA1 and ABCG1 as Potential Therapeutic Targets for the Prevention of Atherosclerosis. *J Pharmacol Sci* **2022**, *148*, 197–203. https://doi.org/10.1016/j.jphs.2021.11.005.

(107) Soumian, S.; Albrecht, C.; Davies, A. H.; Gibbs, R. G. J. ABCA1 and Atherosclerosis. *Vascular Medicine* **2005**, *10*, 109–119. https://doi.org/10.1191/1358863x05vm593ra.